

3.2 Conceptual Model of Geothermal Resources

3.2.1 Reservoir Structure

(1) Major Permeable Structure Controlling Geothermal Activity

From geological information, 4 faults (f1, f2, f3 and f4) are deduced to control geothermal activity near the surface (see Fig. 3.1-5). From gravity information, it is deduced that 3 faults (G1, G2 and G3) are distributed under the ground (see Fig. 3.1-7). An additional 3 faults (R1, R2 and R3) are also estimated (see Fig. 3.1-10). Considering their locations and trending, the following 6 faults are proposed to be the major faults controlling geothermal activity in this field (see Fig. 3.2-1). Although the dipping angles of these faults are uncertain, an angle of 80° is provisionally assumed for every fault in this study, considering the general trend in volcanic regions around the world.

Fault F1, trending north to south, corresponds to G1 and R1, though this fault is not described on the geological map. As there is a high Bouguer anomaly on the eastern side of this fault, the dipping direction of this fault is estimated to be west.

Fault F2, trending north to south, corresponds to f1, G2 and R2. As there is a high Bouguer anomaly on the western side of this fault, the dipping direction of this fault is estimated to be east.

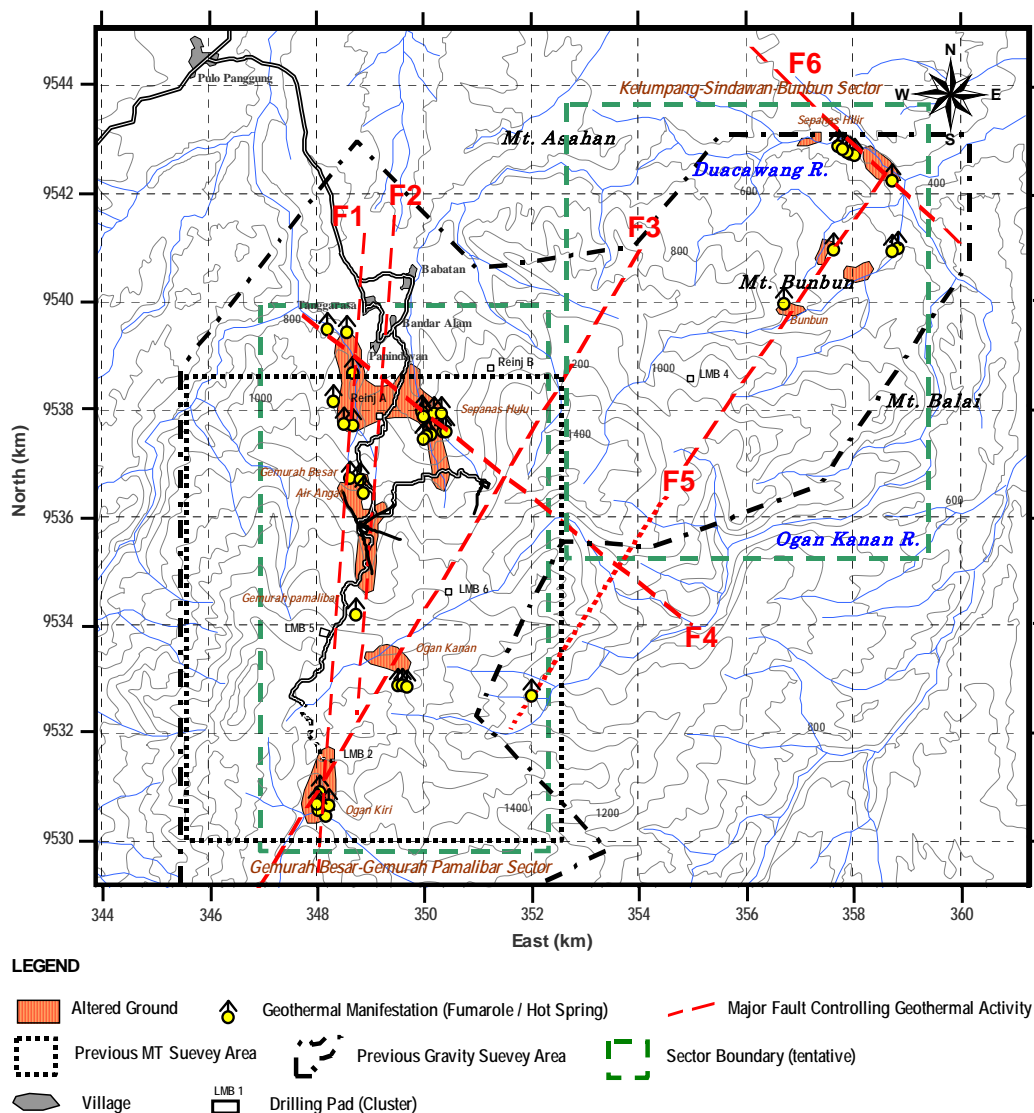
Fault F3, trending northeast to southwest, corresponds to f2 and R3. The dipping direction of this fault is assumed to be northwest, based on the previous geological cross-section.

Fault F4, trending northwest to southeast, corresponds to f3, though this structure is not detected from either gravity data or resistivity data. The dipping direction of this fault is assumed to be southwest, based on the previous geological cross-section.

Fault F5, trending northeast to southwest, corresponds to G3, though this structure is not described on previous geological maps. Its location is outside of the previous MT survey area. As there is a high Bouguer anomaly on the southeastern side of this fault, the dipping direction of this fault is estimated to be northwest. Along the southwestern extent of the estimated F5, there are geothermal manifestations (see Fig. 3.2-1).

Fault F6, trending northwest to southeast, corresponds to f4. This location is outside of the previous MT survey area and is a marginal area of the previous gravity survey. The dipping direction of this fault is uncertain.

Geothermal manifestations and altered ground in the Gemurah Besar-Gemurah Pamalibar sector are distributed along faults F1, F2, F3 and F4, and in the Kelumpang-Sindawan-Bunbun sector are distributed along faults F5 and F6. The southwestern extent of fault F5 is still uncertain, because it is situated outside of the previous MT and gravity survey areas. If this fault extends into the Gemurah Besar-Gemurah Pamalibar sector, there is a possibility that geothermal activity in the Kelumpang-Sindawan-Bunbun sector originates from the Gemurah Besar-Gemurah Pamalibar sector. Therefore, these faults can be regarded as the major permeable structures controlling geothermal activity in this field.



(Based on PGE data)

Fig. 3.2-1 Proposed Major Structure Controlling Geothermal Activity

(2) Cap Rock of Geothermal Resources

A low resistivity layer is detected by MT survey in this field. The elevation of the bottom of this layer around Cluster LMB 1 and Cluster LMB 3 is about 500 m to 800 m above sea level. Considering the well geology (see Fig. 3.1-4), this low resistivity layer can be correlated with an argillized layer. Around Cluster LMB 1, the bottom of the layer characterized by argillization is at a level of 600 m to 900 m above sea level. That around Cluster LMB 3 is at a level of about 500 m above the sea level. Temperature profiles of all drilled wells, at the horizons of the argillized layer, give a rather linear gradient. Moreover, lost circulation can scarcely be recognized at these horizons. This means that the detected low resistivity layer corresponding with the argillized layer can be regarded as a cap rock (impermeable layer).

3.2.2 Fluid Flow

In the Kelumpang-Sindawan-Bunbun sector, it is considered that geothermal fluid flows from southwest to northeast along fault F5 (see Fig. 3.2-2). And this flow branches off at the point where fault F5 crosses fault F6, toward the northwest along fault F6. Around this crossing point, geothermal fluid (hot water) also flows up and discharges on the ground surface. Geothermal fluid must be diluted and cooled by ground water as it flows up. Considering the chemistry of the discharged geothermal fluid, the parental fluid likely has a temperature of 240°C to 300°C and Cl concentration of 5500 to 6500 ppm. This parental fluid must originate from meteoric water and its pH will be neutral. The location of the source of this fluid flow is still uncertain, though this parental fluid must exist southwest of Mt. Bunbun.

In the Gemurah Besar-Gemurah Pamalibar sector, it is considered that geothermal fluid flows from south to north along faults F1 and F2 and also flows from southwest to northeast along fault F3. These flows branch off where fault F4 crosses these faults, toward the northwest along fault F4. Hot water does not flow right up to the ground surface, unlike the flow in the Kelumpang-Sindawan-Bunbun sector. It is considered that an argillized impermeable layer must be preventing the flow to the ground surface. All of the hot spring water in this sector originates from a shallow aquifer heated by steam, gas and conductive heat through the argillized impermeable layer. It is difficult to know the chemistry of the deep geothermal fluid because hot spring water does not contain deep hot water. However, the chemistry of the fumarolic gases in this sector indicates that the pH of the deep hot water must be neutral.

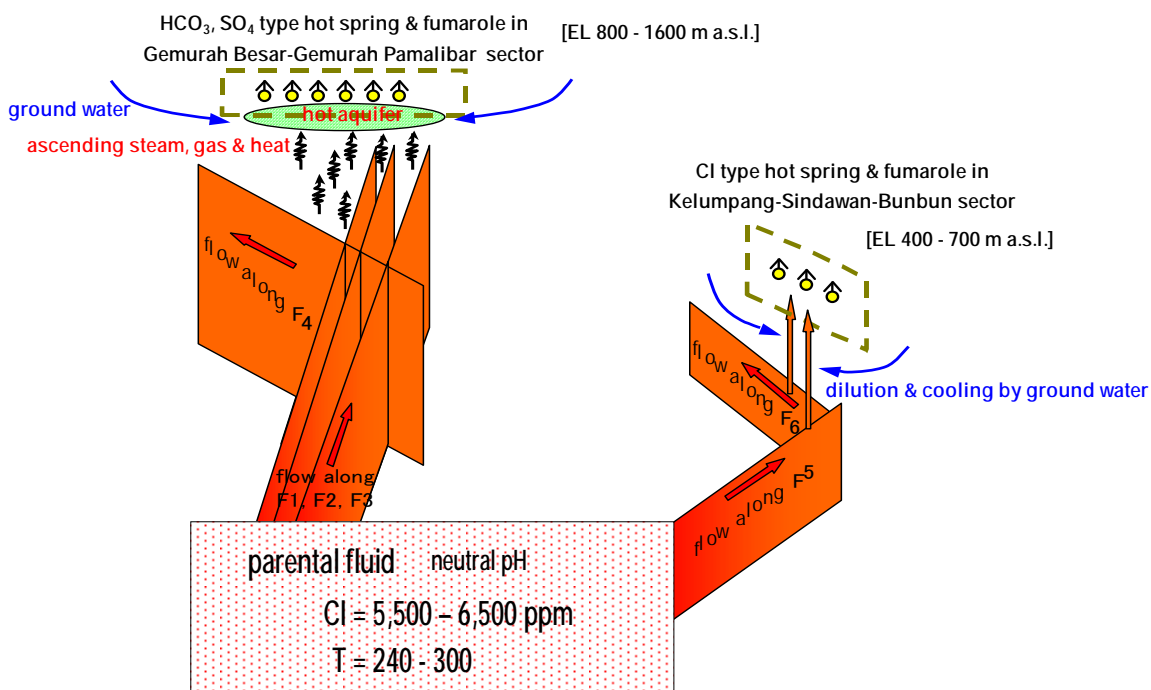


Fig. 3.2-2 Fluid Flow Pattern Model

3.2.3 Reservoir Conceptual Model

In the Gemurah Besar-Gemurah Pamalibar sector (the western part of the Lumut Balai geothermal field), meteoric water is heated at depth and turns into geothermal brine. This brine flows up on the eastern side of the Mt. Lumut summit and flows north along faults F1, F2, F3 and F4. This flowing brine must be neutral in pH. Steam, gas and conductive heat derived from this brine, flowing through an argillized impermeable layer, comes into a shallower aquifer and heats it up. Hot water from this heated aquifer is discharged as hot springs. The bottom of well LMB 1-2 is situated around fault F1 (see Fig. 3.2-3). The bottoms of wells LMB 1-3, LMB 1-4 and LMB 1-5 are situated around the fault F2, and that of well LMB 3-1 is situated around fault F3.

In the Kelumpang-Sindawan-Bunbun sector (the northeastern part of the Lumut Balai geothermal field), geothermal brine flows northeast along fault F5, and this flow branches off where fault F5 crosses fault F6, flowing northwest along fault F6. Geothermal brine also flows up to the ground surface around that crossing point. The source of this geothermal brine flow must be also situated on the eastern side of the Mt. Lumut summit, and the parental fluid has a temperature of 240°C to 300°C and Cl concentration of 5500 to 6500 ppm. However, it is still uncertain whether the source is the same as for the fluid flow system in the Gemurah Besar-Gemurah Pamalibar sector or not. They may be the same.

Considering the chemistry of fumarolic gases, the content of NCG in the geothermal steam produced in this field seems to be relatively low for future geothermal power generation.

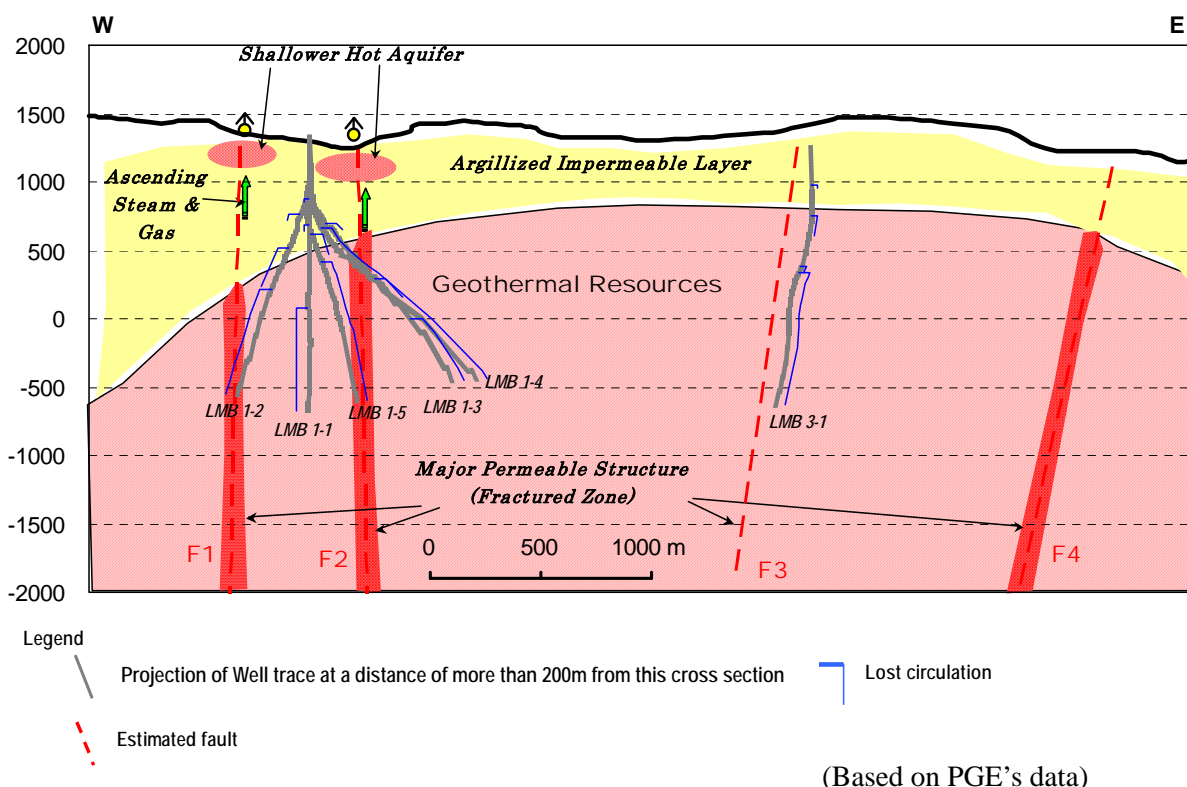


Fig. 3.2-3 Proposed Conceptual Model

3.3 RESERVOIR SIMULATION STUDY

3.3.1 Reservoir Numerical Model

The reservoir simulation study made use of the popular geothermal reservoir simulator program TOUGH2, which was developed at Lawrence Berkeley National Laboratory (LBNL) in the USA.

(1) Creating a grid for the model

After careful consideration of the conceptual model, a grid was generated to discretize the geothermal system in three dimensions. A three-dimensional representation of the simulation grid is presented in Fig. 3.3-1.

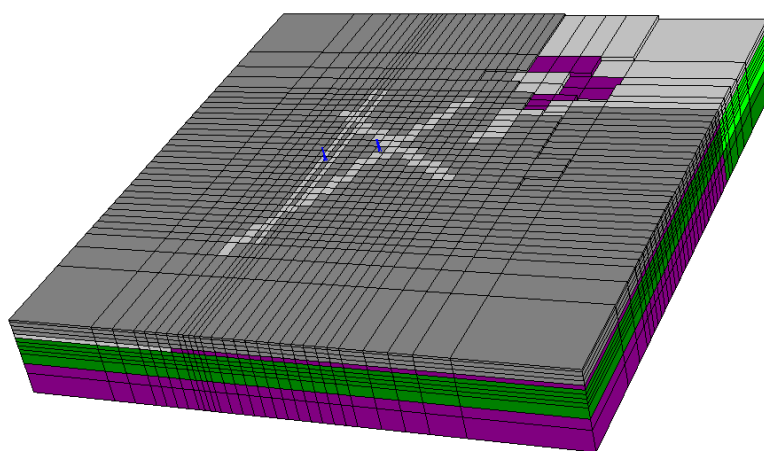


Fig. 3.3-1 General View of 3-dimensional Reservoir Simulation Model

The grid design of the Lumut Balai numerical model is shown in Fig. 3.3-2. The simulation model is oriented North-North-East (NNE) to South-South-West (SSW) along the major structure direction of the field, and includes a total area of 661.5 km². The model is rectangular in outline, and measures 24.5 km in the EWE-WNW direction (the “x” direction) and 27.0 km in the NNE-SSW direction (the “y” direction). The simulation area covers all the Lumut Balai geothermal fields. Each layer of the model is divided into 28 (the “x” direction) by 33 (the “y” direction) blocks, or 924 blocks per layer. In areas where reservoir information is available or where the well density is high, the grid blocks are smaller. Conversely, in areas where no reservoir information is readily available or where the well density is low, the grid blocks are larger. Overall, with twelve layers, the grid contains a total of 11,088 grid blocks. In the vertical dimension, the model extends from an elevation of + 700 m relative to mean sea level (msl) to –3,000 m msl. The overall thickness of 3,700 m is subdivided into 12 layers. Some grid blocks of the model corresponding to an elevation lower than 700 m msl in the top two layers are eliminated, depending on the topographic elevation. The thickness of the top layers is 100 m, that of the next 8 layers is 200 m, the next two layers (layers 10 and 11) are 500 m thick, and the bottom layer is 1000 m thick, as shown in Fig. 3.3-3.

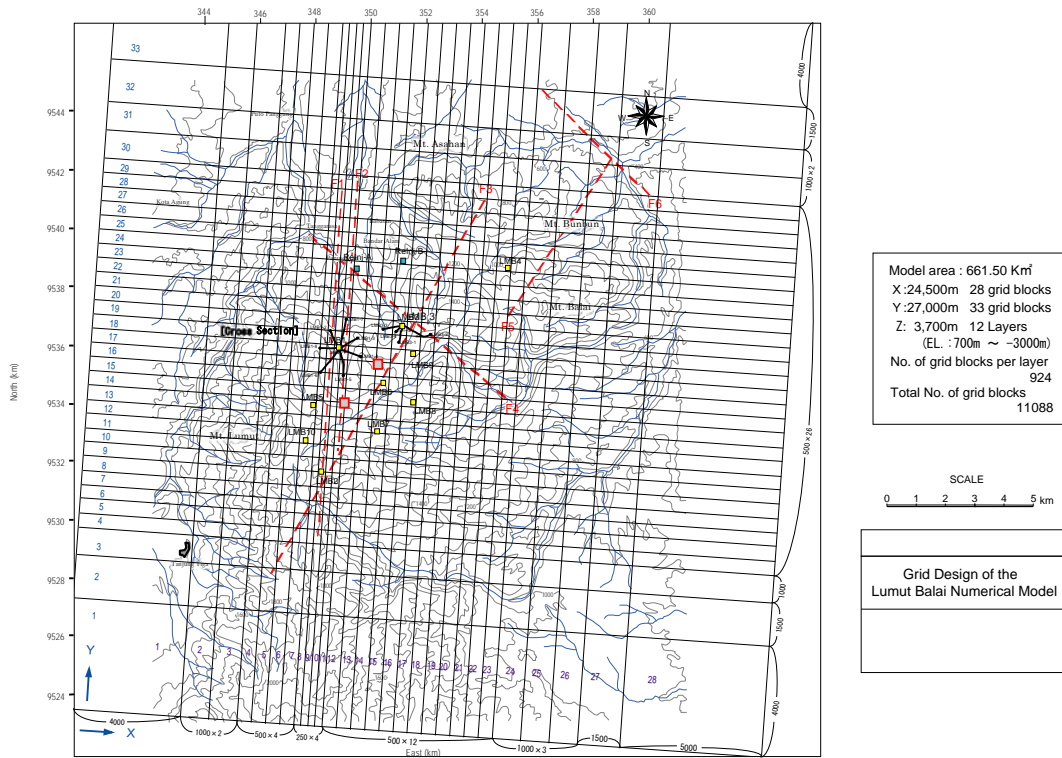


Fig. 3.3-2 Grid Design of the Lumut Balai Numerical Model

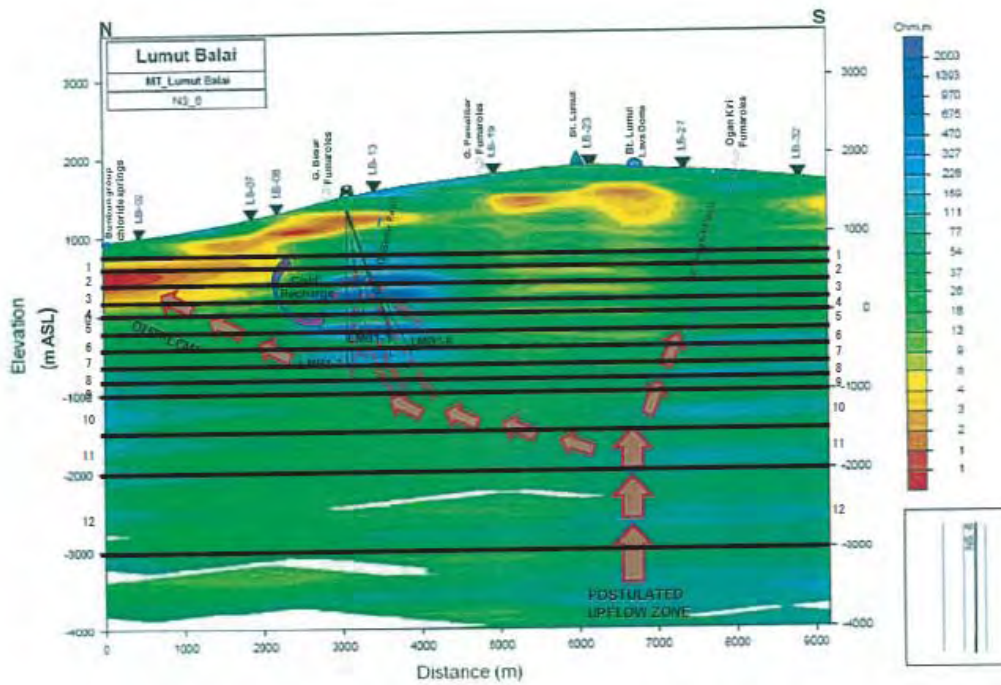


Fig. 3.3-3 Vertical Grid Design of the Lumut Balai Numerical Model

(2) Rock properties

A numerical model is discretized as a network of blocks, in which each block covers a portion of the geothermal reservoir. Each of the reservoir parameters (thermodynamic, geologic, petrophysical, chemical, etc.) within the volume represented by a given grid block has a single, averaged value. Thus, for a given volume, subdivision into more grid blocks enables a more detailed representation of the actual reservoir to be achieved. Once the grid system is constructed, the required grid-block parameters are entered. Rock properties required for the reservoir simulation are density, porosity, permeability, specific heat and thermal conductivity of each rock, as shown in Fig. 3.3-4. The rock properties should be set for all grid blocks.

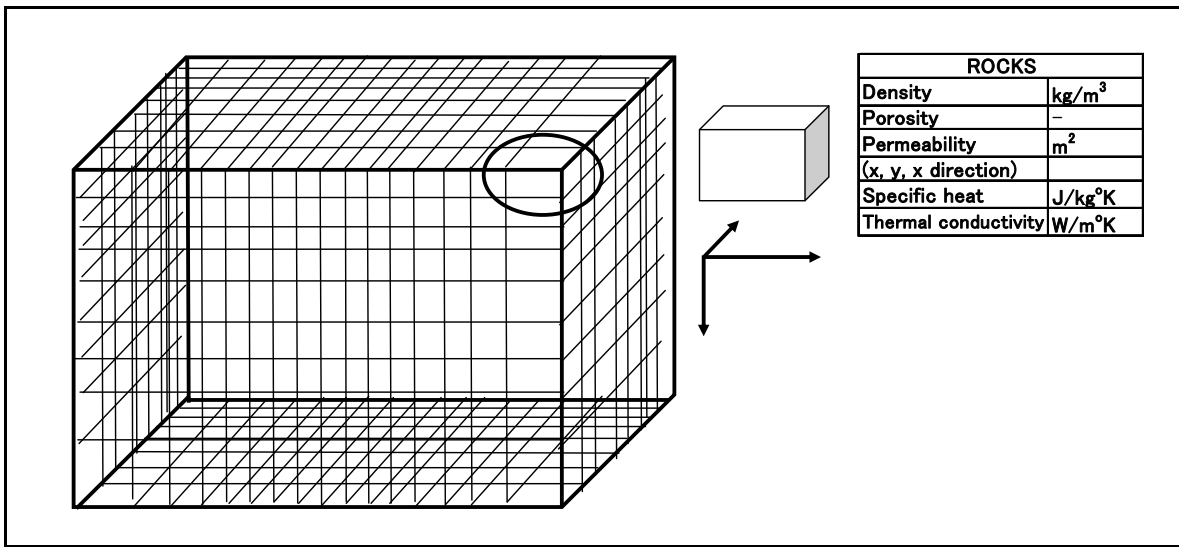


Fig. 3.3-4 Setting of Rock Properties for Numerical Model

The most important parameter is permeability, because permeability of the rocks usually has a wide range depending on the rock type and structure, and depending also on the control flow direction and mass flow rate of the fluids in the reservoirs. In order to estimate the permeability distribution, resistivity distributions are good reference, because low resistivity regions are considered to be low permeability regions that play the role of cap rocks. Cap rocks limit the reservoir extent by preventing high-temperature fluids from flowing out into the surroundings. Thus, reservoirs with high-temperature fluids will be formed beneath the cap rocks, meaning that the distribution of low resistivity that is correlated with cap rocks may represent the reservoir distribution.

The basic distributions of rock properties were examined, with a consideration of the resistivity distribution, geological formations and fault structures in the Lumut Balai geothermal field,. Then, both rock properties and their distribution were repeatedly modified by trial and error until the numerical model could reasonably explain the natural state conditions in the reservoirs. Table 3.3-1 shows the properties of each rock type, and Figs. 3.3-5 to 3.3-12 show the distributions of the rock property set in the numerical model.

Table 3.3-1 Rock Properties

	Density (kg/m ³)	Porosity (-)	Permeability ($\times 10^{-15} \text{ m}^2$)			Cond. (W/m°C)	Spec.Heat (J/kg°C)
			X	Y	Z		
			ROK01	2250.0	0.17		
ROK02	2250.0	0.16	30	30	30	1.60	850.0
ROK03	2250.0	0.15	20	20	20	1.60	850.0
ROK04	2400.0	0.12	15	15	15	1.60	850.0
ROK05	2450.0	0.10	6	6	6	1.60	850.0
ROK06	2500.0	0.07	3	3	3	1.60	850.0
ROK07	2200.0	0.03	1	1	1	1.60	850.0
ROK08	2200.0	0.02	0.1	0.1	0.1	1.60	850.0

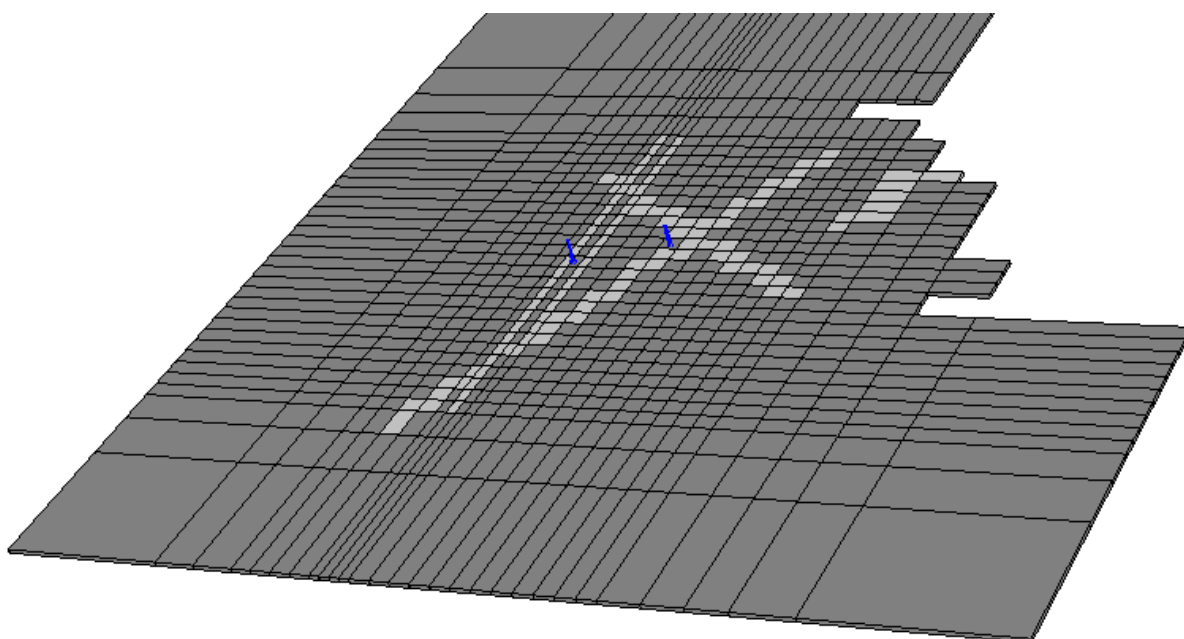


Fig. 3.3-5 Rock Property Distribution in Layer 1 (650 m asl)

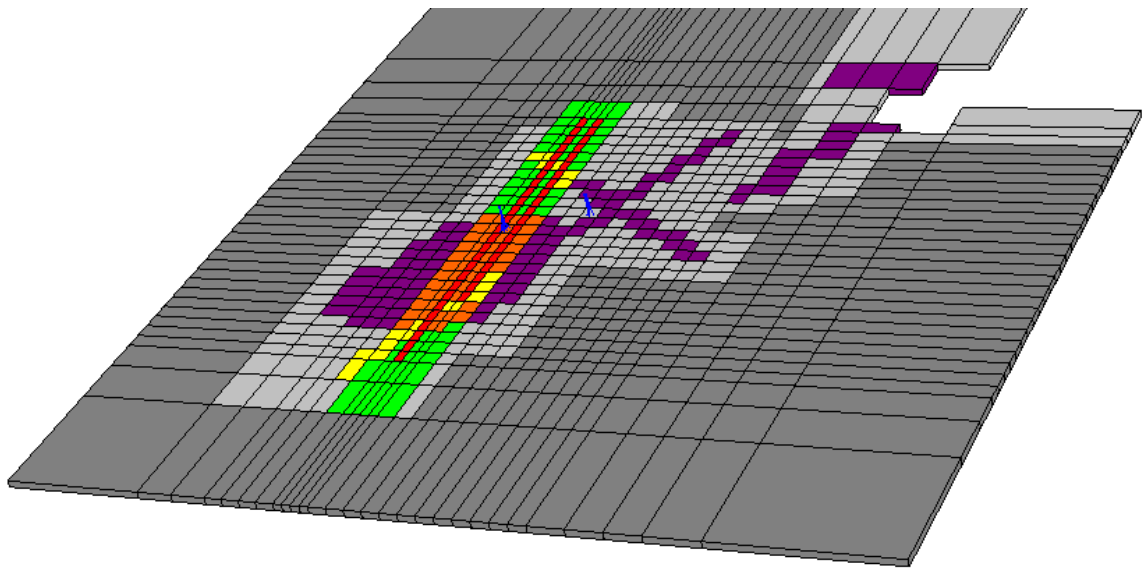


Fig. 3.3-6 Rock Property Distribution in Layer 2 (500 m asl)

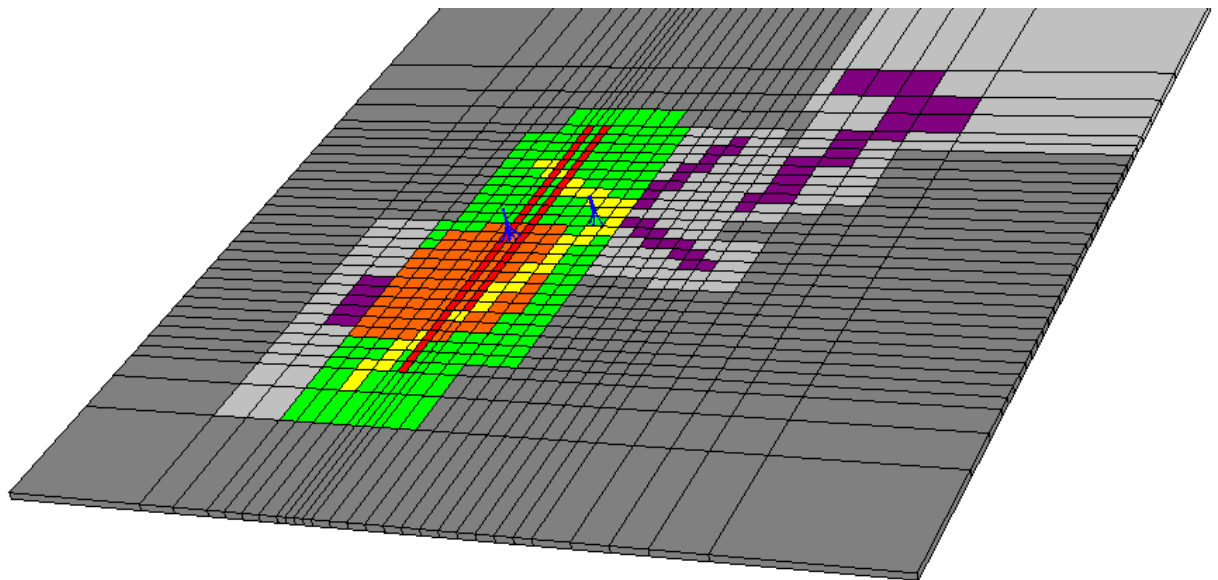


Fig. 3.3-7 Rock Property Distribution in Layer 3 (300 m asl)

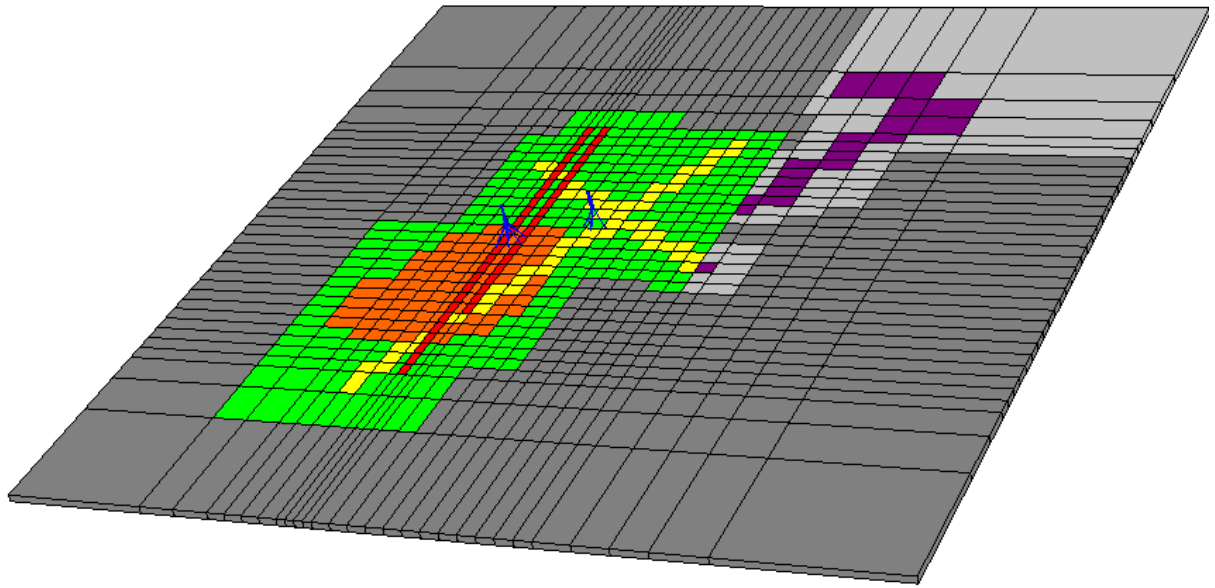


Fig. 3.3-8 Rock Property Distribution in Layer 4 (100 m asl)

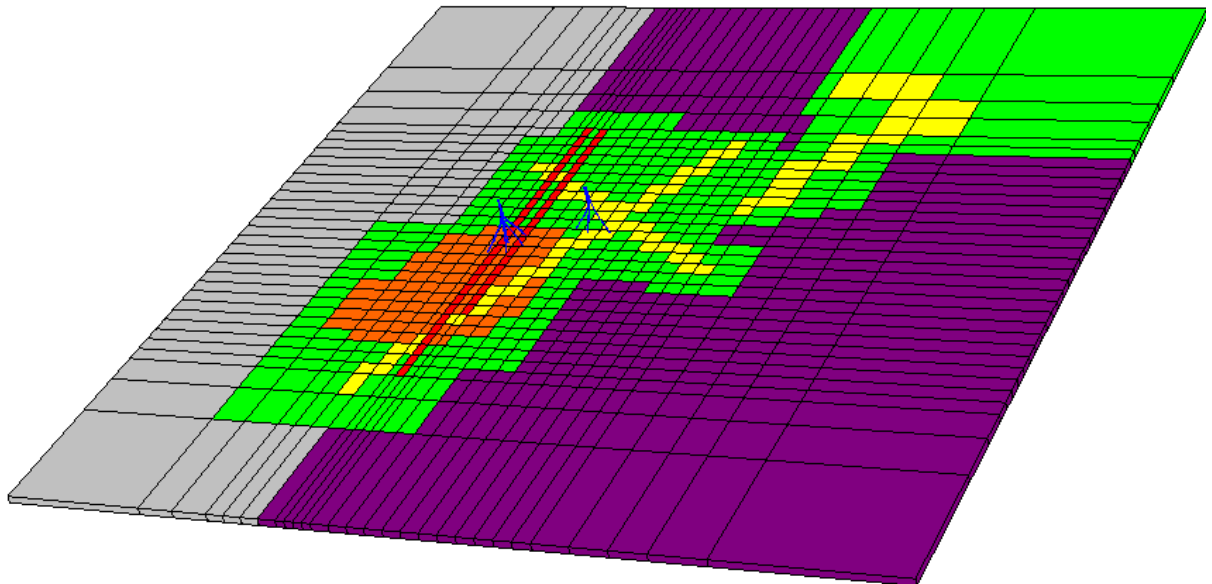


Fig. 3.3-9 Rock Property Distribution in Layer 5 (-100 m asl)

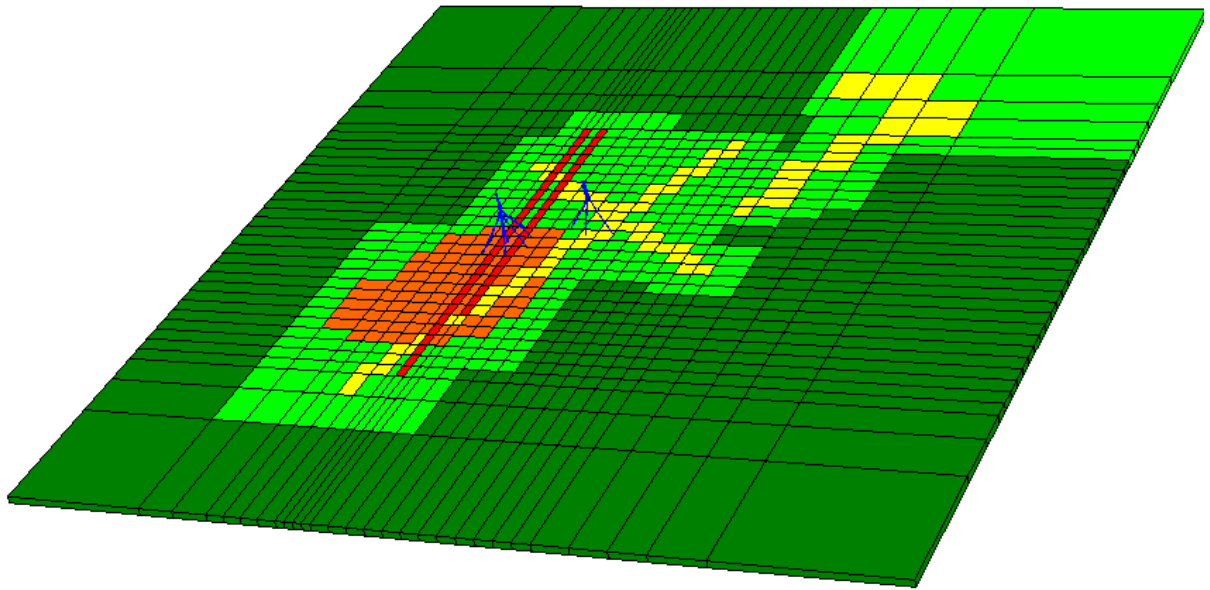


Fig. 3.3-10 Rock Property Distribution in Layers 6 to 10 (-300 to -1250 m asl)

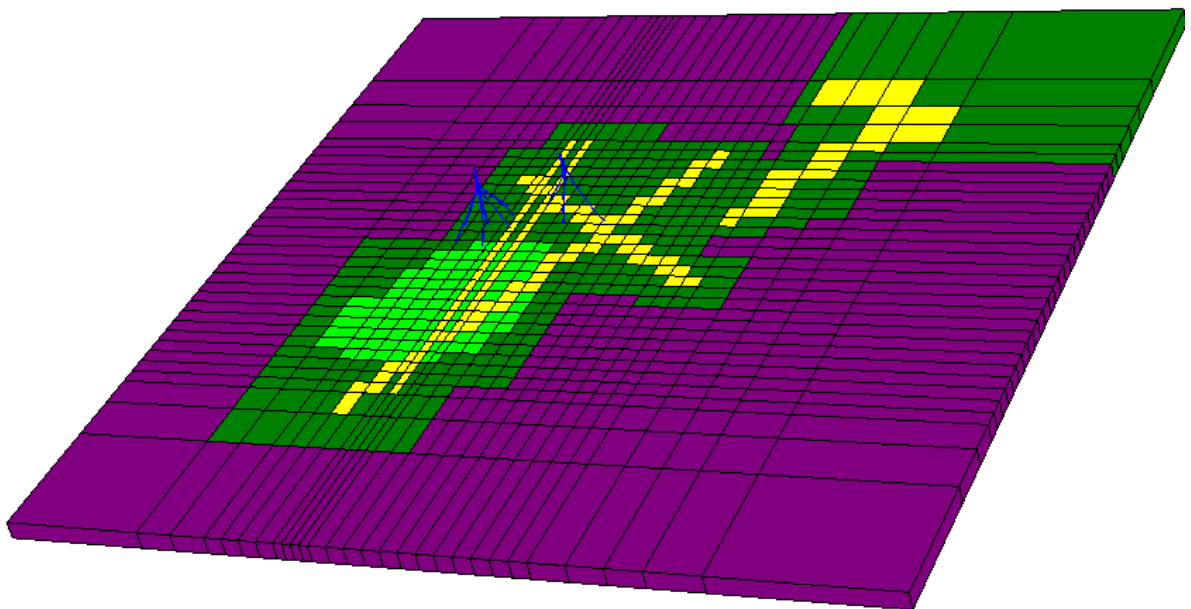


Fig. 3.3-11 Rock Property Distribution in Layer 11 (-1750 m asl)

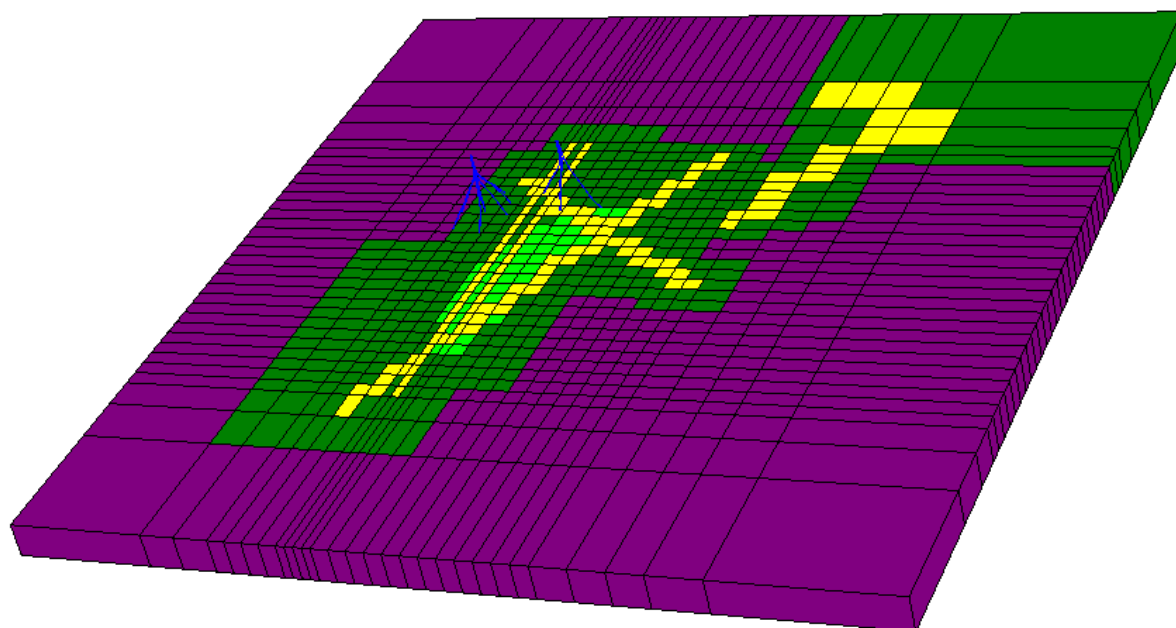


Fig. 3.3-12 Rock Property Distribution in Layer 12 (-2500 m asl)

(3) Boundary Conditions

After setting up the grid block layout and rock properties, boundary conditions are specified to allow for the flow of heat and mass into and out of the model. The boundary conditions are also repeatedly modified by trial and error until satisfactory results matching the natural state conditions in the reservoirs are obtained. The boundary conditions that are finally applied in the initial-state model are as follows:

1) Top boundary condition

The top elevation of Layer 1 of the model is 700 m asl, which approximately corresponds to the water level in the wells at well pads LMB-1 and LMB-3. When we focus on the pressures and temperatures at 700 m asl in the existing wells at both well pads, it is considered that there should be steam and/or gas at this depth. In order to represent the steam cap at around water level, a two-phase condition of steam and liquid which is 5.0 bar absolute (152°C) with a 10% steam mass fraction is assumed around the expected production area at 700 m asl, and for other areas, a constant pressure of 1 bar absolute and temperature of 80°C is assigned to the top of layer 1, as an atmospheric condition, as shown in Fig. 3.3-13.

2) Lateral boundary condition

Closed conditions are set at all lateral boundaries where there is no flow of mass and heat closing the boundaries.

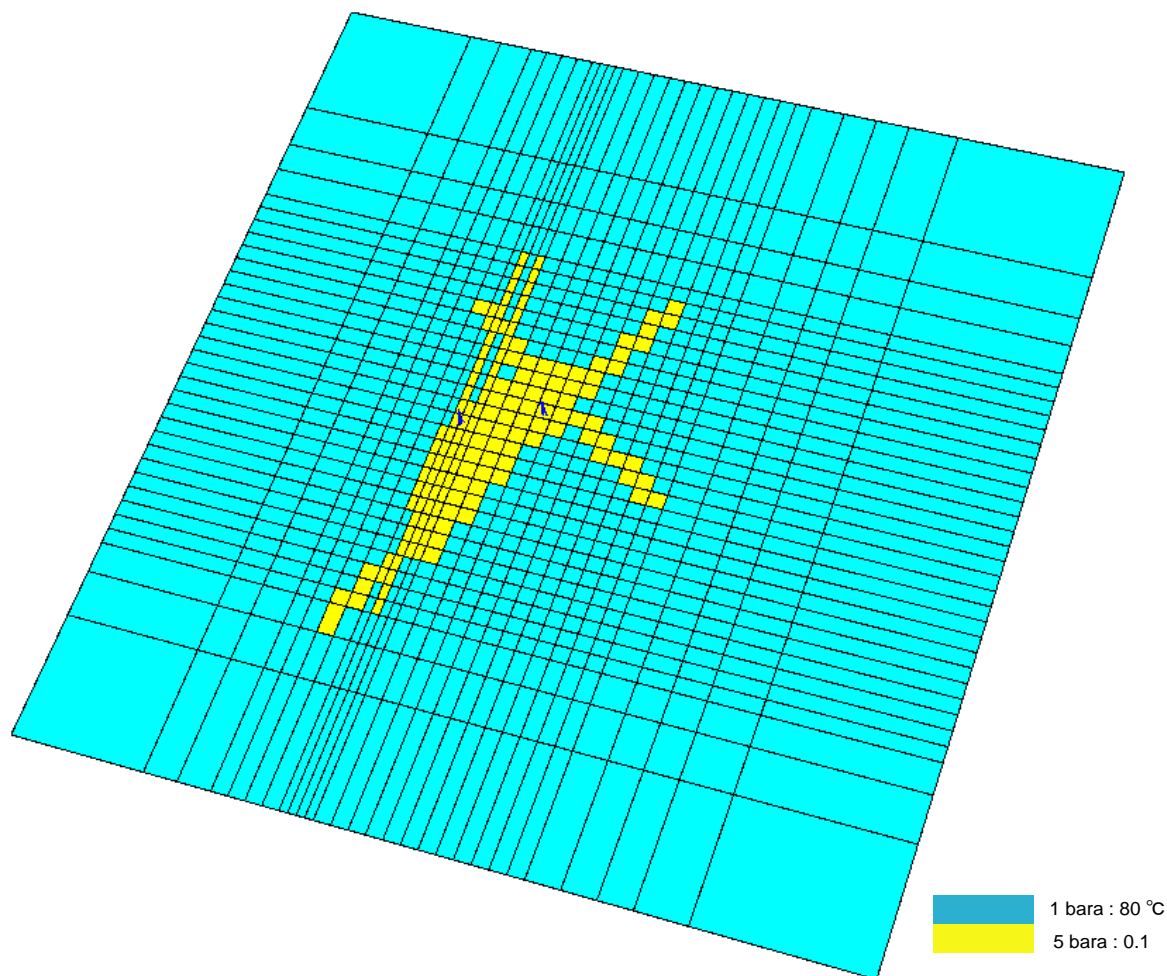


Fig. 3.3-13 Top Boundary Conditions in Layer1 (700 m asl)

3) Bottom boundary conditions

In order to represent up-flow zones of high temperature fluids, constant pressure and temperature conditions are assumed at the expected up-flow zones at the bottom of layer 12 (-3,000 m asl). A lot of revisions were repeated by trial and error to find appropriate bottom boundary conditions. Consequently, it is assumed that primary up-flow zones are found in the south mountain area, where high-temperature fluids of 270°C or 260°C with a pressure of 310 bara flow up. Secondary up-flow zones are assumed in the southern mountain area and in the fault structure in the north-eastern part of the field, where intermediate temperature fluids of 250°C and 230°C with a pressure of 305 bara and 310 bara, respectively, flow up. Other up-flow zones are assumed at the fault structure in the north-eastern part of the entire numerical model and other areas surrounding the central up-flow zones where relatively low-temperature fluids of 210°C and 200°C with a pressure of 305 bara flow up. The bottom boundary conditions of the base model are shown in Fig. 3.3-14.

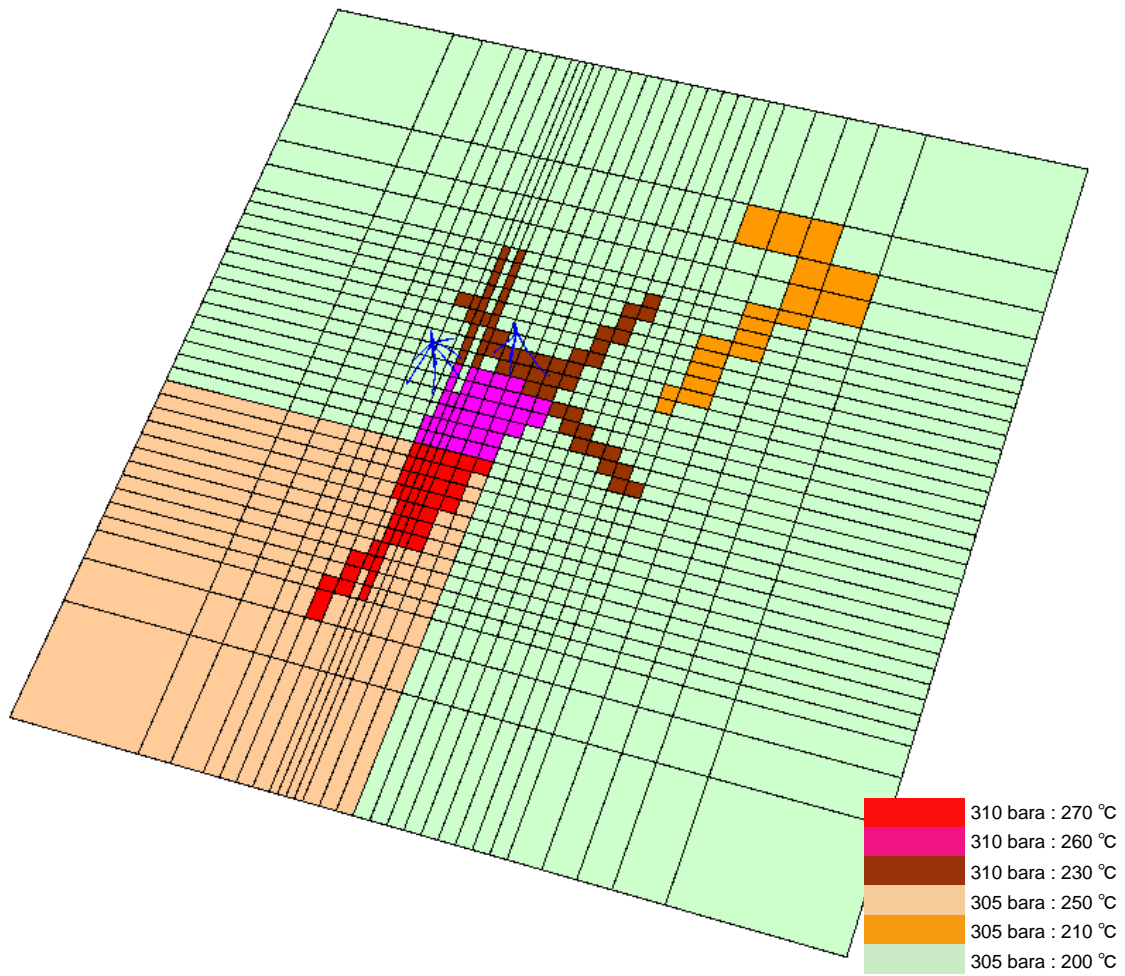


Fig. 3.3-14 Boundary Conditions in the Bottom Layer (-3000 m asl)

3.3.2 Natural State Simulation

(1) Model calibration

Geothermal systems evolve over geologic time, with the thermodynamic and hydrodynamic conditions in the system attaining a dynamic equilibrium. The rate of change in the natural system is very small relative to the changes induced by exploitation. Hence, for all practical purposes, undeveloped geothermal systems are considered to be in a quasi-steady state. Modeling of the natural or initial state of the reservoir has the following objectives: verification that the permeability distribution used in the model is reasonable; verification that assumptions regarding the location and strengths of heat and mass inflows and outflows are reasonable, both conceptually and mathematically; and formulation of a stable starting point for use in matching available production/injection data and for considering future development scenarios.

The initial-state model is based on a conceptual model of the geothermal system, which is derived from as many sources of information as possible, including geological, hydrological, geophysical, geochemical, and reservoir engineering data. The most important set of data used in the initial-state simulation is the subsurface temperature and pressure distribution. Correct interpretation of the temperature and pressure data can not only provide significant insight into how the geothermal fluid is moving through the system, but can also help define the permeability distribution and boundary conditions. Once the required grid-block parameters are entered and the boundary conditions are defined, the model is run until it reaches steady-state conditions. The time required to reach steady-state is not related to the actual geological processes that control the geothermal system, because neither the actual starting conditions nor the evolution of the system are known.

Measured subsurface temperatures and pressure provide the most reliable calibration criteria for the calibration of the initial-state model. Permeabilities in the x, y and z directions are the main variables used to match measured pre-exploitation temperatures. Once a match is obtained, it is assumed that the model represents the permeability distribution reasonably well. After steady-state conditions are reached, the calculated temperature and pressure profiles of the existing wells are compared with the measured data. If the match is not reasonable, changes are made to the model, and the run is repeated. This trial-and-error process is continued until a reasonable match is obtained. The final initial-state model then provides a stable starting point for the history-matching stage of model calibration and for forecasting future reservoir behavior. As a result of natural state simulation, a reasonable model was obtained.

The results of matching of simulated and measured temperature and pressure profiles of all the existing 12 wells – LMB 1-1, 1-2, 1-3, 1-4, 1-5, 1-6, 1-7, 1-8 at LMB1 pad and LMB3-1, 3-2, 3-3 and 3-3 at LMB3 pad – are shown in Figs. 3.3-15 to 3.3-26. As shown in these figures, considering that the conditions of measurement are not sufficient for full recovery to the natural state, the numerical model provides fair matching results, which indicates that the model is reasonable and capable of forecasting simulation, which is the next step in evaluating the sustainability of the 110 MW operation of units 3 and 4 of the Lumut Balai power plant. However, it should be noted that this numerical model is a preliminary reference model, because there is no data for the southern part of the field in spite of the fact that it is the production development area for Units 3 and 4 of the power plant, and the measured data are currently concentrated only around well pads LMB 1 and LMB3, where the production wells will be used for Units 1 and 2.

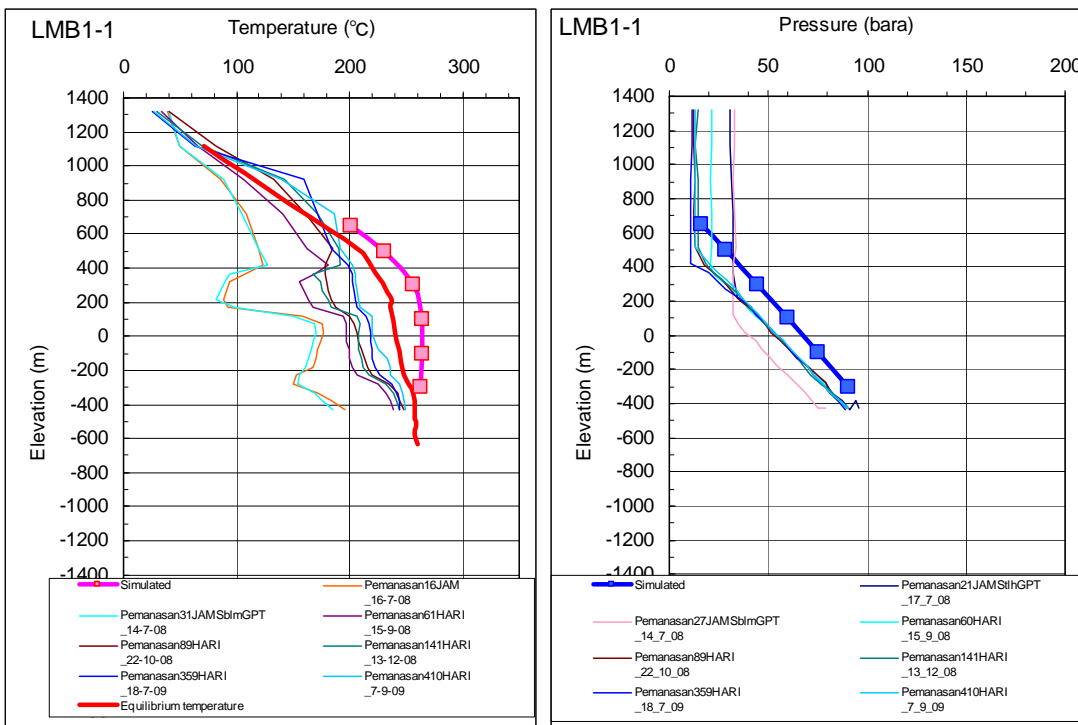


Fig. 3.3-15 Matching of Temperature/Pressure Profiles of LMB1-1

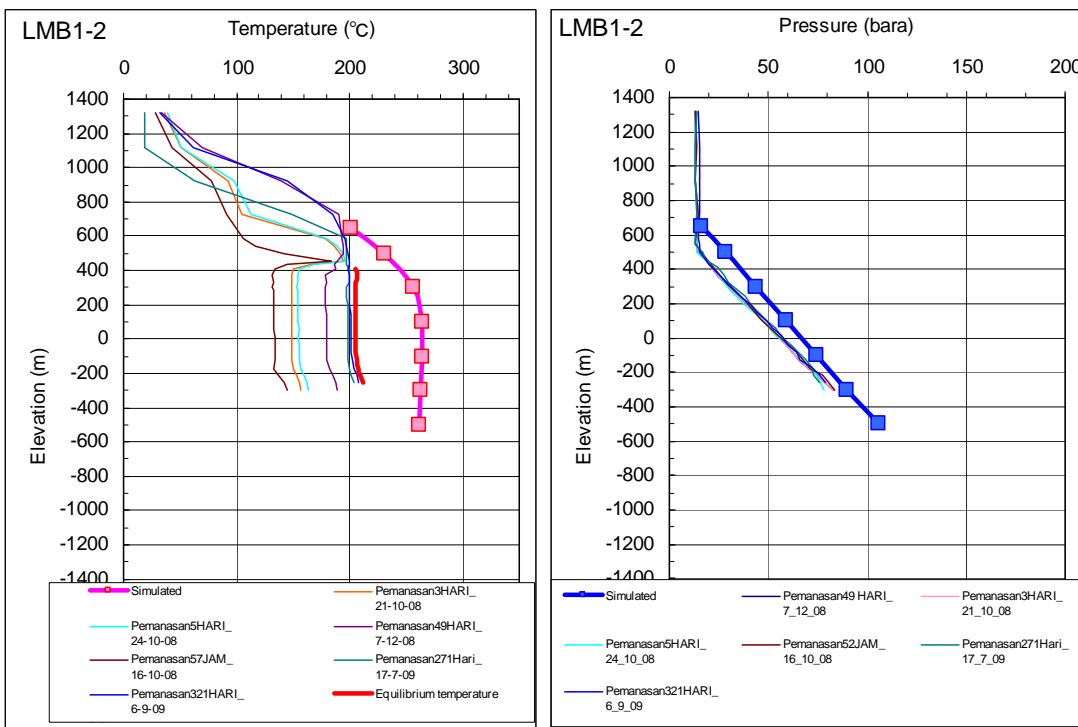


Fig. 3.3-16 Matching of Temperature/Pressure Profiles of LMB1-2

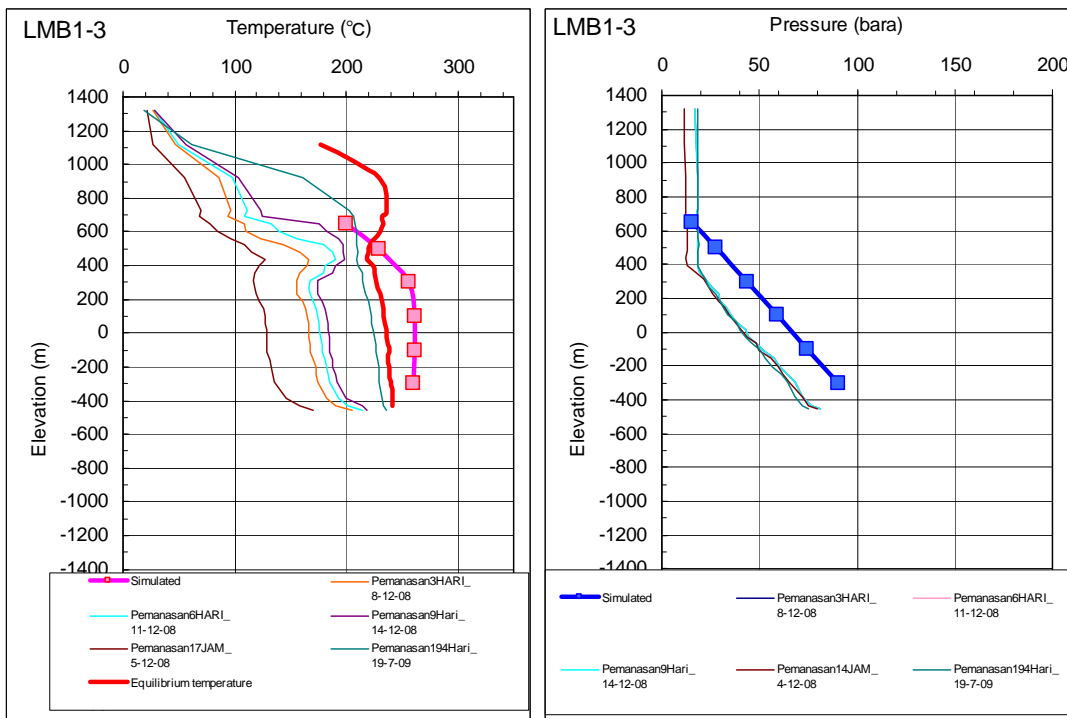


Fig. 3.3-17 Matching of Temperature/Pressure Profiles of LMB1-3

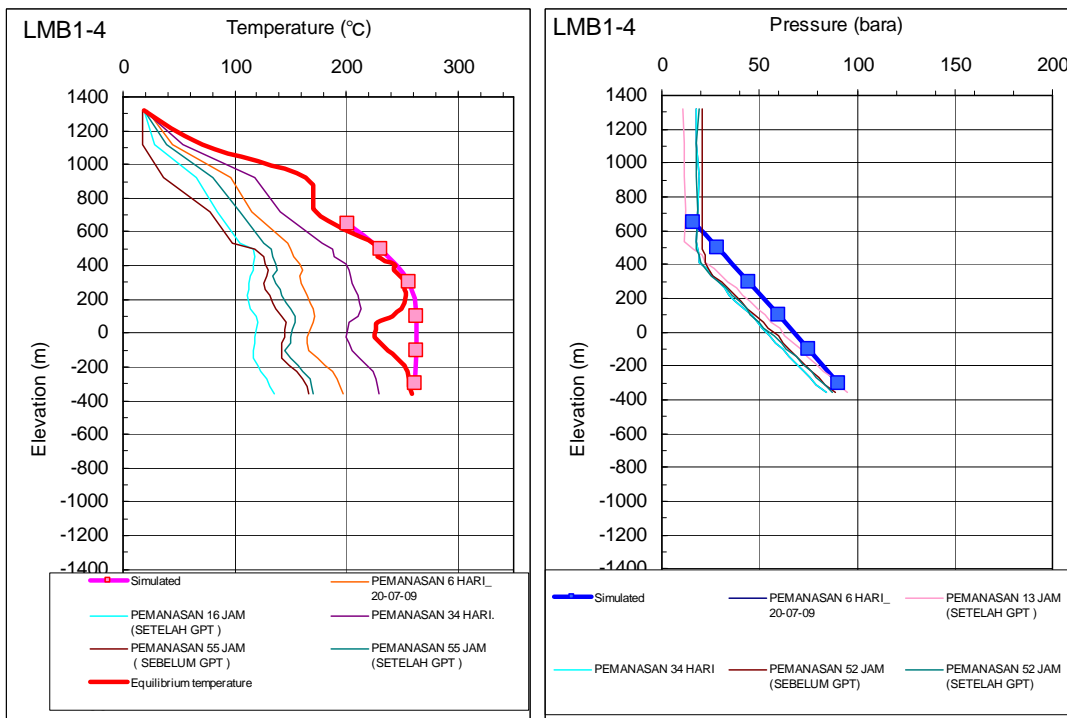


Fig. 3.3-18 Matching of Temperature/Pressure Profiles of LMB1-4

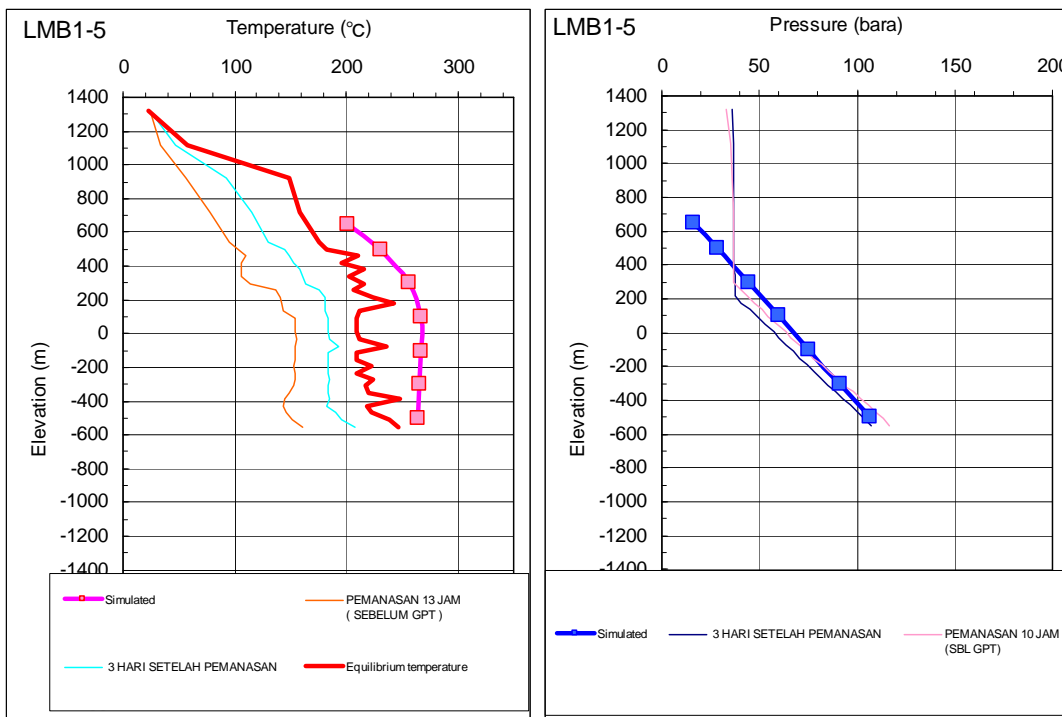


Fig. 3.3-19 Matching of Temperature/Pressure Profiles of LMB1-5

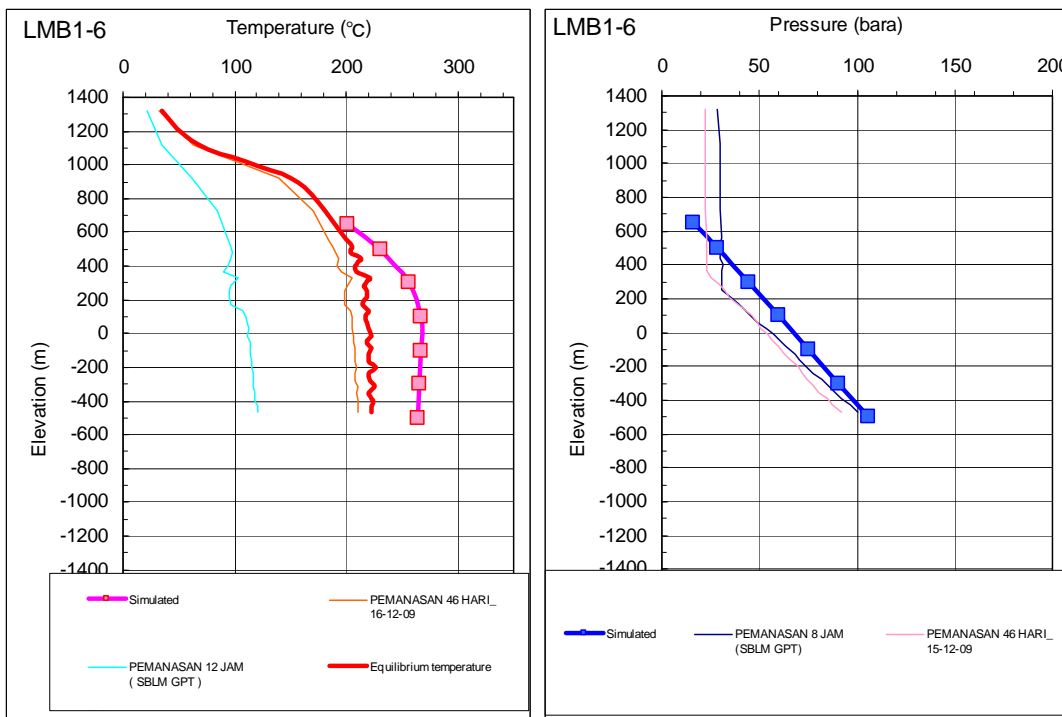


Fig. 3.3-20 Matching of Temperature/Pressure Profiles of LMB1-6

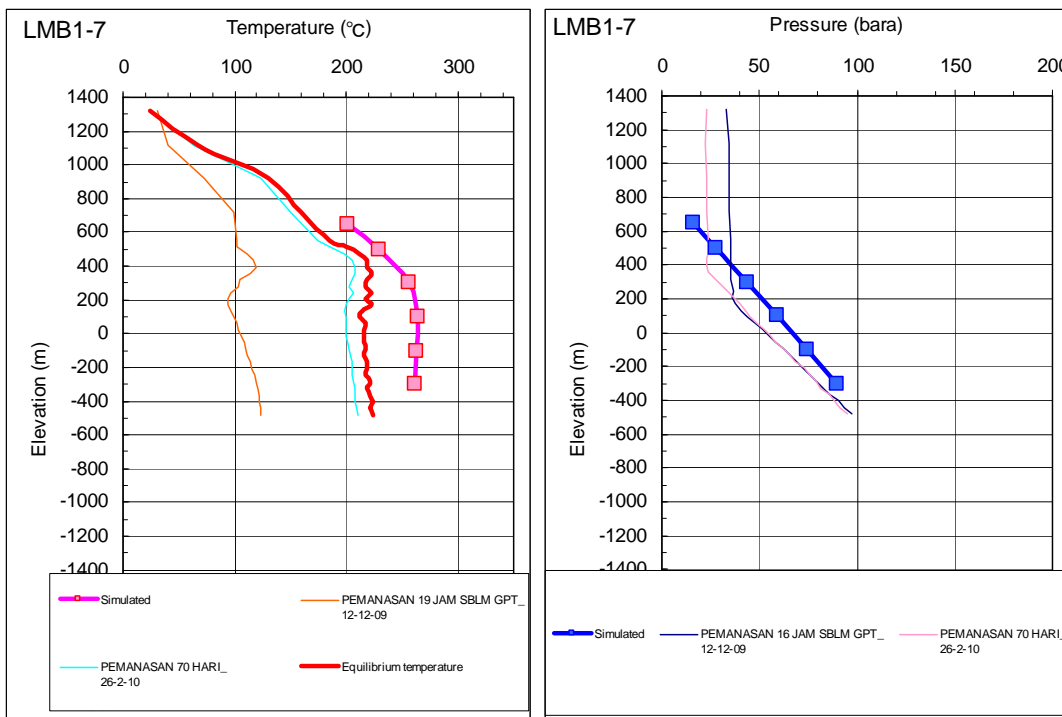


Fig. 3.3-21 Matching of Temperature/Pressure Profiles of LMB1-7

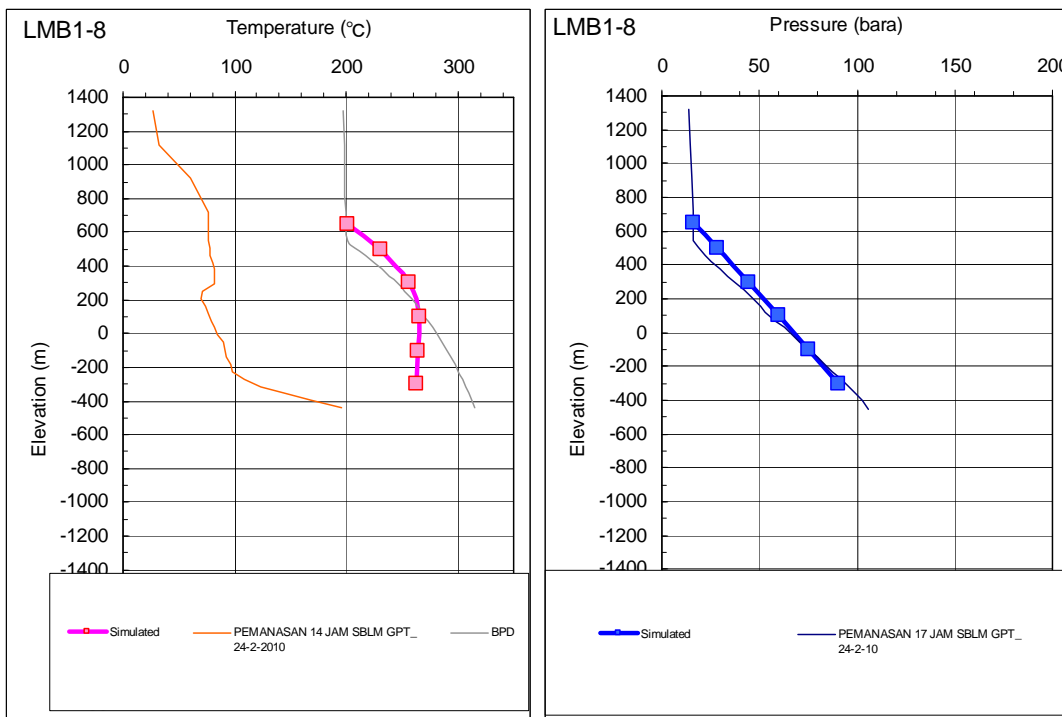


Fig. 3.3-22 Matching of Temperature/Pressure Profiles of LMB1-8

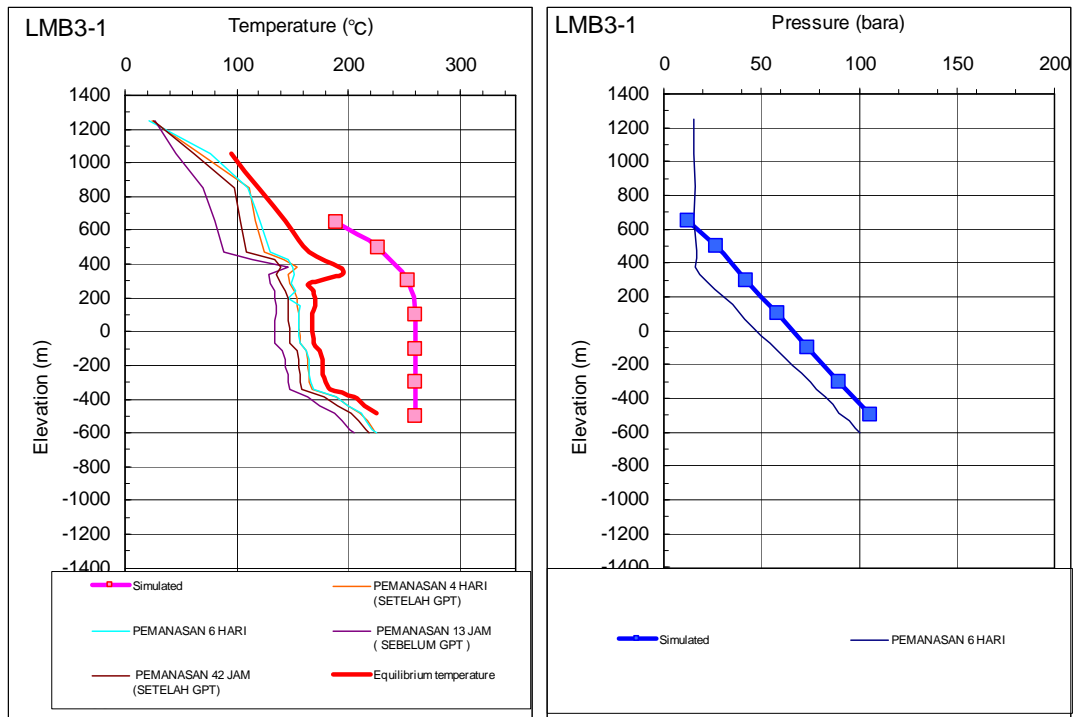


Fig. 3.3-23 Matching of Temperature/Pressure Profiles of LMB3-1

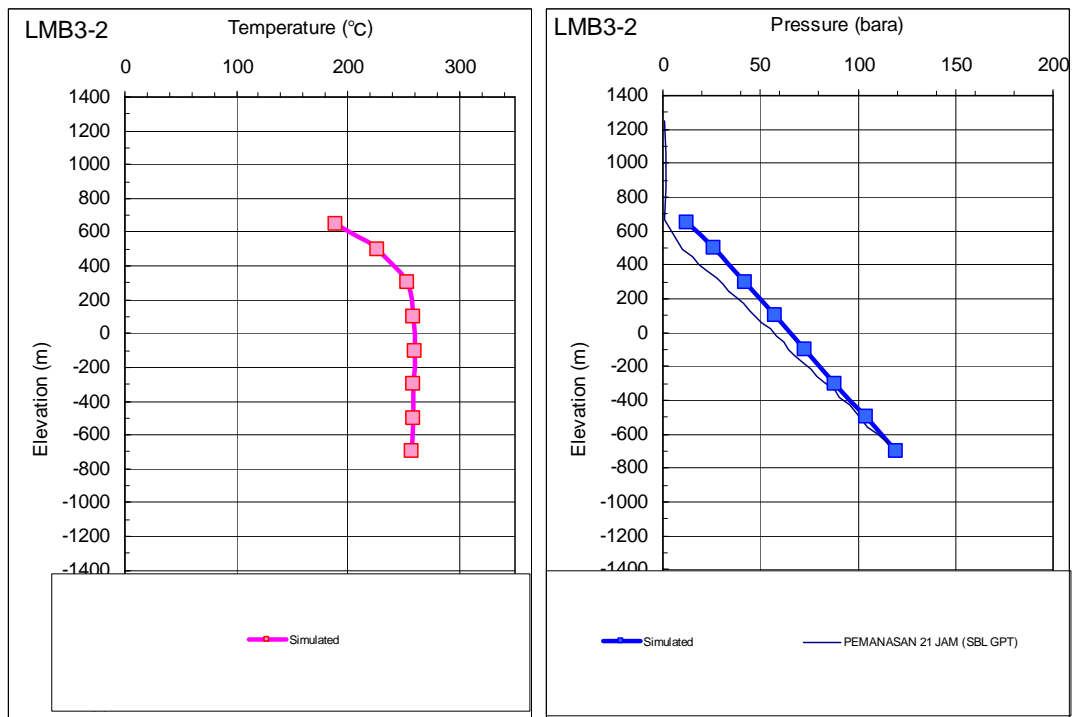


Fig. 3.3-24 Matching of Temperature/Pressure Profiles of LMB3-2

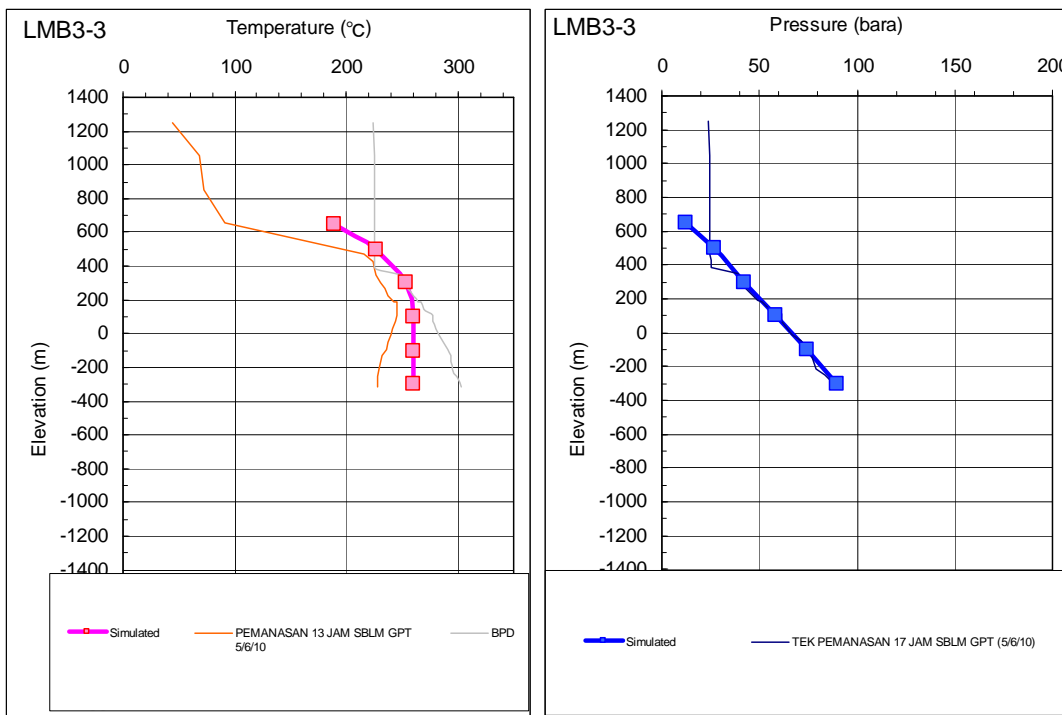


Fig. 3.3-25 Matching of Temperature/Pressure Profiles of LMB3-3

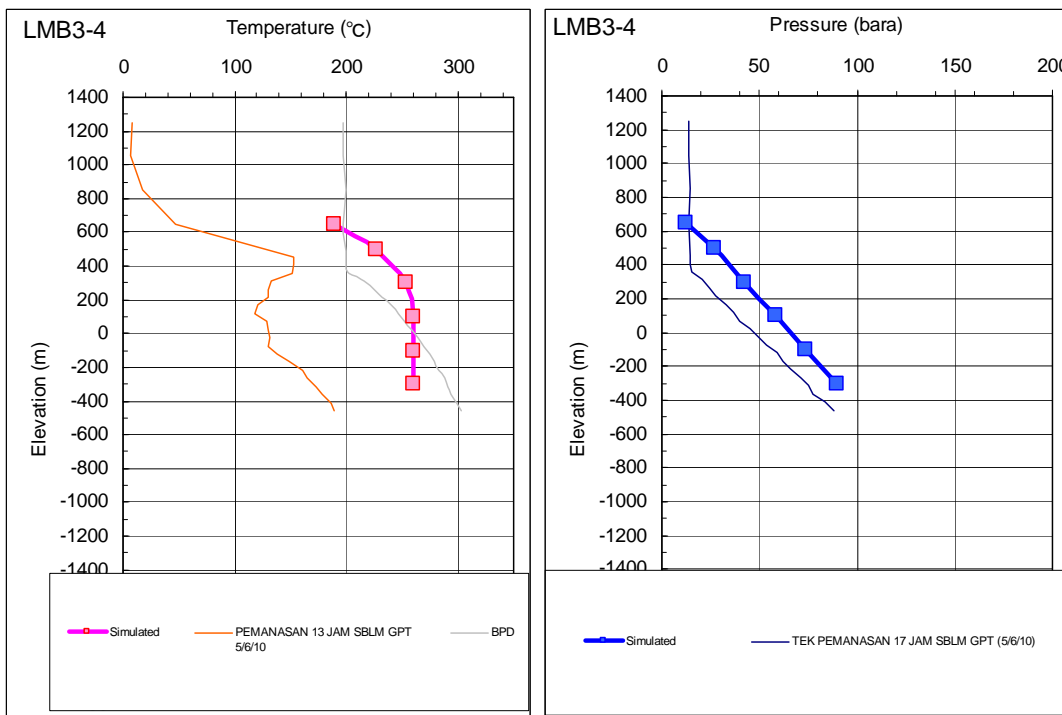


Fig. 3.3-26 Matching of Temperature/Pressure Profiles of LMB3-4

(4) Current reservoir conditions

Once a reasonable numerical model is obtained, the model provides the current reservoir conditions such as temperature, pressure and steam distribution in the reservoirs.

Figs 3.3-27 to 3.3-38 show the current pressure contours in layers 1 (650 m asl.) to 12 (-3000 m asl.), which are obtained from the natural state simulation. The pressure contours indicate that there is a higher-pressure region in the development area of the field, reflecting the up-flow zone.

Similarly, Figs 3.3-39 to 3.3-50 show the current temperature contours in layers 1 to 12. The temperature contours indicate that there is a higher-temperature region involving the current development area where there is a promising reservoirs with a temperature of 260°C or higher. The higher temperature fluids flow up from the deep up-flow zones and extend horizontally along the fault structures where there are more highly permeable zones. The development area of the Lumut Balai geothermal field is located in a region where the reservoir temperature is more than 250°C in layer 5 (-100 m asl.) and below this layer. The reservoir extends along the NE-SW trending fault structure from the southwest to the northeast. Since the location of the development area for Units 3 and 4 is closer to the primary up-flow zone compared to that for Units 1 and 2, the reservoir temperature in the former is expected to be higher than that for the latter. This means that the productivity of the production wells in the development area for Units 3 and 4 will be greater than that for Units 1 and 2, unless the reservoir is less permeable in the former than in the latter development area.

Figs 3.3-51 to 3.3-52 show steam saturation contours in the top three layers (650 to 300 m asl). The steam saturation contours indicate that a two-phase flow of steam and liquid water is widespread in the higher-temperature regions in the top three layers, which correspond to a drilling depth up to around 1000 to 1350 m. Beneath the steam cap there are water-dominated reservoirs at depth. Considering that the produced steam ratio of well LMB1-5 at a wellhead pressure of 8 bara is around 20%, the production reservoir at the Lumut Balai geothermal field should be water-dominated.

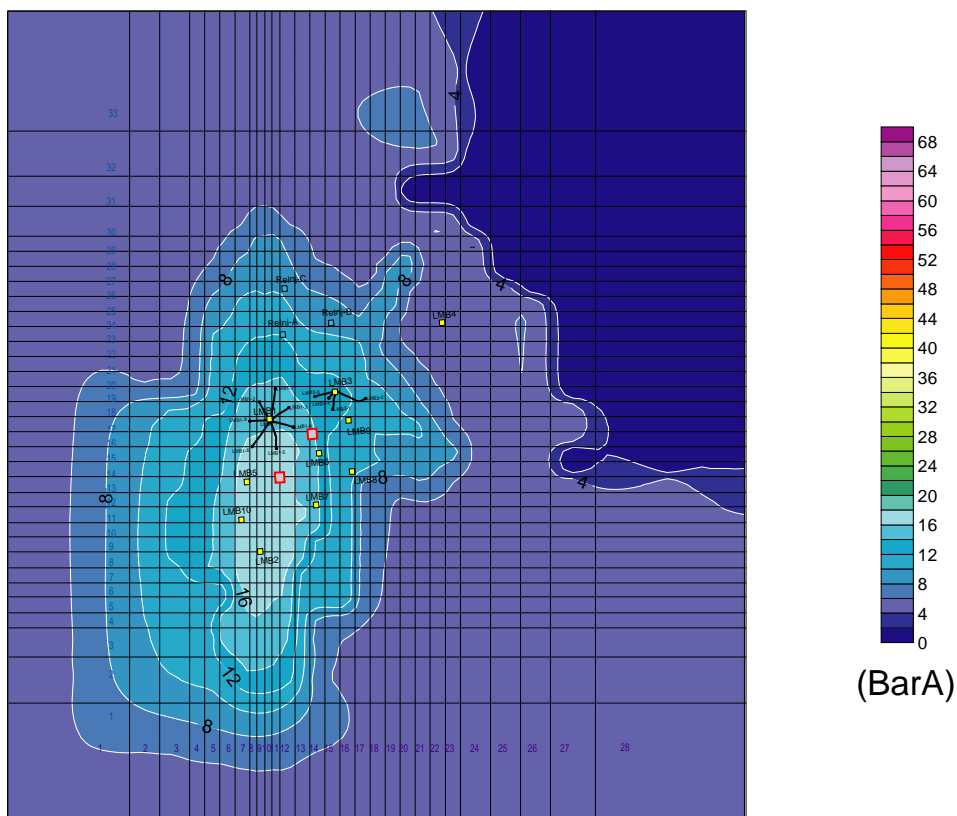


Fig. 3.3-27 Pressure Distribution in Layer 1 (650 m asl)

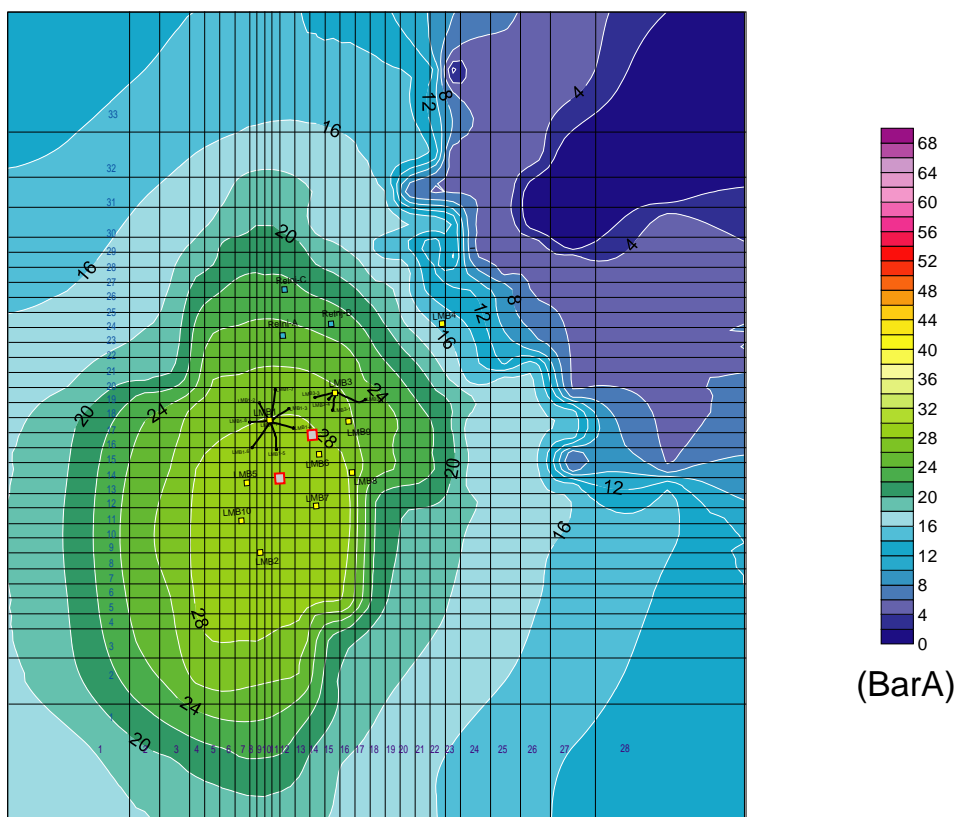


Fig. 3.3-28 Pressure Distribution in Layer 2 (500 m asl)

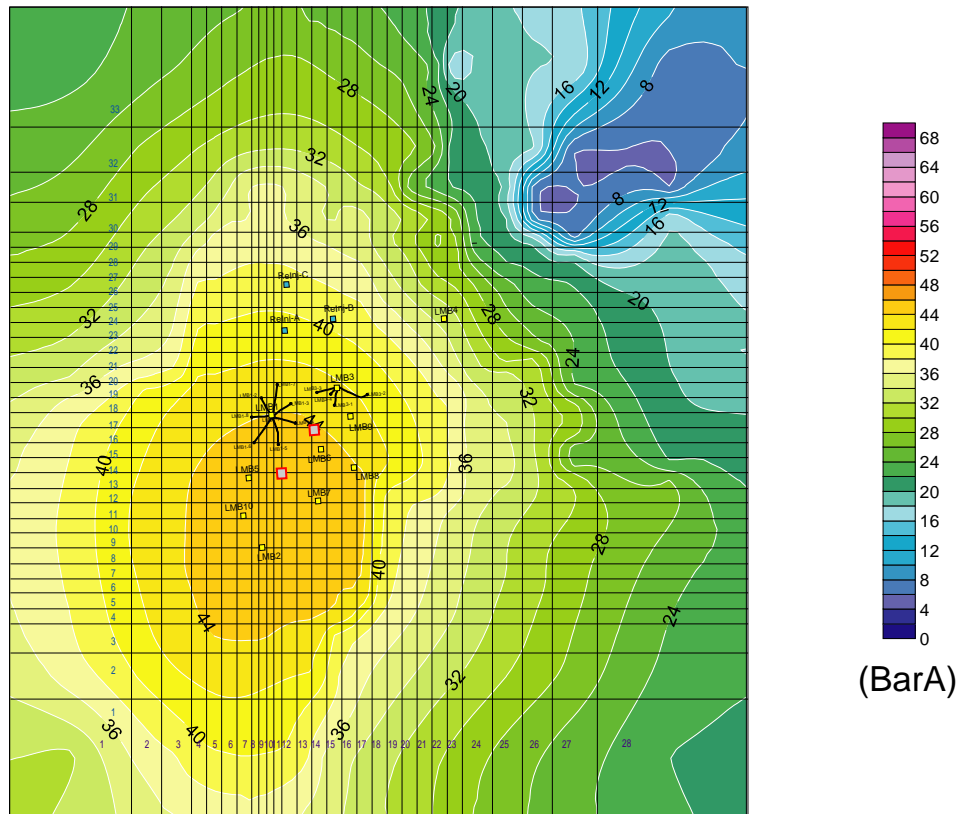


Fig. 3.3-29 Pressure Distribution in Layer 3 (300 m asl)

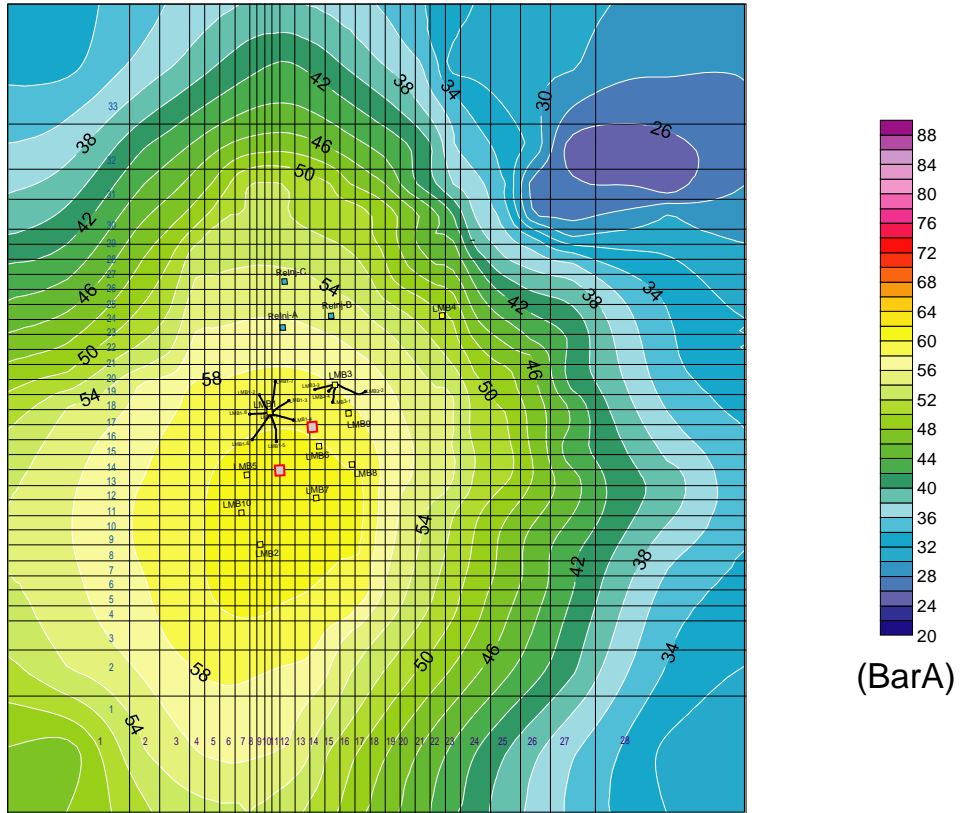


Fig. 3.3-30 Pressure Distribution in Layer 4 (100 m asl)

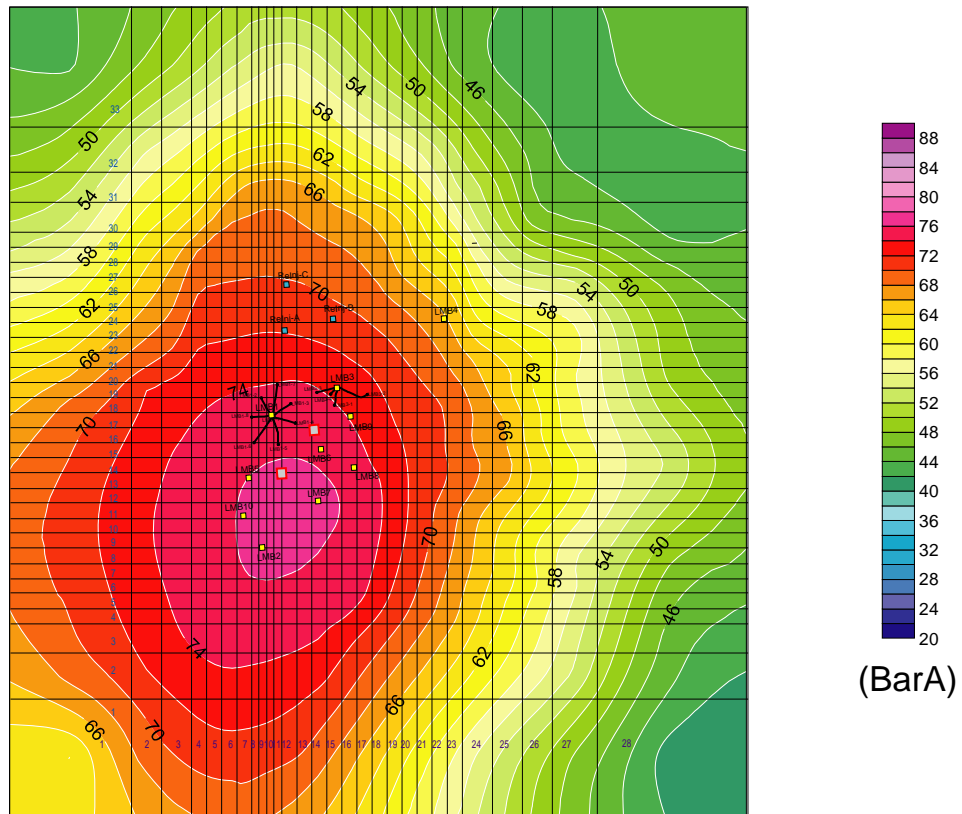


Fig. 3.3-31 Pressure Distribution in Layer 5 (-100 m asl)

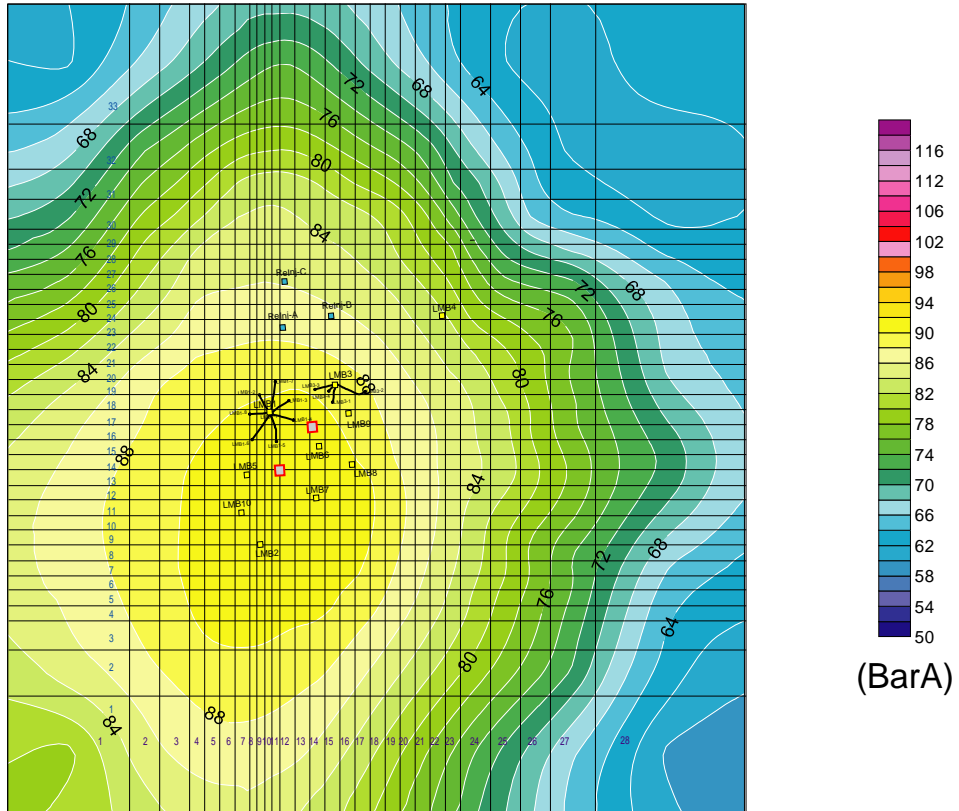


Fig. 3.3-32 Pressure Distribution in Layer 6 (-300 m asl)

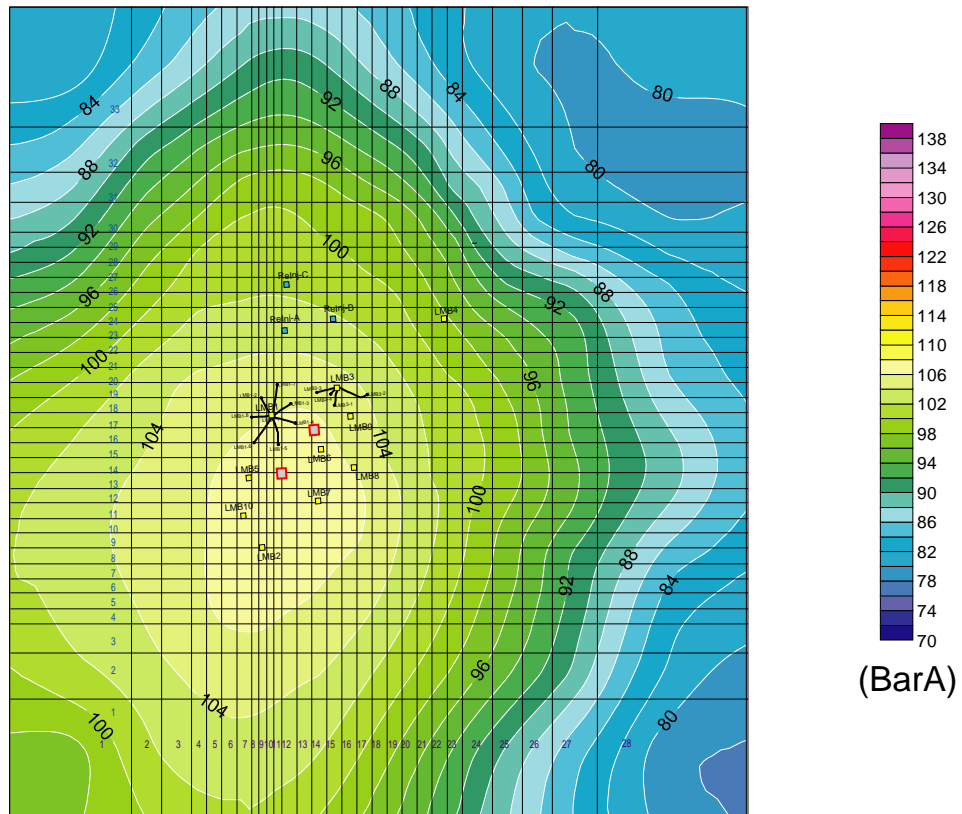


Fig. 3.3-33 Pressure Distribution in Layer 7 (-500 m asl)

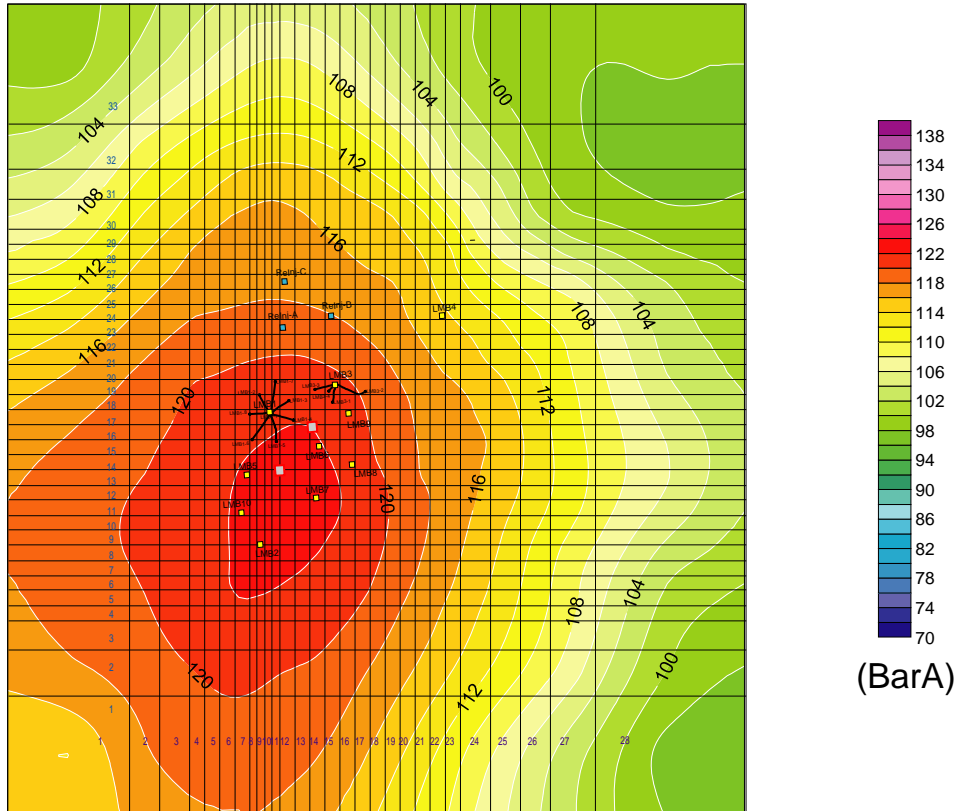


Fig. 3.3-34 Pressure Distribution in Layer 8 (-700 m asl)

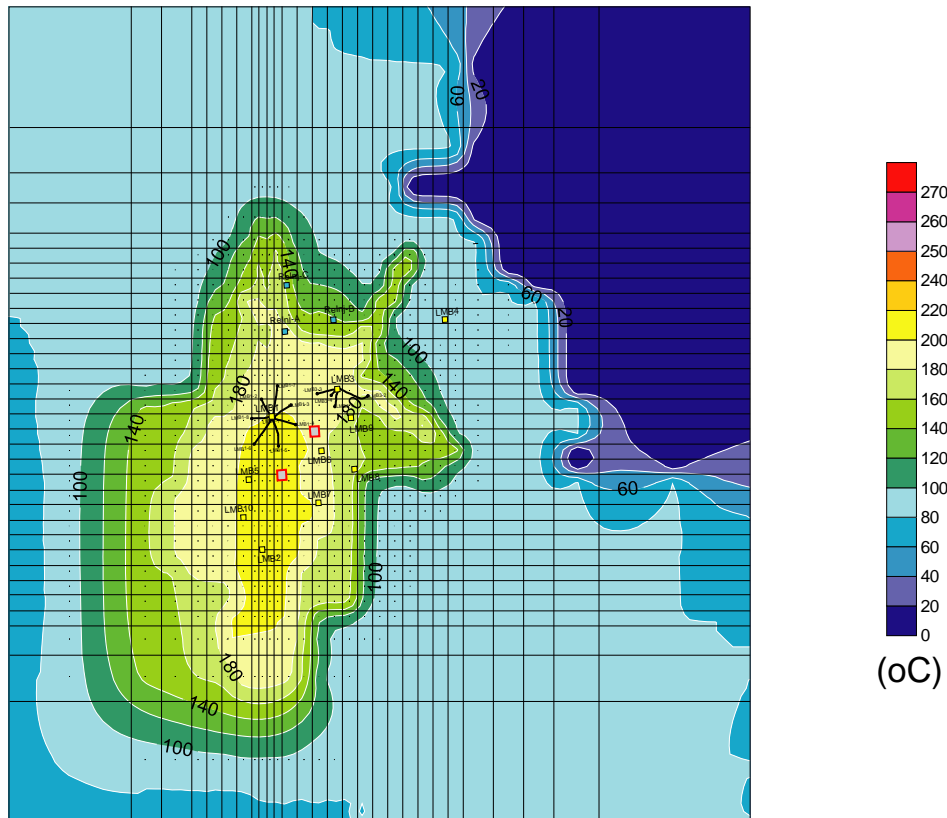


Fig. 3.3-39 Temperature Distribution in Layer 1 (650 m asl)

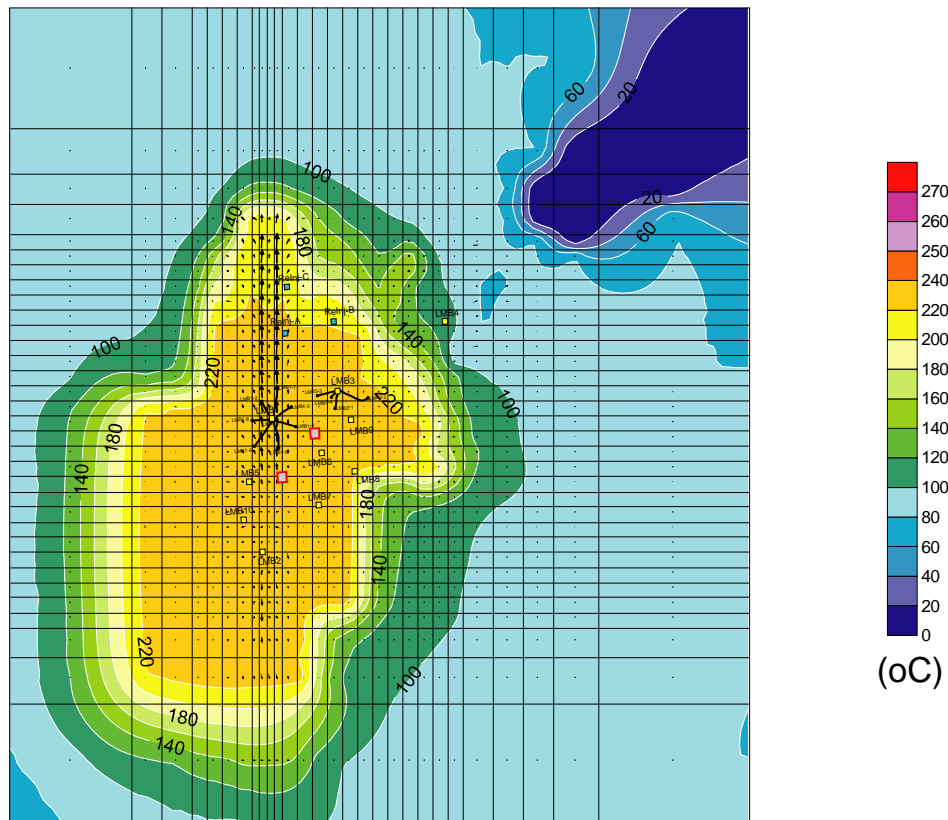


Fig. 3.3-40 Temperature Distribution in Layer 2 (500 m asl)

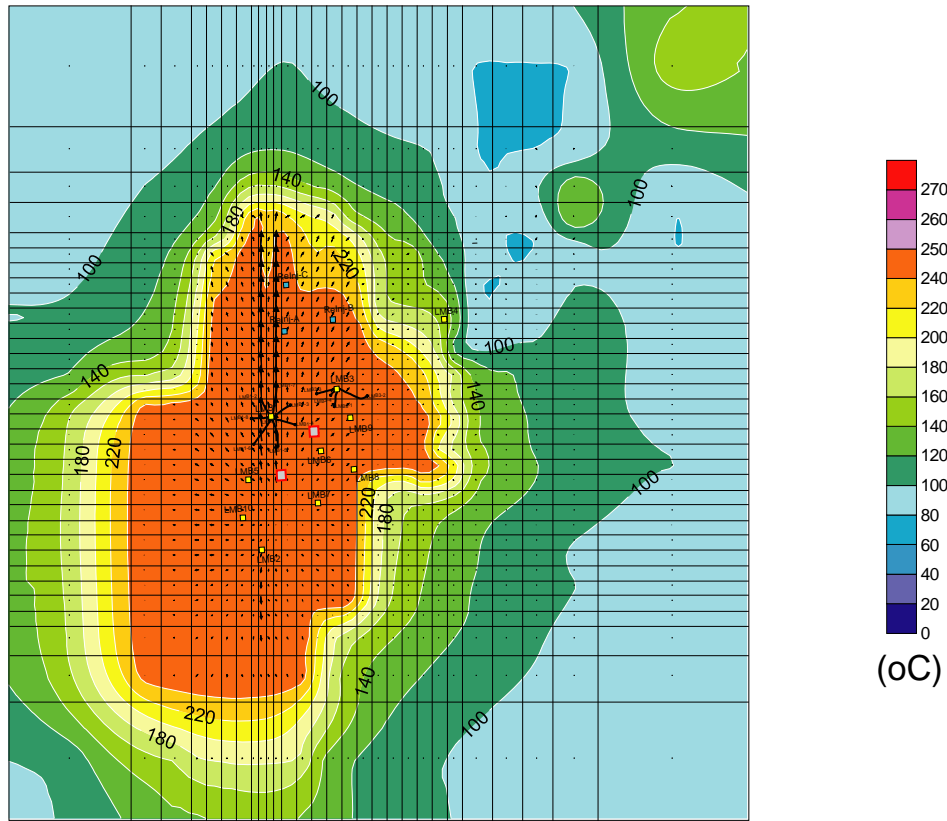


Fig. 3.3-41 Temperature Distribution in Layer 3 (300 m asl)

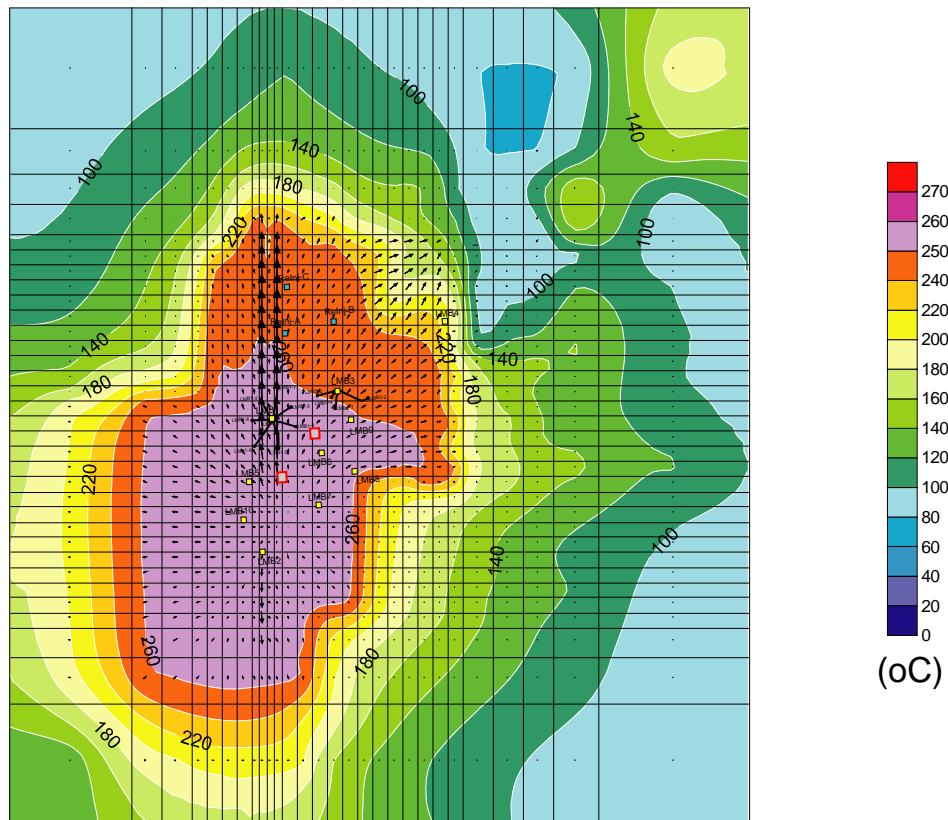


Fig. 3.3-42 Temperature Distribution in Layer 4 (100 m asl)

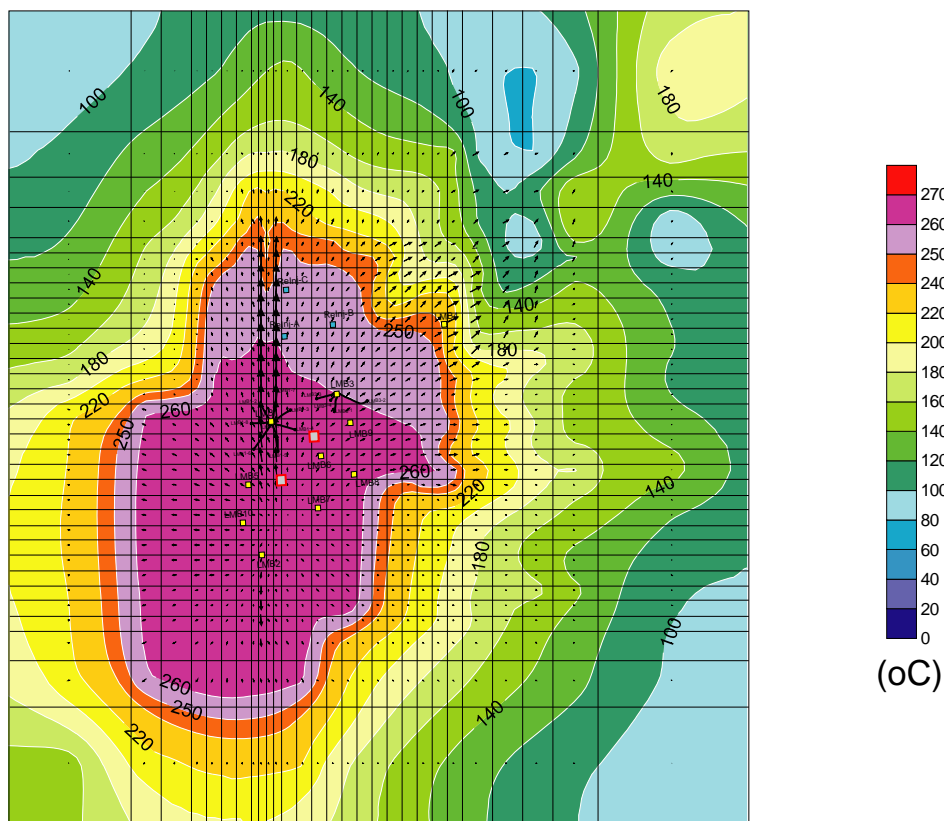


Fig. 3.3-43 Temperature Distribution in Layer 5 (-100 m asl)

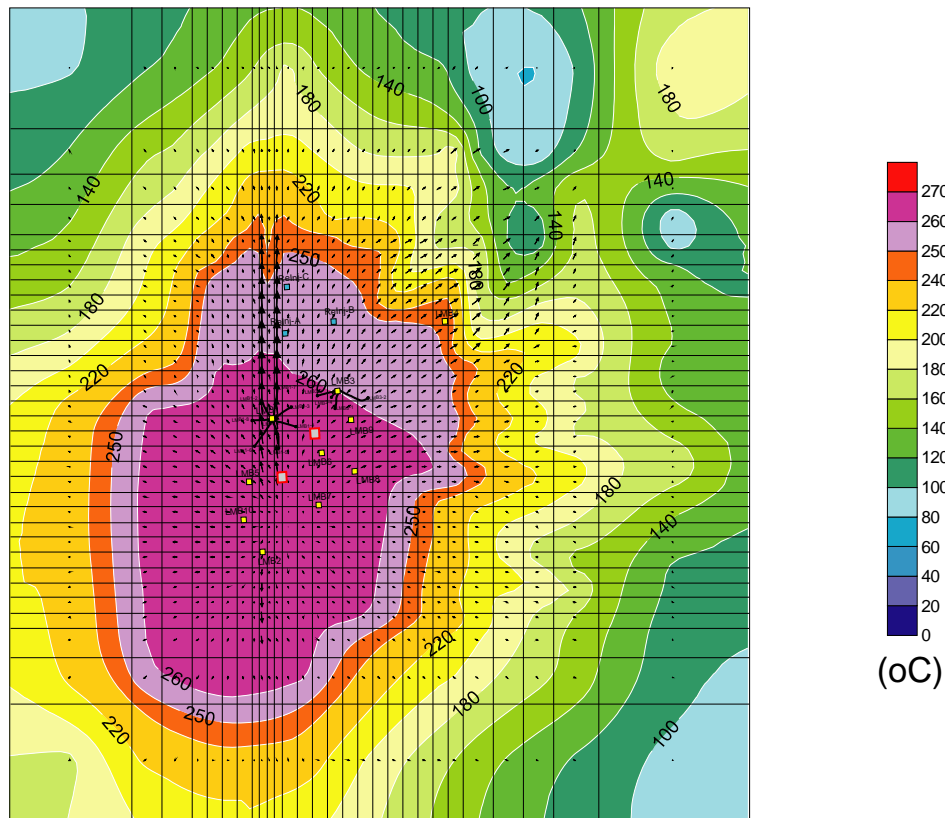


Fig. 3.3-44 Temperature Distribution in Layer 6 (-300 m asl)

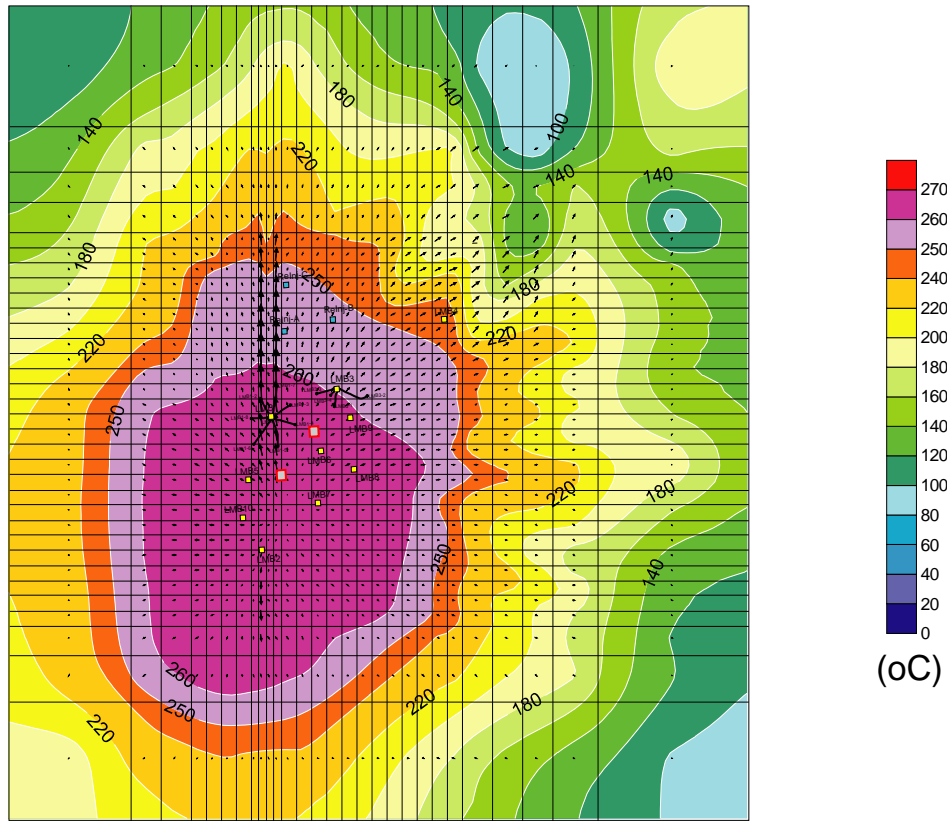


Fig. 3.3-45 Temperature Distribution in Layer 7 (-500 m asl)

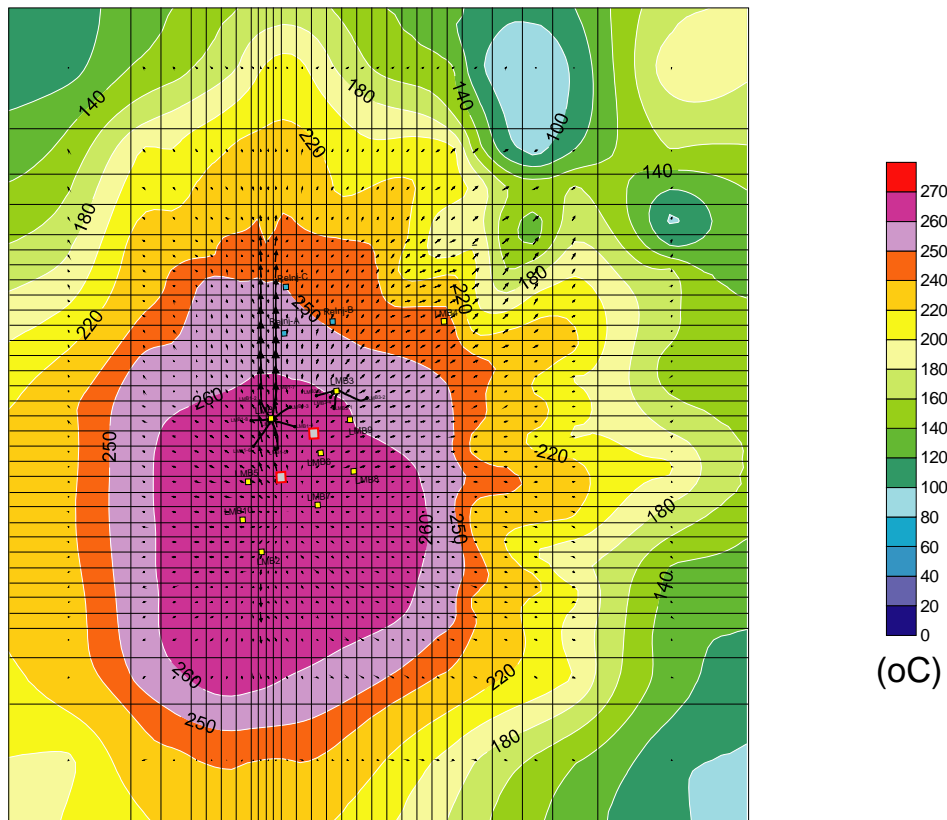


Fig. 3.3-46 Temperature Distribution in Layer 8 (-700 m asl)

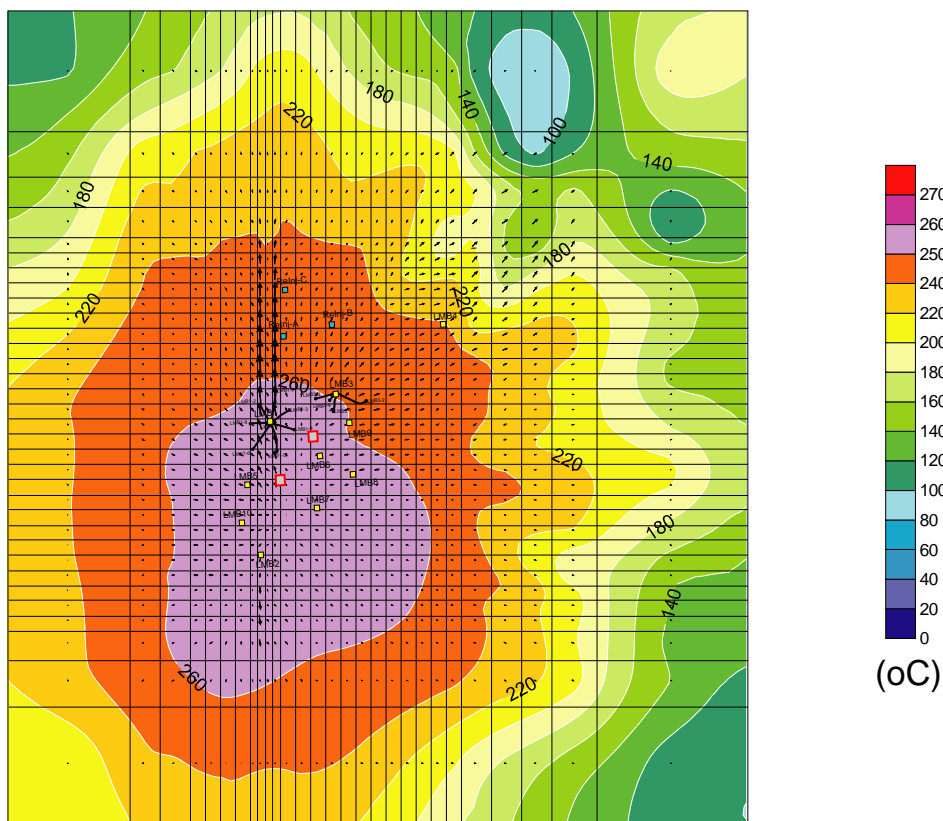


Fig. 3.3-47 Temperature Distribution in Layer 9 (-900 m asl)

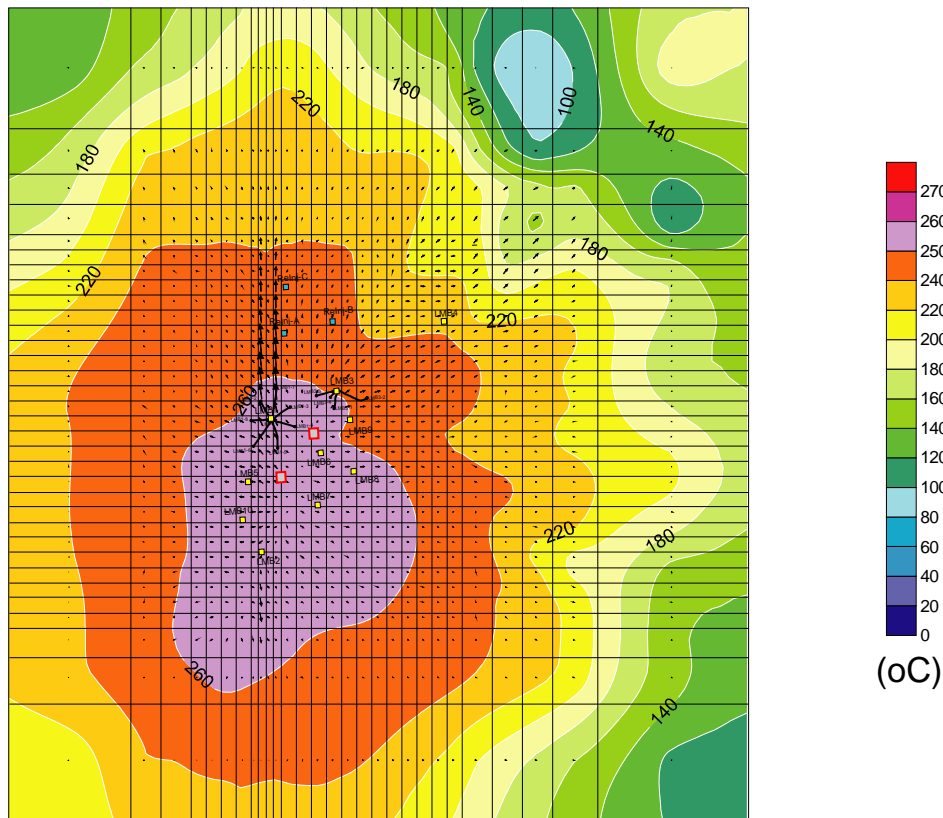


Fig. 3.3-48 Temperature Distribution in Layer 10 (-1250 m asl)

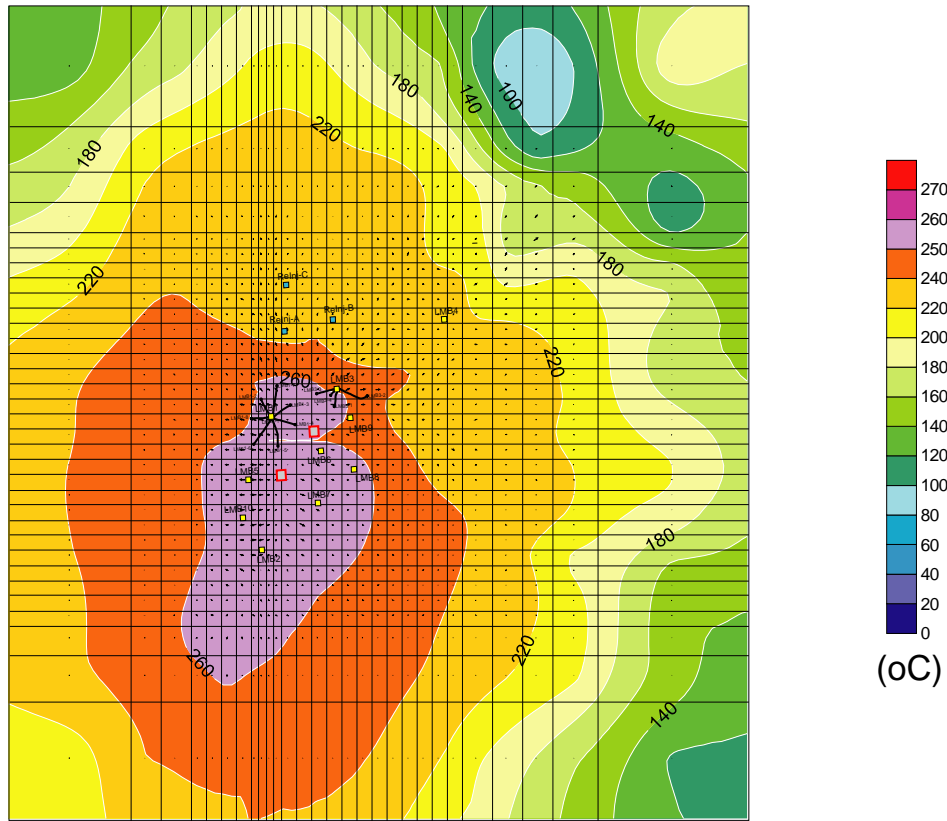


Fig. 3.3-49 Temperature Distribution in Layer 11 (-1750 m asl)

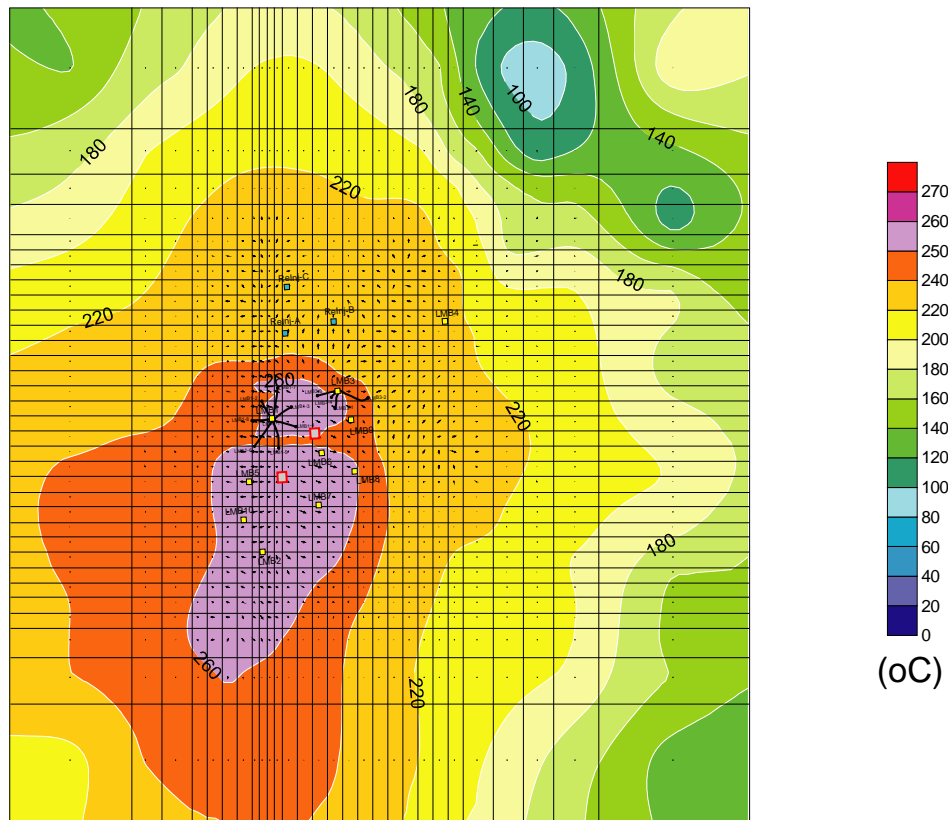


Fig. 3.3-50 Temperature Distribution in Layer 12 (-2500 m asl)

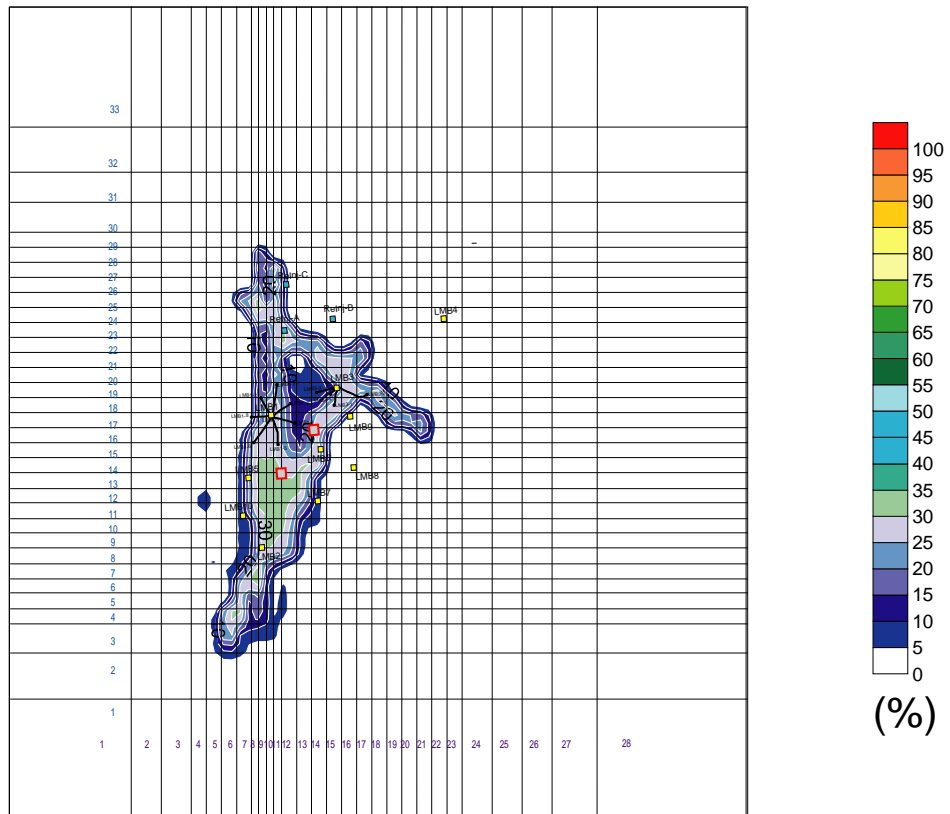


Fig. 3.3-51 Steam Saturation Distribution in Layer 1 (650 m asl)

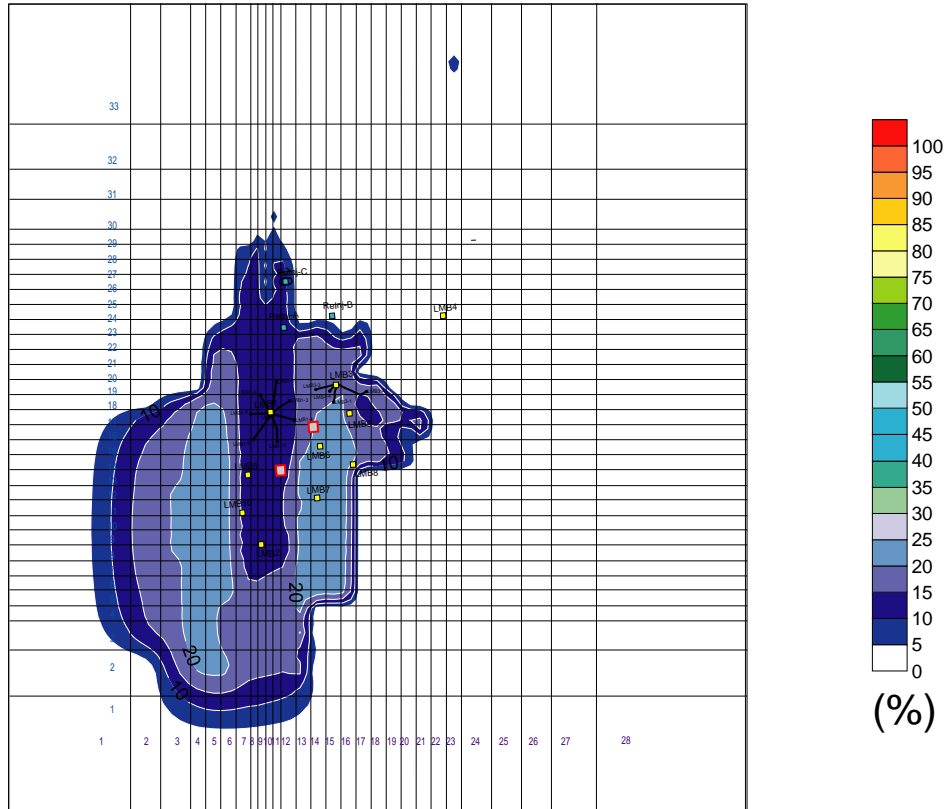


Fig. 3.3-52 Steam Saturation Distribution in Layer 2 (500 m asl)

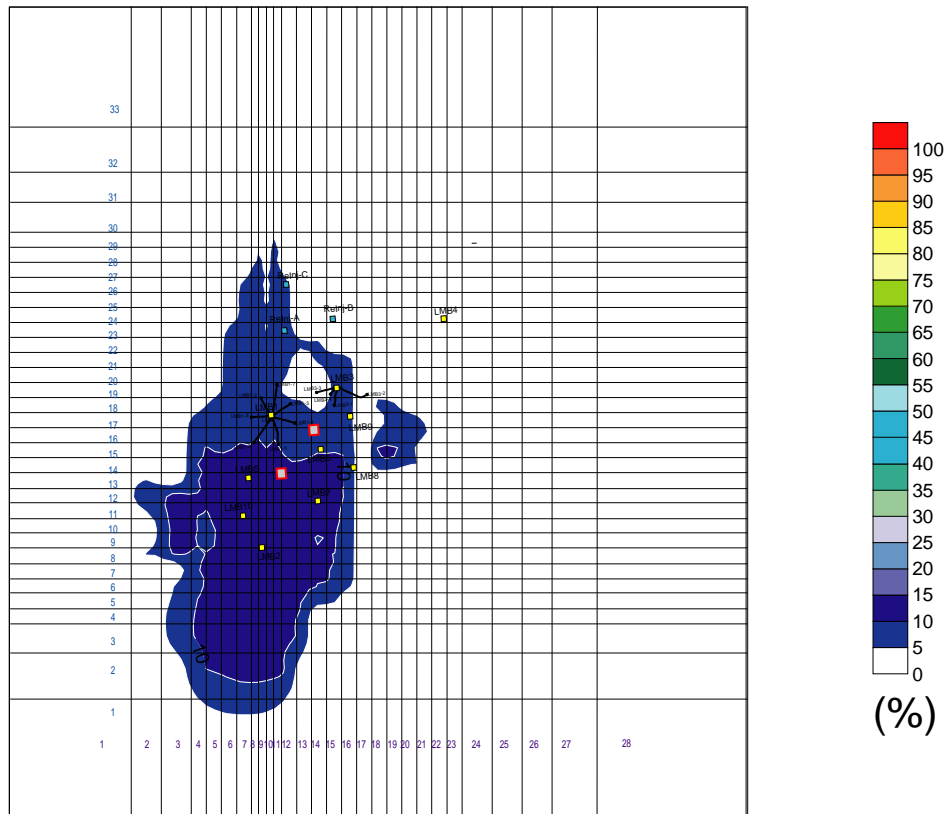


Fig. 3.3-53 Steam Saturation Distribution in Layer 3 (300 m asl)

3.3.3 Forecasting Simulation

(1) Methodology and calculation conditions

Since the reservoir numerical model is considered to be reasonable from the natural state simulation, a forecasting simulation was done as a preliminary study. In order to generally estimate the resource potential and evaluate the sustainability of the entirety of reservoirs in the Lumut Balai geothermal field, all the units from 1 to 4 with their total power output of 220 MW were assumed to be operated for 30 years in parallel, as a basic scenario for the forecasting simulation. The calculation conditions for the forecasting simulation are shown in Table 3.3-2.

Table 3.3-2 Calculation Conditions for Forecasting Simulation

Power Output (MW)	Unit 1&2	Unit 3&4
Wellhead pressure (bara)	8.0	8.0-8.5
Separator pressure (bara)	6.8	6.8
Turbine inlet pressure (bara)	5.5	5.5
Steam requirement (t/h)	924	924

The forecasting simulation was conducted by coupling the reservoir simulator TOUGH2 with the wellbore simulator WELLFLOW that was developed by West Japan Engineering Consultants, Inc. (West JEC). The wellbore simulator calculates the mass flow rate and power output of each production well at the given wellhead pressure on the basis of the reservoir conditions that are calculated by the reservoir simulator. The coupling concept is shown in Fig. 3.3-54.

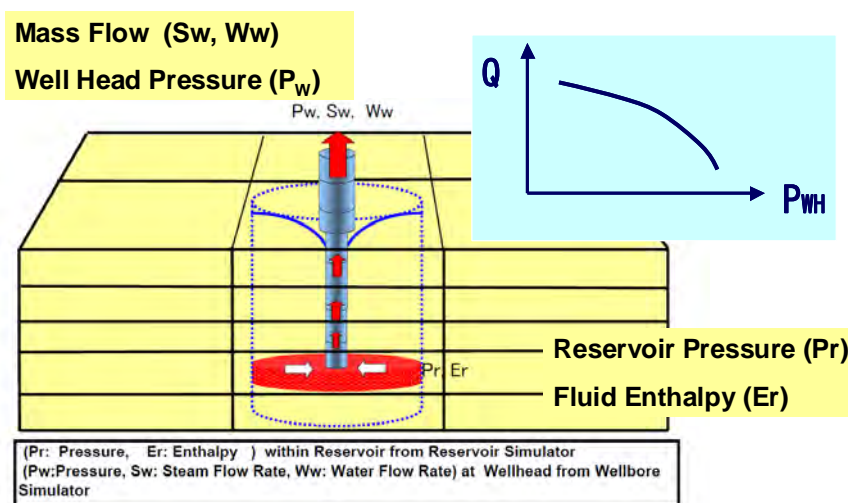


Fig. 3.3-54 Concept of Coupling Reservoir Simulator and Wellbore Simulator

The primary reservoir parameters that affect the productivity of each production well are reservoir pressure, temperature and permeability. The reservoir pressure and temperature at the productive depth surrounding the production well can be estimated from those of the corresponding grid block of the reservoir numerical model. Compared to the reservoir pressure and temperature, the reservoir permeability is difficult to correctly estimate because the reservoir permeability generally indicates a wide range of values, depending on the geological structure and formation condition. Accordingly, the measured permeability or productivity of the production well is very helpful in distinguishing the representative permeability of wells. However, it should be noted that the measured permeability obtained through injection tests often indicates a larger value than the true value of the feed zone, because it often indicates the integrated permeability of all the lost circulation zones where injected water flows out from inside the well into the formation during injection. Therefore, when we can estimate reservoir pressure and temperature, the measured productivity of production wells will be useful for estimating the corresponding reservoir permeability. For this preliminary simulation study, the permeability was estimated using the measured deliverability of production well LMB1-5 through a matching process, which was done by repeatedly correcting the assumption of the permeability-thickness products (kh value) of well LMB1-5 until satisfactory matching between the simulated and measured deliverability is achieved, as shown in Fig. 3.3-55. The results suggested that a reasonable kh value for well LMB1-5 is 2.0 darcy-m. Therefore, as a representative kh value for wells, 2.0 darcy-m was assumed for all wells in the forecasting simulation. For reinjection wells, the injection capacity of each reinjection well was calculated based on the reservoir pressure of the corresponding grid block of the numerical model and an assumed kh value of 10 darcy-m, on the basis of the kh of 10.27 darcy-m for well LMB1-1 that was obtained by a gross permeability test (GPT).

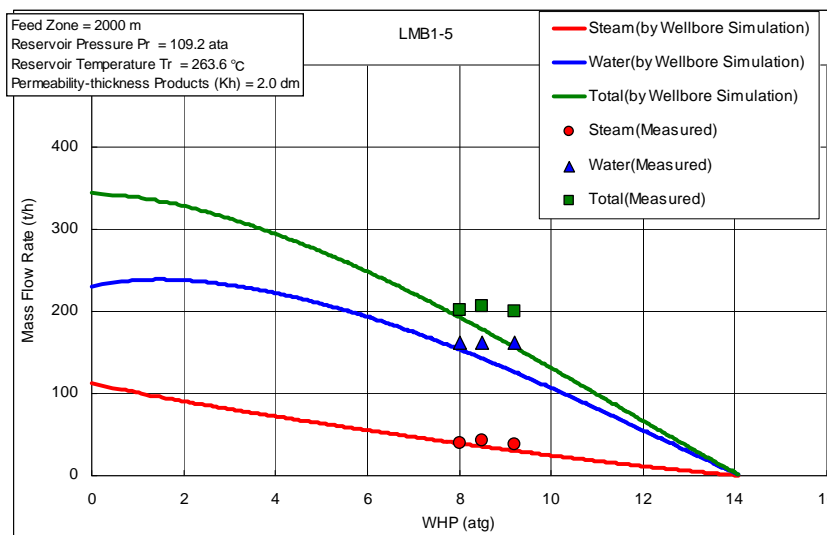


Fig. 3.3-55 Comparison of Measured and Simulated Deliverability of LMB1-5

Figs 3.3-56 to 3.3-59 show drilling targets of the reinjection wells in layer 5 (-100 m asl.), and production wells in layer 6 (-300 m asl.), layer 7 (-500 m asl.) and layer 8 (-700 m asl.), respectively, which are assumed for the forecasting simulation. With respect to the well pads, the well pads LMB 1, 3, 5, 6 and 9 were used for Units 1 and 2, and LMB 2, 7, 8, 10, and another one (LMBX) were used for Units 3 and 4, following the current plan of PGE.

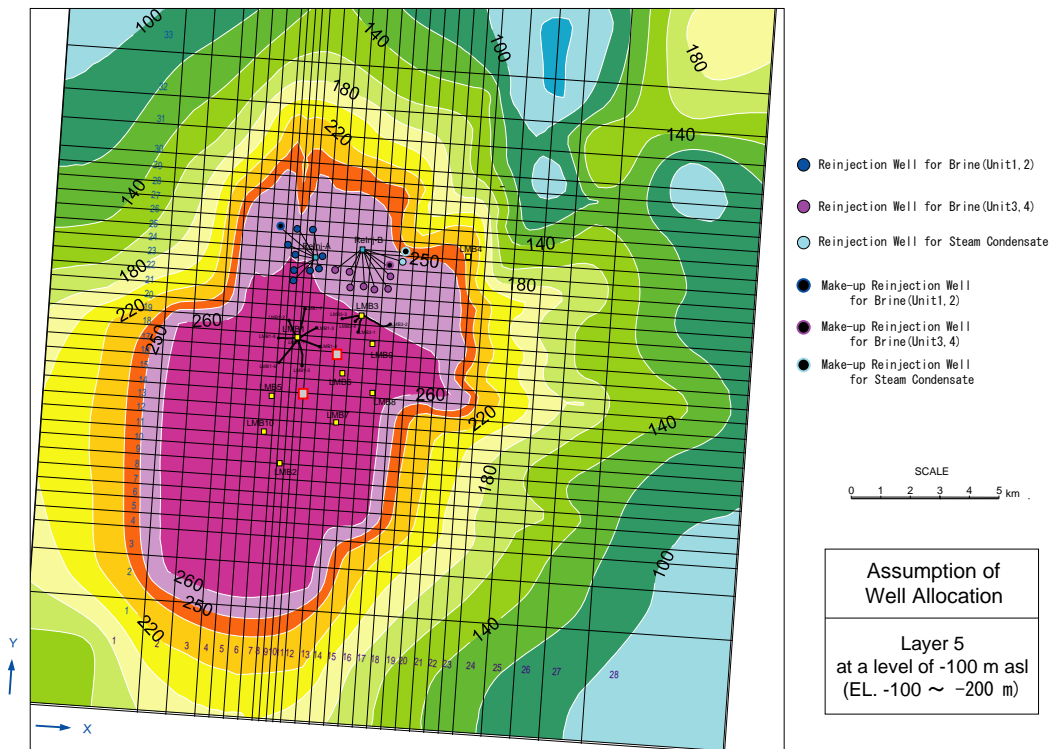


Fig. 3.3-56 Reinjection Well Allocation in Layer 5 (-100 m asl)

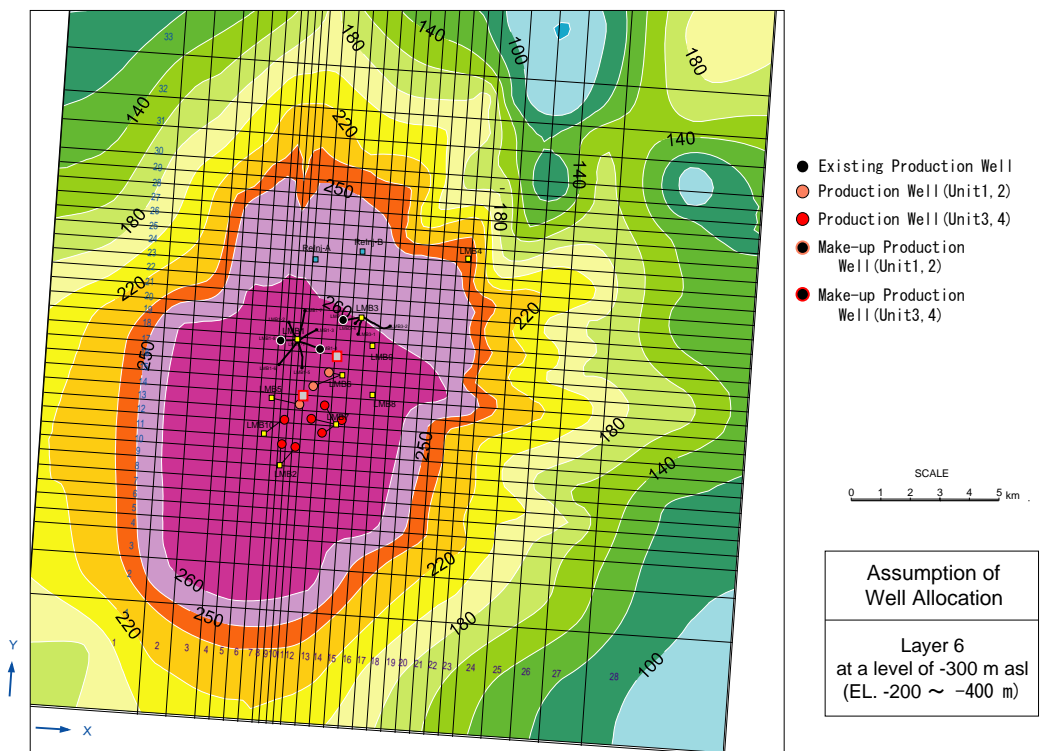


Fig. 3.3-57 Production Well Allocation in Layer 6 (-300 m asl)

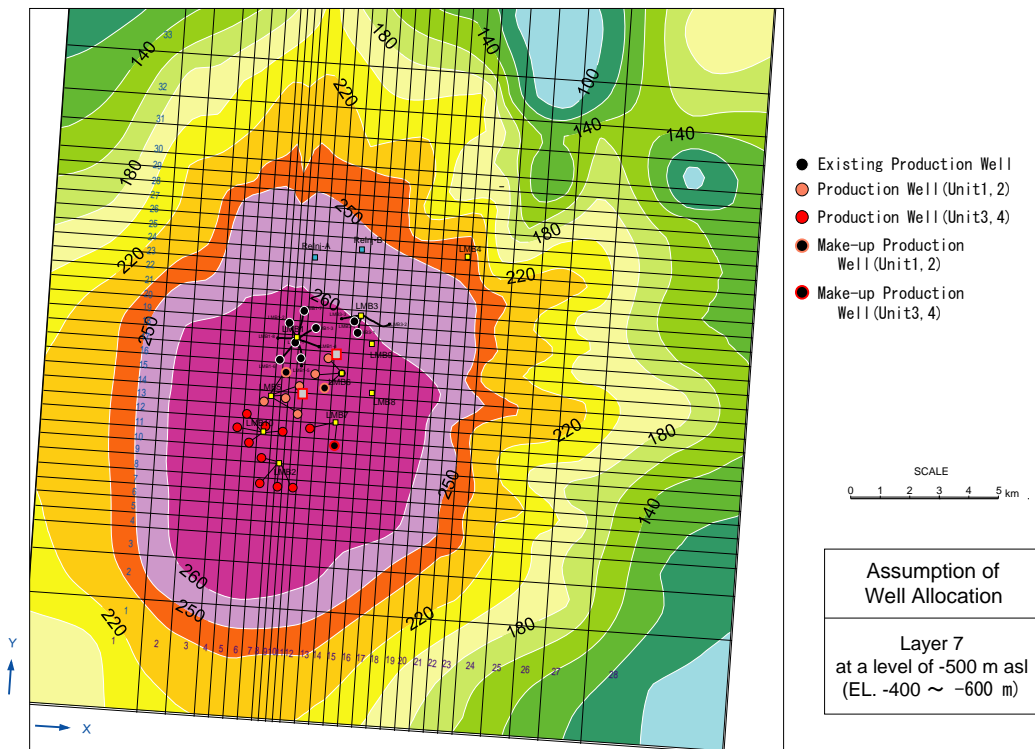


Fig. 3.3-58 Production Well Allocation at Layer 7 (-500 m asl)

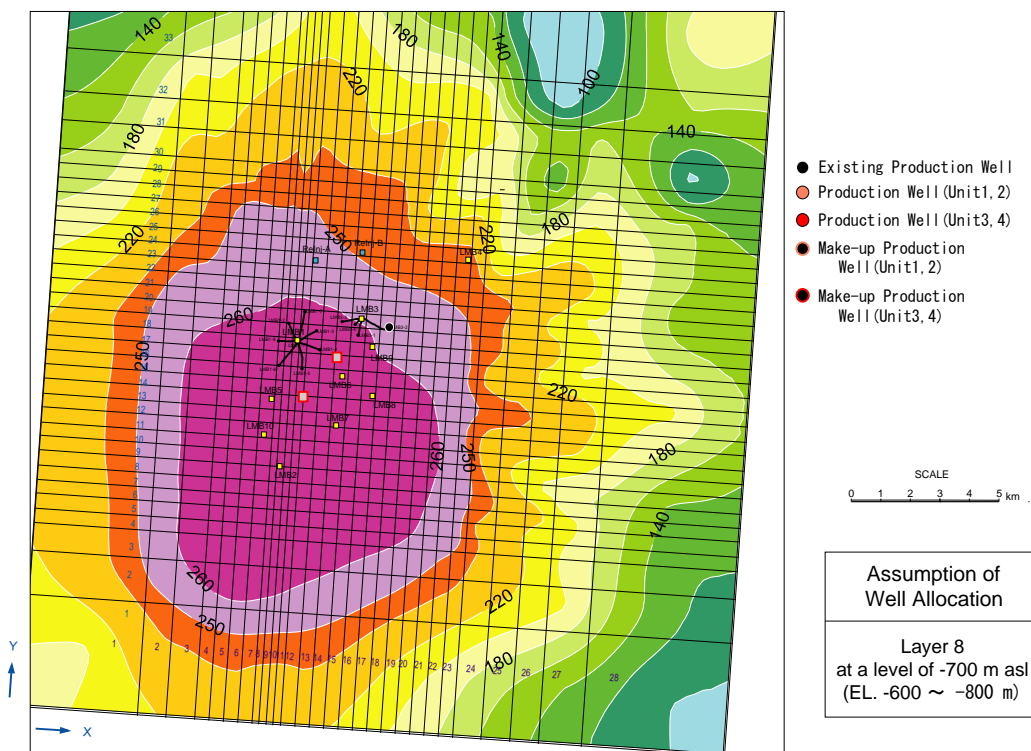


Fig. 3.3-59 Production Well Allocation at Layer 8 (-700 m asl)

(2) Forecasting results

These suggest that the reservoir has enough capacity to sustain a power output of 220 MW (Units 1 to 4) during the plant operating life of 30 years.

1) Number of start-up wells

Table 3.3-3 summarizes the number of wells required for commencing the power plant operation (start-up wells). The number of start-up wells that is required to commence the power plant operation of Units 3 and 4 (110 MW) is 17 for production and 8 for reinjection, consisting of 7 for brine reinjection and one for steam condensate reinjection. One make-up production well and another two make-up reinjection wells (one for brine and one for steam condensate reinjection) are required over the 30 years of operation.

2) Steam and brine flow rates at each production well pad

Figs 3.3-60 to 3.3-62 indicate the simulated deliverability of each well pad. According to the results of the simulation, the three well pads LMB 2, 7, and 10 should be used as production well pads to commence the power plant operation of Units 3 and 4, while the four well pads LMB 1, 3, 5 and 6 should be used for Unit 1 and 2. The reason for the required number of production well pads for Units 3 and 4 being smaller than that for Unit 1 and 2 is that the expected productivity of the wells for the former is greater than that for the latter because of the higher reservoir temperature. In this forecasting simulation, the maximum number of production wells at each well pad is estimated as six. Consequently, the simulated numbers of wells at well pads LMB10, 2 and 7 are six, six, and five, respectively. The simulated steam flow rate at each well pad is around 280 to 340 t/h and the brine flow rate is around 900 to 1100 t/h, as shown in Table 3.3-3.

3) Optimum turbine inlet pressure

The power output of a turbine is determined by the adiabatic heat drop and steam flow rate at the turbine. As the turbine inlet pressure increases, the required steam flow rate becomes smaller due to the larger adiabatic heat drop, and therefore the turbine itself can be smaller, which is an advantage in terms of manufacturing costs. Hence, the turbine inlet pressure should be designed to be higher, for greater turbine efficiency and lower manufacturing cost, as long as the required steam flow rate can be secured. However, a higher inlet pressure of the turbine requires the production wells to maintain a higher wellhead pressure, which will increase the number of production wells required because the steam flow rate produced from the production wells will be reduced at higher wellhead pressure. Therefore, optimum turbine inlet pressure should be decided based on an integrated evaluation in terms of both turbine efficiency and the deliverability of production wells. Figs 3.3-63 to 3.3-66 show the results of a study of the range of optimum turbine inlet pressures for well pads LMB 2, 5, 10 and 7. In this study, pressure loss between the turbine and the steam separator at the well pads is assumed to be 2.0 to 3.0 bar, and the operation wellhead pressures of production wells are assumed to be 8.0 bara at well pads LMB 5, 10 and LMB 7, and 8.5 bara at LMB 2. When the steam separator is installed at each well pad, the separator pressure is estimated to be 6.8 bara, assuming the pressure loss between the steam separator and the production well to be 1.0 to 2.0 bar. Although the maximum power output will be given at a turbine inlet pressure of around 3 bara in terms of the expected deliverability of production wells, it is recommended that the optimum turbine inlet pressure be 5.5 bara, taking into account appropriate turbine size in terms of the manufacturing cost. In future, detailed turbine design should be discussed after obtaining additional

data from production wells at these well pads.

4) Number of make-up wells and change in the mass flow rate of the produced fluids over time

Table 3.3-4 and Figs 3.3-67 to 3.3-69 show the forecasted number of make-up wells which are required for 30 years of plant operating life and the timing of their drilling,. Furthermore, Table 3.3-5 and 3.3-6 indicate the forecasted change over 30 years in the mass flow rate of the produced fluids at each production well pad and the reinjection flow rate at each reinjection well pad, respectively. The forecasted results suggest that the reservoir can sustain power generation of 220 MW for 30 years by adding only one make-up production well and one make-up reinjection well for brine disposal at 4 years after commencement of power plant operation, and one make-up well for steam condensate at 12 years. That is to say, only one production well and two reinjection wells will be required to maintain the required steam production and injection capacity of the wells, meaning that the reservoir will be very stable even as geothermal fluid is produced for power generation and reinjected .

However, it is recommended that an annual rate of decline of 3% should be assumed in counting the number of make-up wells for the calculation of O&M cost in order to avoid overly optimistic predictions, considering that the precision of this reservoir numerical model is still low because the existing well data available for model construction are currently derived only from well pads LMB1 and 3. Therefore, as a future task, the model should be revised to increase its reliability on the basis of additional data from the wells that will be drilled at well pads LMB 5, 10 and LMB 2.

5) Changes of properties in the reservoir over time

In this reservoir simulation study, layer 5 (-100 m asl.) is the depth of the reinjection zones, and layers 6 (-300 m asl.) and 7 (-500 m asl.) are the depths of the production zones. Figs 3.3-70 to 3.3-73 show the change over time in pressure distributions in the reservoir every 10 years in layers 5 to 8 (-700 m asl.), and Figs 3.3-74 to 3.3-77 focus on the change over time (every 10 years) in pressure in the reservoir in these layers compared to that in the natural state. The latter figures are derived from the former figures to highlight the regions affected by production and reinjection.

Similarly, Figs 3.3-78 to 3.3-81 show the change over time in temperature distributions in the reservoir every 10 years in layers 5 to 8, and Figs 3.3-82 to 3.3-85 focus on the change over time (every 10 years) of temperatures in the reservoir compared to those in the natural state. The latter figures are derived from the former figures to highlight the regions affected by production and reinjection. Figs 3.3-86 to 3.3-89 show the change over time of distributions of reinjected water in layers 5 to 8, which represents where and how deep the reinjected water has flowed and spread over time in the reservoir.

The simulated pressure contours indicated that the reservoir pressure around reinjection zones in layers 5 to 8 would increase by 5 to 15 bar due to reinjection, while that around the production zones would decrease by 5 to 10 bar due to production within 10 years after the commencement of power plant operation. On the other hand, the simulated temperature contours indicated that the reservoir temperature around the reinjection zones in layers 5 to 8 would decrease by 25 to 30°C due to reinjection within 10 years after the commencement of power plant operation. By contrast, the reservoir temperatures around the production zones would be almost stable except in the northern area where well pad LMB 3 is located. Accordingly, it is forecasted that the productivity of production wells at LMB 3 will be slightly reduced. Cooling in the production zones affected by reinjection will be the main reason for reduced power output. However, the degree of cooling in the

production zones will be very small, because distances between production and reinjection zones are great enough to avoid cooling effects due to the migration of reinjected water into production zones, which is indicated by the simulated distribution of reinjected water in the reservoir. Therefore, the plant power output will be relatively stable over the operating life of 30 years.

Table 3.3-3 The Forecasted Number of Wells

UNIT	Pad	WHP (bara)	WellName	Forecasted Mass Flow Rate at Turbine Inlet Pressure of 5.5 bara					
				30 days			1 year		
				Steam (t/h)	Water (t/h)	Total (t/h)	Steam (t/h)	Water (t/h)	Total (t/h)
UNIT1,2 (21wells)	LMB1 (8wells)	8.0	LMB1-1	49.8	178.8	228.6	49.9	178.9	228.7
			LMB1-2	36.5	131.5	168.0	36.5	131.6	168.1
			LMB1-3	36.9	134.1	171.0	37.0	134.4	171.4
			LMB1-4	38.1	135.1	173.2	37.9	134.2	172.0
			LMB1-5	47.8	167.3	215.1	47.4	166.1	213.5
			LMB1-6	33.2	115.8	149.0	33.0	115.1	148.1
			LMB1-7	42.8	154.4	197.2	43.2	155.8	199.0
			LMB1-8	41.1	147.2	188.3	41.0	147.0	188.0
		Total		326.1	1164.3	1490.4	325.8	1163.1	1488.8
	LMB3 (4wells)	8.0	LMB3-1	48.7	178.7	227.3	49.2	180.5	229.7
			LMB3-2	21.1	80.3	101.3	21.8	83.3	105.1
			LMB3-3	35.7	131.0	166.7	36.7	134.5	171.2
			LMB3-4	47.9	176.3	224.2	48.8	179.8	228.6
		Total		153.4	566.2	719.5	156.5	578.1	734.6
	LMB5 (5wells)	8.0	LMB5-1	58.5	188.8	247.3	58.0	187.0	245.0
			LMB5-2	53.4	172.4	225.8	52.4	169.1	221.5
			LMB5-3	58.8	189.9	248.7	58.4	188.7	247.1
			LMB5-4	58.8	189.6	248.4	58.3	187.9	246.2
			LMB5-5	59.0	191.2	250.2	57.1	185.2	242.2
				Total		288.6	931.8	1220.4	284.2
	LMB6 (4wells)	8.0	LMB6-1	47.4	163.2	210.6	46.9	161.5	208.4
LMB6-2			40.0	143.7	183.7	39.8	143.2	183.0	
LMB6-3			53.3	173.6	226.9	52.4	170.4	222.7	
LMB6-4			47.7	164.0	211.7	47.4	162.7	210.0	
	Total		188.5	644.4	832.9	186.5	637.6	824.1	
UNIT1,2 Total				956.5	3306.7	4263.2	952.9	3296.6	4249.5
UNIT3,4 (17wells)	LMB10 (6wells)	8.0	LMB5-1	53.3	171.9	225.2	52.7	169.8	222.5
			LMB5-2	58.7	189.4	248.1	58.4	188.1	246.5
			LMB5-3	57.0	186.0	243.0	56.8	185.2	242.0
			LMB5-4	54.6	180.5	235.1	54.4	179.7	234.1
			LMB5-5	58.7	189.4	248.0	58.3	188.3	246.6
			LMB5-6	57.7	187.3	245.0	57.4	186.4	243.8
		Total		340.0	1104.4	1444.4	337.9	1097.6	1435.5
	LMB2 (6wells)	8.5	LMB2-1	56.6	182.6	239.2	56.5	182.0	238.5
			LMB2-2	52.7	169.8	222.5	52.2	168.2	220.3
			LMB2-3	52.6	169.5	222.1	52.1	167.8	219.9
			LMB2-4	56.4	182.3	238.7	56.3	181.7	238.0
			LMB2-5	55.7	179.9	235.6	55.6	179.5	235.1
			LMB2-6	55.9	180.6	236.5	55.6	179.8	235.4
		Total		329.9	1064.7	1394.6	328.1	1059.1	1387.2
	LMB7 (5wells)	8.0	LMB7-1	54.4	175.3	229.6	53.8	173.4	227.2
			LMB7-2	54.5	176.3	230.8	53.9	174.4	228.3
			LMB7-3	58.5	188.6	247.1	58.1	187.4	245.5
LMB7-4			52.9	170.4	223.3	52.1	168.0	220.1	
LMB7-5			55.8	180.5	236.3	52.7	170.4	223.1	
	Total		276.1	891.1	1167.1	270.6	873.6	1144.2	
UNIT3,4 Total				946.0	3060.1	4006.1	936.6	3030.3	3966.9
Start-up			Production			Reinjection			
Unit 1,2			21			Brine		Steam Condensate	
Unit 3,4			17			8			
Total			38			7		1	
						16			

(6 wells)

Wellhead Pressure (bara)	Forecasted Mass Flow Rate at Wellhead Condition				
	Steam (t/h)	Water (t/h)	Total (t/h)	Quality (%)	Enthalpy (KJ/kg)
1	466.90	961.13	1428.03	32.70	1155.75
2	439.10	979.96	1419.06	30.94	1185.94
3	410.67	999.89	1410.56	29.11	1191.23
4	381.67	1014.60	1396.27	27.34	1187.72
5	352.14	1018.93	1371.07	25.68	1181.38
6	322.13	1008.87	1330.99	24.20	1175.04
7	291.68	981.57	1273.24	22.91	1170.10
8	260.83	935.32	1196.15	21.81	1167.21
9	229.65	869.56	1099.21	20.89	1166.65
10	198.17	784.91	983.07	20.16	1168.50
11	166.43	683.10	849.53	19.59	1172.66
12	134.49	567.05	701.54	19.17	1178.84
13	102.39	440.80	543.19	18.85	1186.17
14	70.17	309.57	379.75	18.48	1191.84
15	37.89	179.72	217.61	17.41	1183.38
16	6.93	58.75	65.68	10.55	1062.50
17					
18					

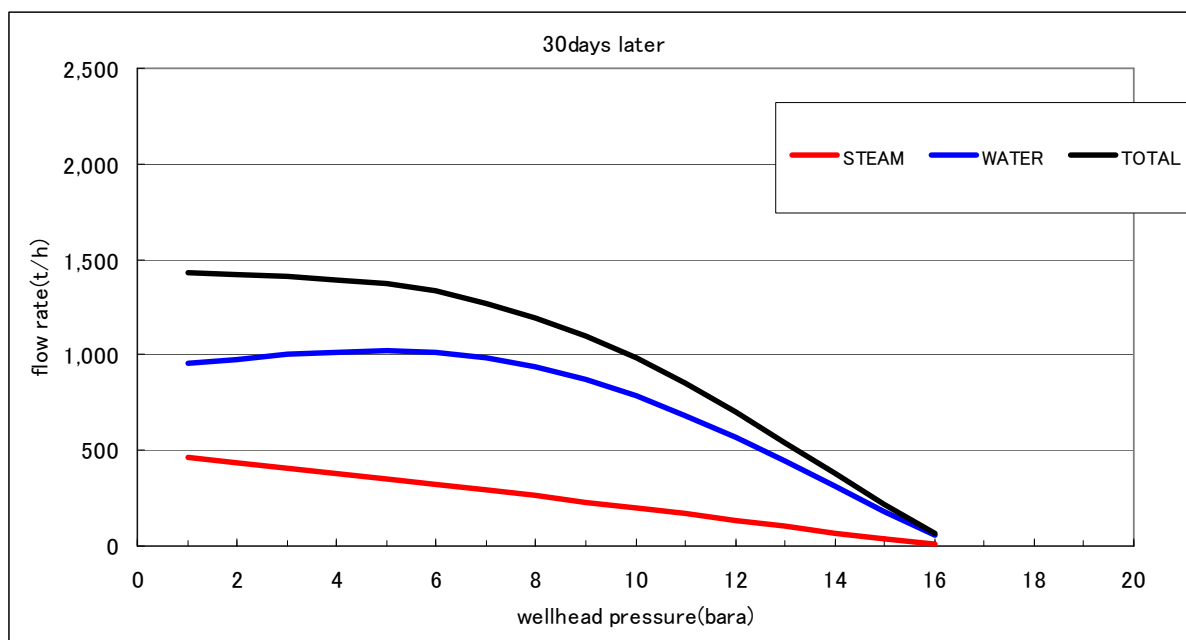


Fig. 3.3-60 Simulated Deliverability at Well Pad LMB 10

(30 days after Commencing Power Plant Operation)

(6 wells)

Wellhead Pressure (bara)	Forecasted Mass Flow Rate at Wellhead Condition				
	Steam (t/h)	Water (t/h)	Total (t/h)	Quality (%)	Enthalpy (KJ/kg)
1	633.10	1240.23	1873.33	33.80	1180.59
2	586.72	1266.12	1852.84	31.67	1201.86
3	541.06	1285.13	1826.19	29.63	1202.34
4	496.10	1292.35	1788.45	27.74	1196.34
5	451.83	1283.85	1735.68	26.03	1188.72
6	408.23	1256.76	1664.99	24.52	1181.64
7	365.28	1209.20	1574.48	23.20	1176.13
8	322.97	1140.33	1463.30	22.07	1172.63
9	281.28	1050.33	1331.60	21.12	1171.34
10	240.19	940.40	1180.59	20.34	1172.26
11	199.68	812.77	1012.45	19.72	1175.29
12	159.75	670.67	830.42	19.24	1180.15
13	120.36	518.39	638.75	18.84	1186.06
14	81.52	361.20	442.72	18.41	1190.54
15	43.19	205.43	248.62	17.37	1182.57
16	5.36	58.41	63.77	8.41	1021.05
17					
18					

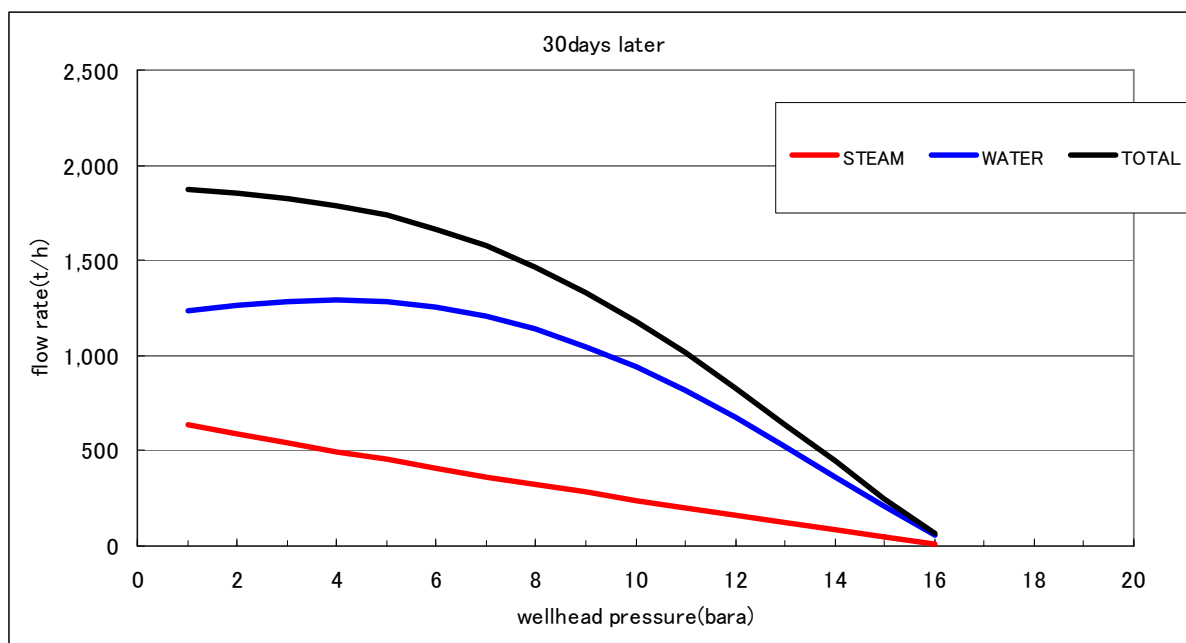


Fig. 3.3-61 Simulated Deliverability at Well Pad LMB 2

(30 days after Commencing Power Plant Operation)

(5 wells)

Wellhead Pressure (bara)	Forecasted Mass Flow Rate at Wellhead Condition				
	Steam (t/h)	Water (t/h)	Total (t/h)	Quality (%)	Enthalpy (KJ/kg)
1	654.72	1294.84	1949.56	33.58	1175.79
2	604.21	1327.13	1931.35	31.28	1193.46
3	554.82	1343.90	1898.72	29.22	1193.54
4	506.51	1342.76	1849.27	27.39	1188.88
5	459.25	1322.02	1781.27	25.78	1183.46
6	413.02	1280.68	1693.71	24.39	1178.87
7	367.79	1218.45	1586.24	23.19	1175.84
8	323.52	1135.74	1459.26	22.17	1174.66
9	280.19	1033.64	1313.84	21.33	1175.46
10	237.77	913.97	1151.74	20.64	1178.30
11	196.23	779.20	975.43	20.12	1183.18
12	155.54	632.55	788.09	19.74	1190.05
13	115.66	477.91	593.57	19.49	1198.71
14	76.58	319.87	396.45	19.32	1208.23
15	38.26	163.73	201.99	18.94	1213.09
16					
17					
18					

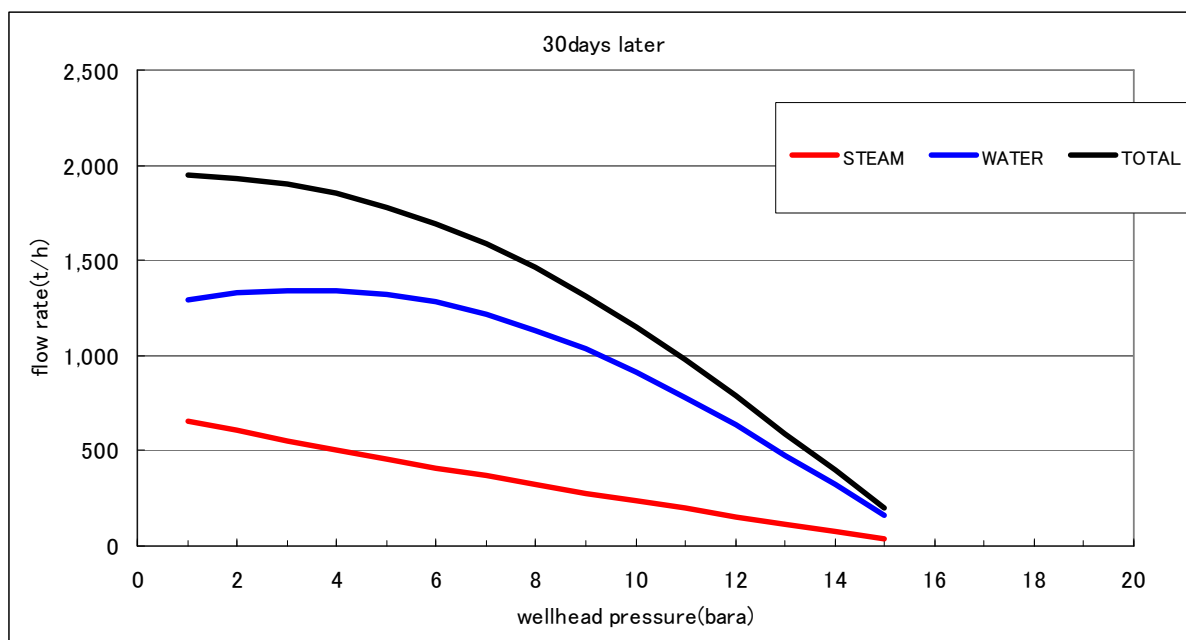


Fig. 3.3-62 Simulated Deliverability at Well Pad LMB 7

(30 days after Commencing Power Plant Operation)

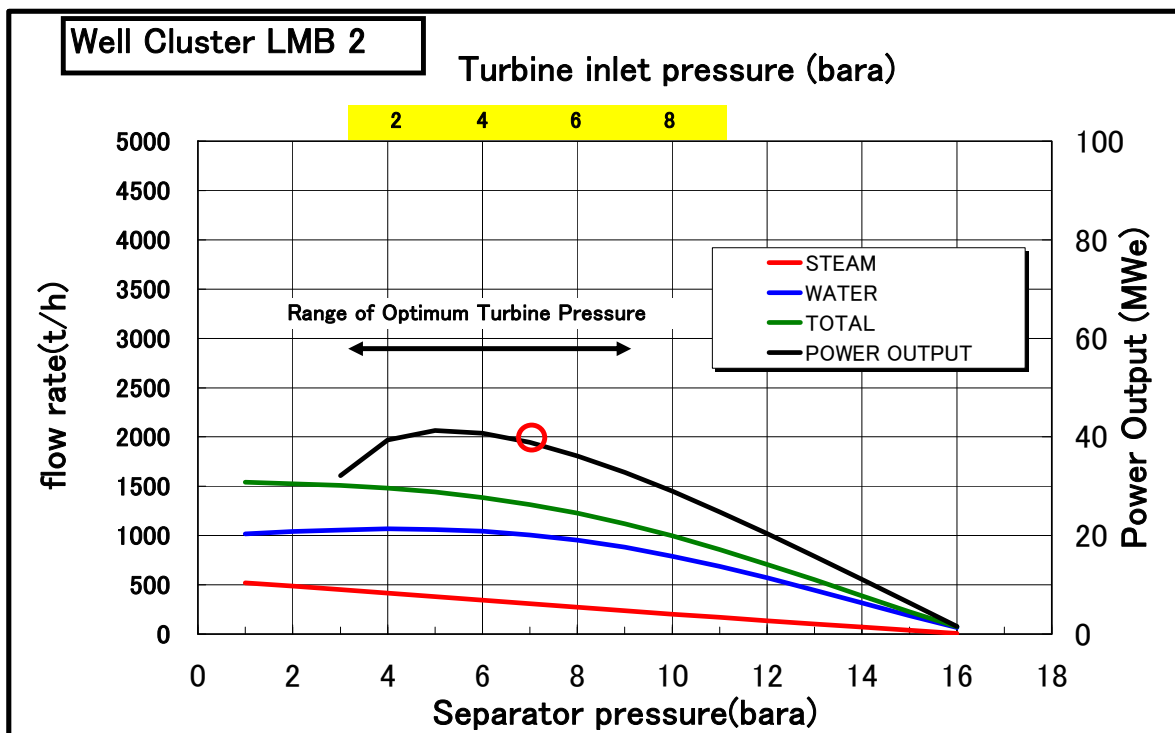


Fig. 3.3-63 Study of Range of Optimum Turbine Inlet Pressure at Well Pad LMB 2

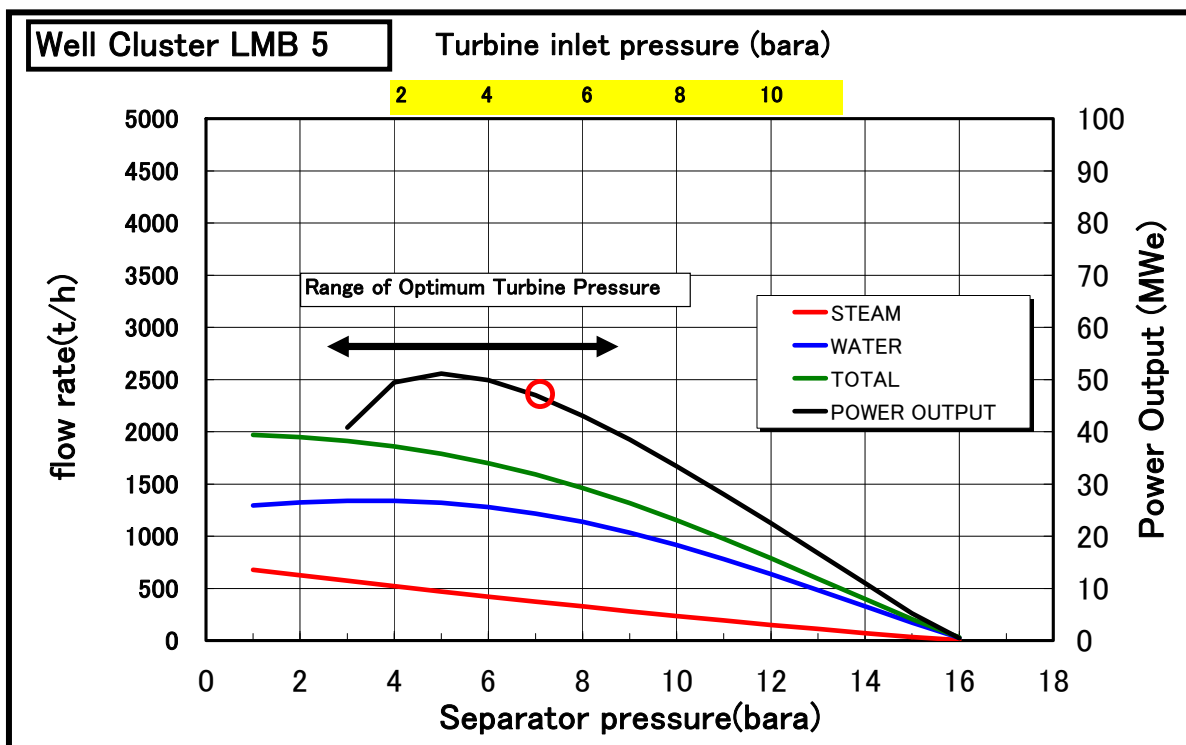


Fig. 3.3-64 Study of Range of Optimum Turbine Inlet Pressure at Well Pad LMB 5

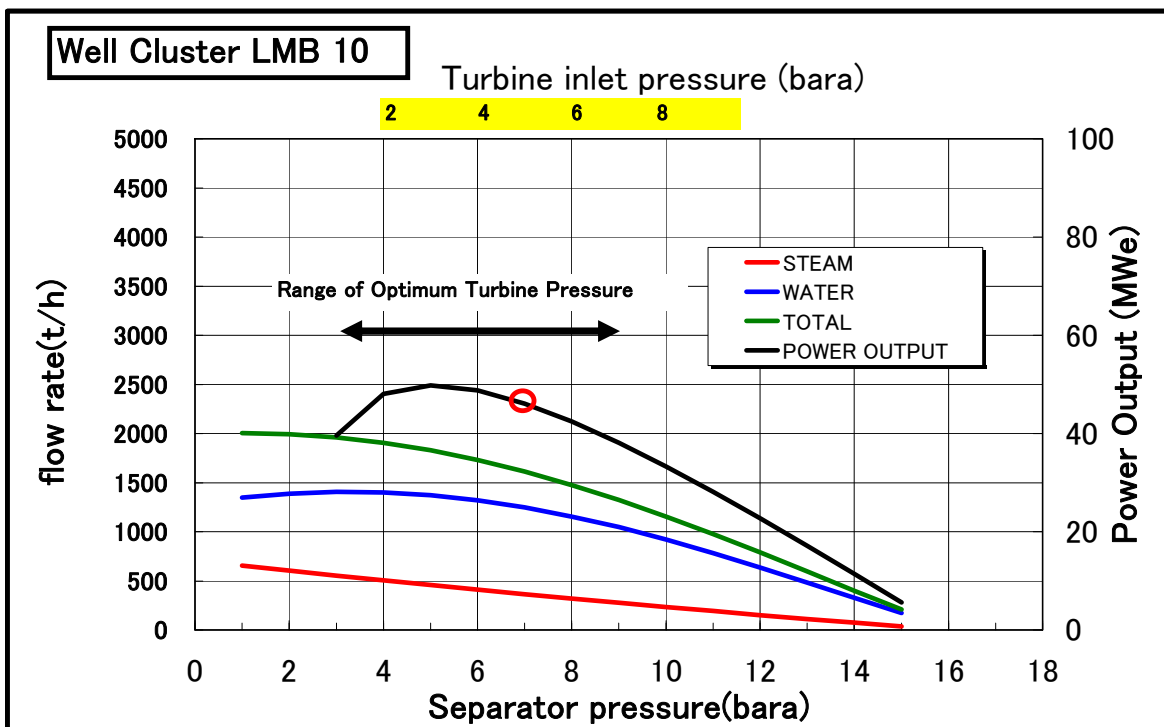


Fig. 3.3-65 Study of Range of Optimum Turbine Inlet Pressure at Well Pad LMB10

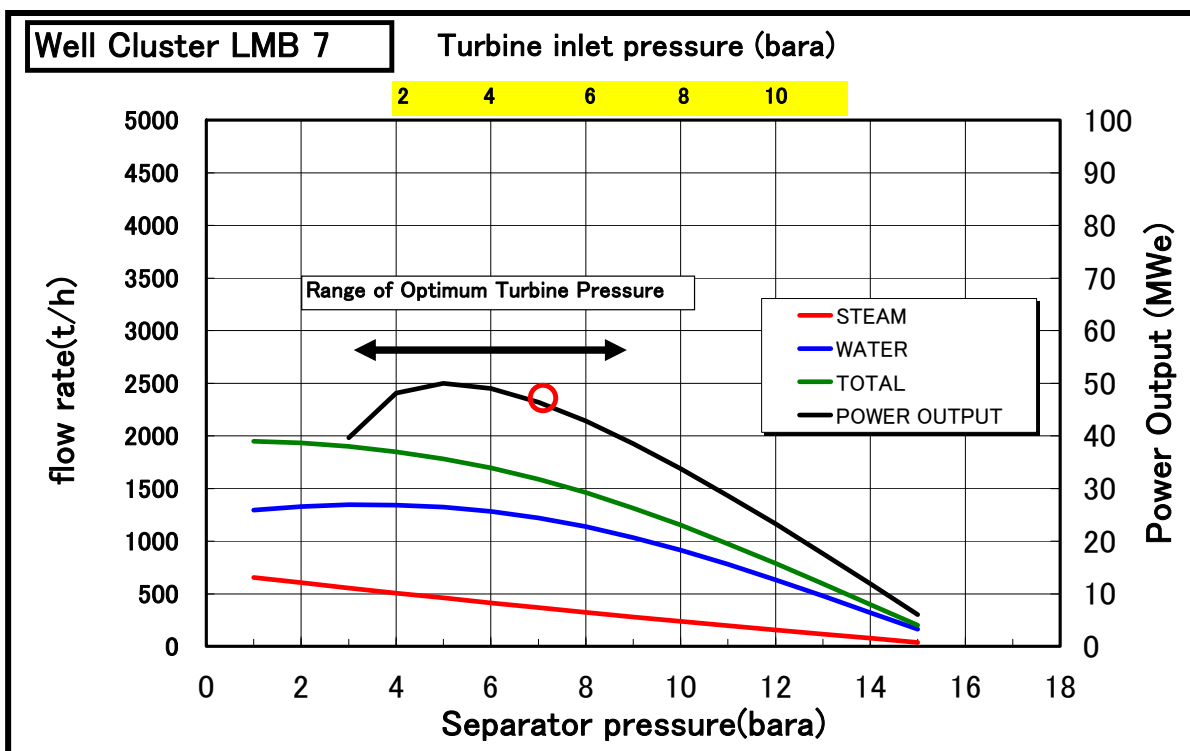


Fig. 3.3-66 Study of Range of Optimum Turbine Inlet Pressure at Well Pad LMB 7

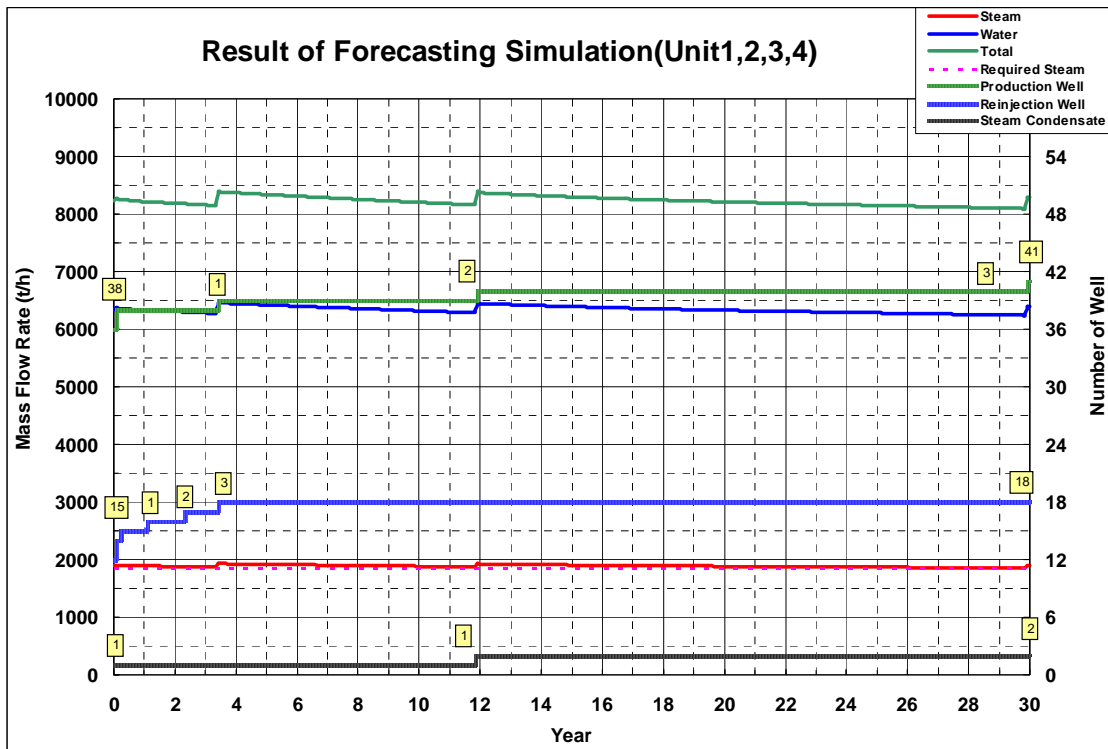


Fig. 3.3-67 Result of Forecasting Simulation (Unit 1, 2, 3, 4)

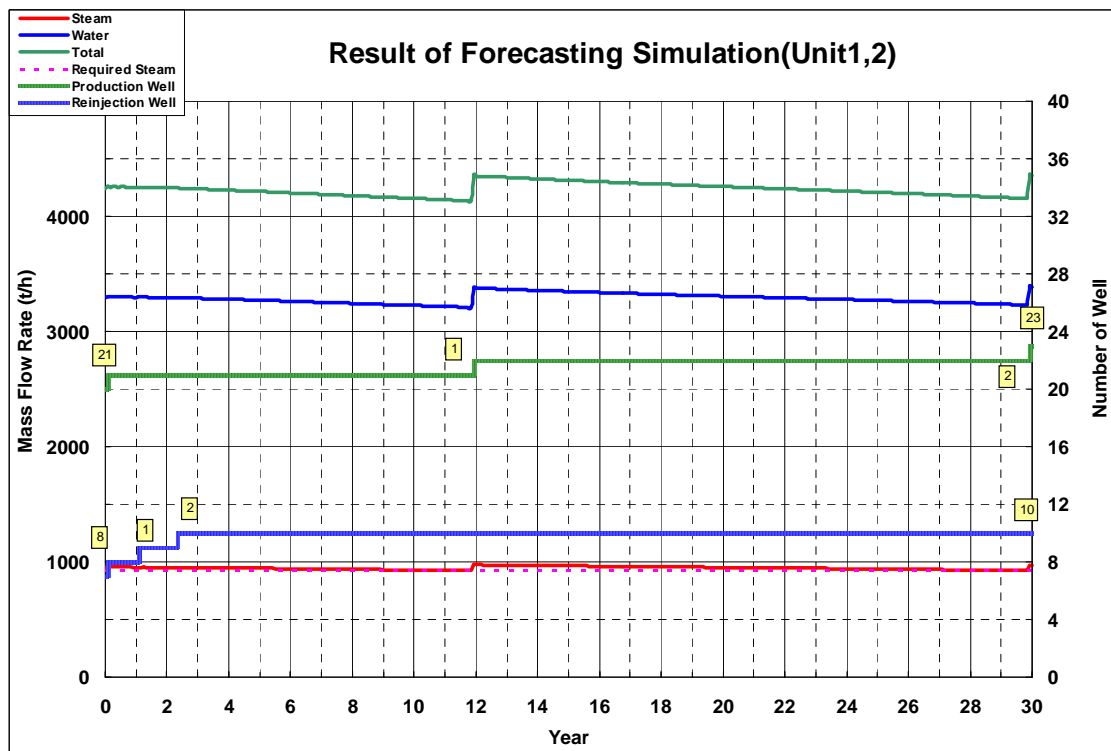


Fig. 3.3-68 Result of Forecasting Simulation (Unit 1, 2)

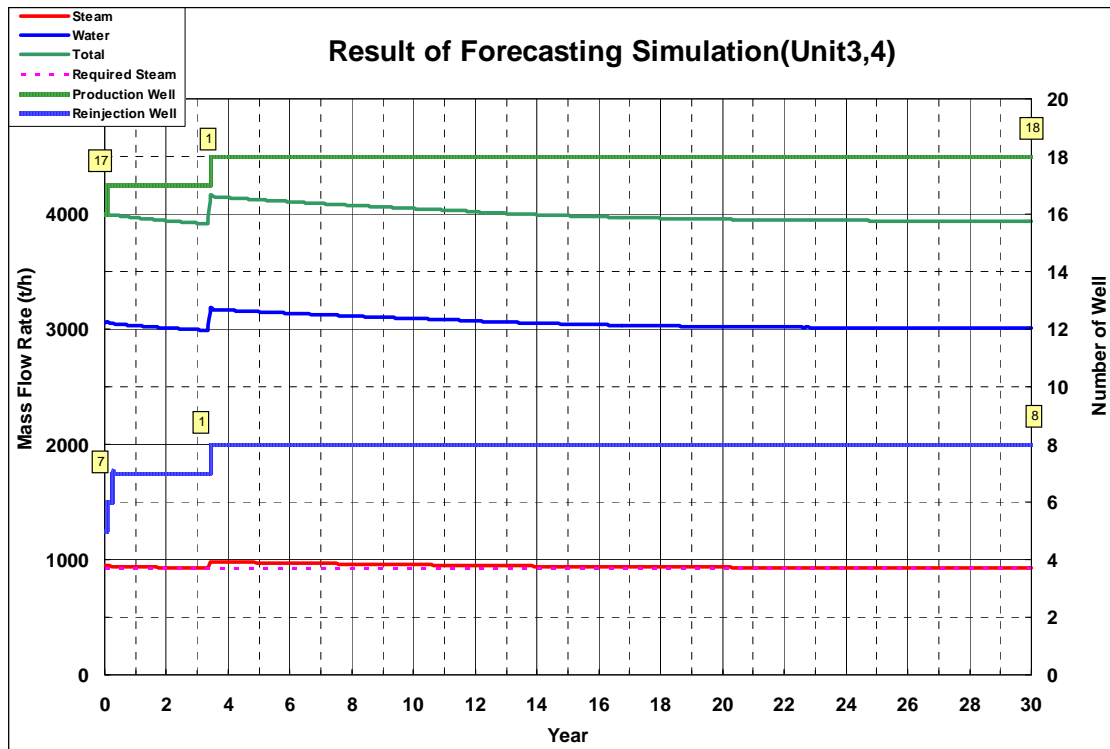


Fig. 3.3-69 Result of Forecasting Simulation (Unit 3, 4)

Table 3.3-4 Required Number and Timing of Drilling of Make-up Wells (Lumut Balai)

Turbine inlet pressure : 6.8 bara

Year	UNIT 1&2						UNIT 3&4						Grand Total	
	Steam (t/h)	Water (t/h)	Total (t/h)	Make-up Production Well	Make-up ReInjection Well for Brine	Total	Steam (t/h)	Water (t/h)	Total (t/h)	Make-up Production Well	Make-up ReInjection Well for Brine	Total		Make-up ReInjection Well for Steam Condensate
0	957	3307	4263				946	3060	4006					
1	953	3297	4250				937	3030	3967					
2	952	3295	4247		1	1	930	3011	3941					1
3	950	3288	4237		1	1	926	2995	3921					1
4	947	3280	4227				924 ↓ 984	2990 ↓ 3183	3914 ↓ 4167	1	1	2		2
5	944	3271	4215				973	3150	4124					
6	941	3262	4203				970	3138	4107					
7	938	3253	4191				966	3125	4091					
8	935	3244	4180				962	3114	4076					
9	932	3234	4166				958	3103	4061					
10	930	3226	4155				955	3093	4048					
11	924 ↓ 979	3209 ↓ 3387	4133 ↓ 4366	1		1	952	3083	4035					1
12	974	3374	4348				948	3069	4017				1	1
13	972	3366	4338				945	3060	4005					
14	968	3356	4324				942	3052	3994					
15	966	3347	4313				940	3045	3985					
16	962	3338	4300				938	3039	3977					
17	959	3329	4289				936	3033	3970					
18	957	3322	4279				935	3028	3963					
19	954	3314	4268				934	3025	3958					
20	951	3306	4258				933	3022	3954					
21	949	3299	4248				932	3019	3950					
22	947	3293	4239				931	3017	3948					
23	944	3284	4228				930	3015	3946					
24	941	3277	4218				930	3014	3944					
25	938	3270	4208				930	3013	3942					
26	936	3262	4197				929	3012	3941					
27	933	3254	4186				929	3011	3940					
28	930	3246	4176				929	3011	3939					
29	924 ↓ 972	3229 ↓ 3392	4153 ↓ 4364	1		1	928	3010	3939					1
30	969	3382	4351				928	3009	3937					
No. of Make-up	-	-	-	2	2	4	-	-	-	1	1	2	1	7

Table 3.3-6 Forecasted Mass Flow Rate of each Reinjection Well

Pad	WellName	30 days		1 year		2 year		3 year		4 year		5 year		6 year		7 year		8 year		9 year		10 year		11 year		12 year		13 year		14 year		15 year						
		Brine (t/h)	Total (t/h)	Brine (t/h)	Total (t/h)	Brine (t/h)	Total (t/h)	Brine (t/h)	Total (t/h)	Brine (t/h)	Total (t/h)	Brine (t/h)	Total (t/h)	Brine (t/h)	Total (t/h)	Brine (t/h)	Total (t/h)	Brine (t/h)	Total (t/h)	Brine (t/h)	Total (t/h)	Brine (t/h)	Total (t/h)	Brine (t/h)	Total (t/h)	Brine (t/h)	Total (t/h)	Brine (t/h)	Total (t/h)	Brine (t/h)	Total (t/h)	Brine (t/h)	Total (t/h)					
Brine	ReinjeksiA	InjA-1	427.7		420.1		391.3		378.4		374.4		373.0		371.9		371.5		371.2		370.8		370.8		370.8		369.7		369.4		369.7		370.1					
		InjA-2	420.5		410.4		373.0		358.7		354.6		353.4		352.2		351.7		351.2		350.7		350.4		350.2		348.2		347.8		347.8		347.8					
		InjA-3	435.2		403.2		368.3		356.8		353.2		352.2		351.4		350.9		350.4		349.8		349.5		349.3		347.8		347.3		347.3		347.3					
		InjA-4	436.7		423.7		377.6		360.0		356.5		355.5		354.6		354.1		353.6		353.2		352.9		352.9		349.3		349.0		348.8		348.8					
		InjA-5	469.1	3306.6	459.0	3297.1	410.8	3295.6	387.0	3287.4	383.4	3279.9	382.7	3271.0	382.0	3261.6	381.6	3253.0	381.6	3244.2	381.2	3233.8	381.2	3225.9	381.2	3225.9	381.2	3216.3	381.2	3216.3	381.2	3216.3	381.2	3216.3	381.2			
		InjA-6	468.0		452.2		405.7		387.4		384.1		383.4		382.7		382.3		382.0		381.6		381.2		381.2		381.2		378.0		377.3		376.9		376.9			
		InjA-7	441.4		355.2		325.5		317.1		314.0		313.2		312.3		311.7		310.9		310.1		309.4		309.4		308.8		307.3		306.6		306.2		305.9			
		InjA-8	208.0		373.3		341.2		331.0		328.1		327.5		326.8		326.3		325.5		324.8		324.2		323.5		323.5		321.6		320.8		320.3		320.0			
		InjA-9					302.2		349.3		344.2		342.0		340.2		338.7		337.5		336.3		335.2		334.4		334.4		327.8		327.5		327.1		326.6			
		InjA-10							61.8		87.3		88.2		87.6		84.2		80.5		75.2		71.0		64.7		249.4		246.1		237.3		229.6		229.6			
	ReinjeksiB	InjB-1	508.3		454.3		436.0		431.3		427.0		425.5		424.4		423.4		422.3		421.6		420.8		420.1		419.4		418.7		418.0		417.6		417.6			
		InjB-2	500.4		457.6		439.9		435.2		429.8		428.4		427.3		426.6		425.5		424.8		423.7		423.0		422.3		421.6		421.2		420.8		420.8			
		InjB-3	497.9		464.4		445.3		440.6		433.8		432.4		431.3		430.6		429.5		428.8		428.0		427.3		426.6		425.9		425.5		425.2		425.2			
		InjB-4	488.2		476.3		454.7		449.6		439.9		438.5		437.8		437.0		436.3		435.6		434.9		434.9		434.5		433.8		433.4		433.2		432.7		432.7	
		InjB-5	547.6	3060.0	461.5	3030.9	437.4	3010.3	430.2	2995.2	426.6	3164.3	425.5	3150.0	424.1	3137.3	423.0	3125.5	421.9	3113.6	421.2	3102.8	420.1	3092.7	419.4	3082.9	418.0	3069.5	417.2	3060.4	416.9	3052.4	416.2	3045.5	416.2	3045.5		
		InjB-6	517.7		452.2		432.0		425.9		421.2		420.1		419.0		418.3		417.2		416.2		415.4		414.4		413.6		412.6		412.2		411.5		411.5			
		InjB-7			264.6		365.0		382.3		442.8		441.7		441.0		440.3		439.9		439.2		438.8		438.5		438.5		437.0		437.0		437.0		437.0			
		InjB-8							143.2		138.3		133.3		126.4		120.9		115.6		110.8		105.7		98.1		88.6		84.5		84.5		84.5		84.5			
Brine Total		6366.6		6328.0		6305.9		6282.6		6444.1		6421.0		6398.8		6378.5		6357.8		6336.6		6318.6		6299.2		6443.4		6426.1		6407.9		6392.5		6392.5				
Condensate	ReinjeksiB	InjB-9	380.5	380.5	378.0	378.0	376.6	376.6	375.1	375.1	384.8	384.8	383.4	383.4	382.0	382.0	380.9	380.9	379.4	379.4	378.0	378.0	376.9	376.9	375.8	375.8	373.3	373.3	366.1	366.1	362.5	362.5	381.1	381.1				
		InjB-10																																				
	Condensate Total	380.5		378.0		376.6		375.1		384.8		383.4		382.0		380.9		379.4		378.0		376.9		375.8		373.3		366.1		362.5		381.1		381.1				

Pad	WellName	16 year		17 year		18 year		19 year		20 year		21 year		22 year		23 year		24 year		25 year		26 year		27 year		28 year		29 year		30 year		Average				
		Brine (t/h)	Total (t/h)	Brine (t/h)	Total (t/h)	Brine (t/h)	Total (t/h)	Brine (t/h)	Total (t/h)	Brine (t/h)	Total (t/h)	Brine (t/h)	Total (t/h)	Brine (t/h)	Total (t/h)	Brine (t/h)	Total (t/h)	Brine (t/h)	Total (t/h)	Brine (t/h)	Total (t/h)	Brine (t/h)	Total (t/h)	Brine (t/h)	Total (t/h)	Brine (t/h)	Total (t/h)	Brine (t/h)	Total (t/h)	Total (t/h)						
Brine	ReinjeksiA	InjA-1	370.4		370.4		370.8		370.8		371.2		371.2		371.2		370.8		370.8		370.8		370.8		371.2		371.2		371.2		371.2		371.2			
		InjA-2	348.0		348.0		348.0		348.0		348.2		348.0		347.8		347.5		347.3		347.3		347.1		347.3		347.5		347.7		347.7		347.7			
		InjA-3	347.3		347.3		347.3		347.3		347.5		347.3		347.1		346.6		346.5		346.3		346.1		346.1		346.1		346.3		346.3		346.3		346.3	
		InjA-4	348.8		348.8		348.7		348.8		348.8		348.5		348.3		348.0		347.8		347.7		347.7		347.7		347.8		348.0		348.3		348.3		348.3	
		InjA-5	374.0	3337.9	374.0	3328.8	374.0	3322.1	374.4	3314.2	374.4	3306.5	374.0	3298.6	373.7	3292.7	373.7	3284.0	374.0	3277.1	374.0	3269.5	374.0	3261.6	374.0	3253.7	374.4	3246.1	375.1	3237.0	371.2	3382.2	3290.7	3290.7		
		InjA-6	376.9		376.9		376.9		376.9		376.9		376.9		376.6		376.2		376.2		375.8		375.8		375.8		376.2		376.6		376.9		376.9		376.9	
		InjA-7	305.5		305.2		305.0		304.7		304.6		304.1		303.7		303.3		302.9		302.9		302.6		302.3		302.1		302.0		302.0		301.5		301.5	
		InjA-8	319.6		319.3		319.0		318.7		318.5		318.2		317.9		317.2		316.9		316.9		316.5		316.2		316.1		316.1		316.1		315.4		315.4	
		InjA-9	326.4		326.3		326.1		325.9		325.9		325.6		325.2		325.1		325.1		325.1		324.9		324.9		325.2		325.6		325.9		325.9		325.9	
		InjA-10	220.8		212.5		206.3		198.5		190.5		185.3		180.9		175.7		169.6		165.1		163.5		156.5		147.3		137.9		128.8		286.5		286.5	
	ReinjeksiB	InjB-1	417.2		416.9		416.5		416.2		415.8		415.4		414.7		414.7		414.7		414.0		414.0		413.6		413.6		413.6		413.3		413.3		413.3	
		InjB-2	420.5		420.1		419.4		419.0		418.7		418.3		418.0		417.8		417.8		417.2		417.2		417.2		416.9		416.9		416.5		416.5		416.5	
		InjB-3	424.8		424.4		423.7		423.4		423.0		422.6		422.3		422.3		422.3		422.3		421.9		421.9		421.6		421.2		421.2		420.8		420.8	
		InjB-4	432.4		432.0		432.0		431.6		431.3		430.9		430.6		430.6		430.2		430.2		430.2		430.2		429.8		429.8		429.5		429.1		429.1	
		InjB-5	415.4	3038.7	415.4	3033.7	415.1	3028.5	414.4	3024.8	414.0	3021.3	413.6	3018.3	413.6	3017.3	412.9	3014.9	412.6	3014.2	412.2	3012.6	411.8	3012.6	411.8	3011.0	411.8	3011.0	411.5	3010.7	411.5	3010.5	411.1	3008.9	3050.4	
		InjB-6	410.8</																																	

Layer 5 (EL. 0 m ~ -200 m)

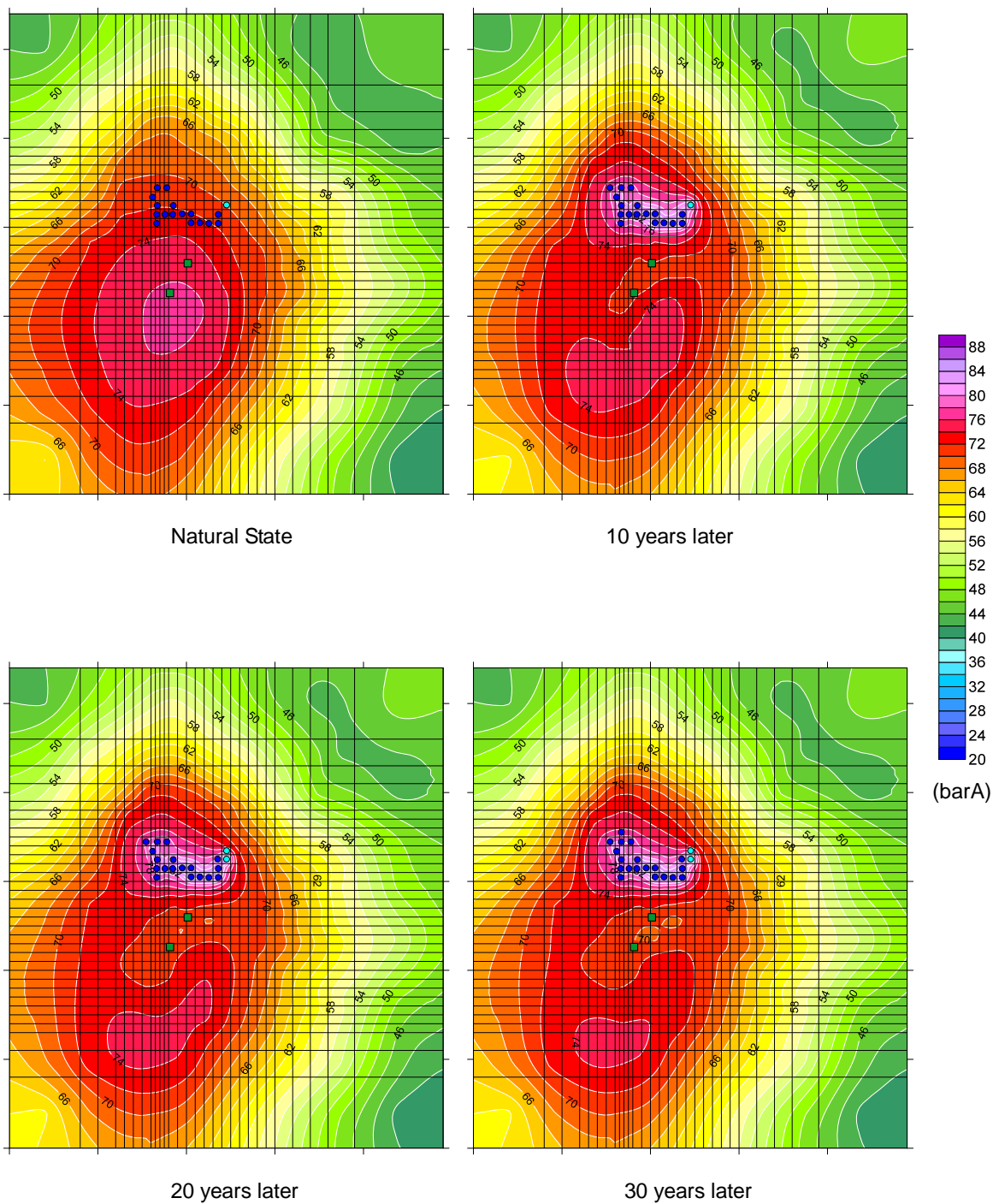


Fig. 3.3-70 Forecasted Pressure Distributions in Layer 5 (EL. -100 m asl)

Layer 6 (EL. -200 m ~ -400 m)

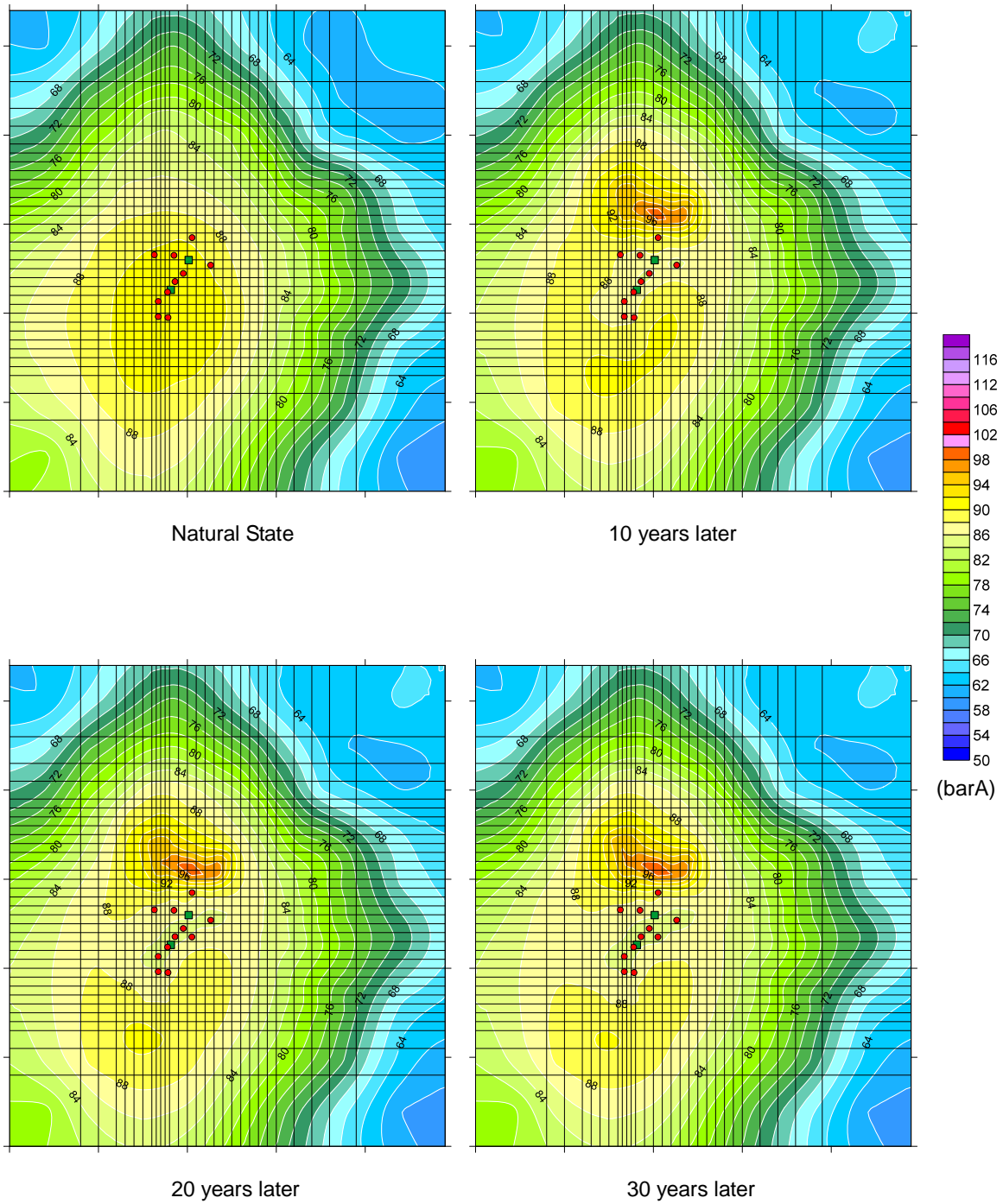


Fig. 3.3-71 Forecasted Pressure Distributions in Layer 6 (EL. -300 m asl)

Layer 7 (EL. -400 m ~ -600 m)

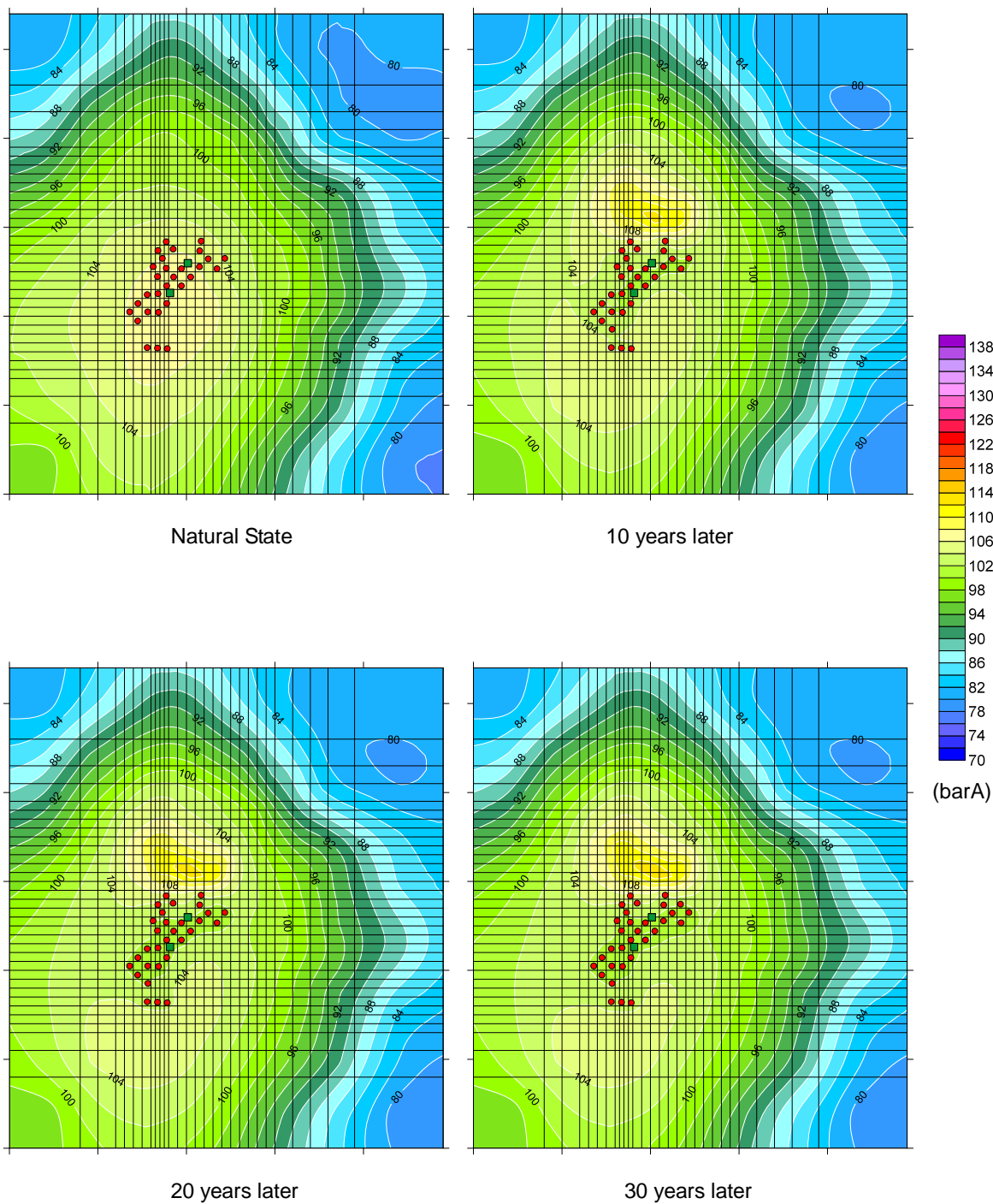


Fig. 3.3-72 Forecasted Pressure Distributions in Layer 7 (EL. -500 m asl)

Layer 8 (EL. -600 m ~ -800 m)

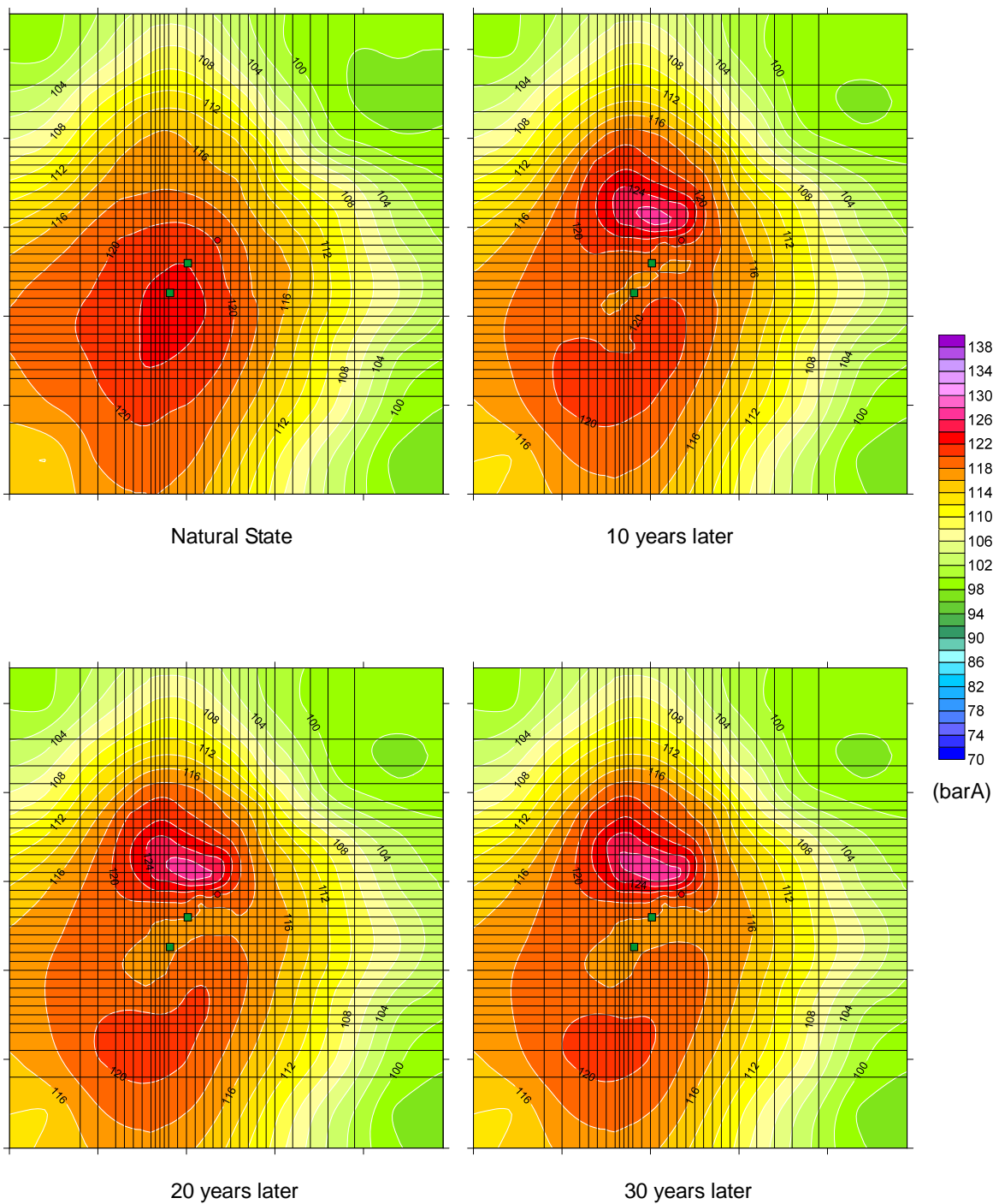


Fig. 3.3-73 Forecasted Pressure Distributions in Layer 8 (EL. -700 m asl)

Layer 5 (EL. 0 m ~ -200 m)

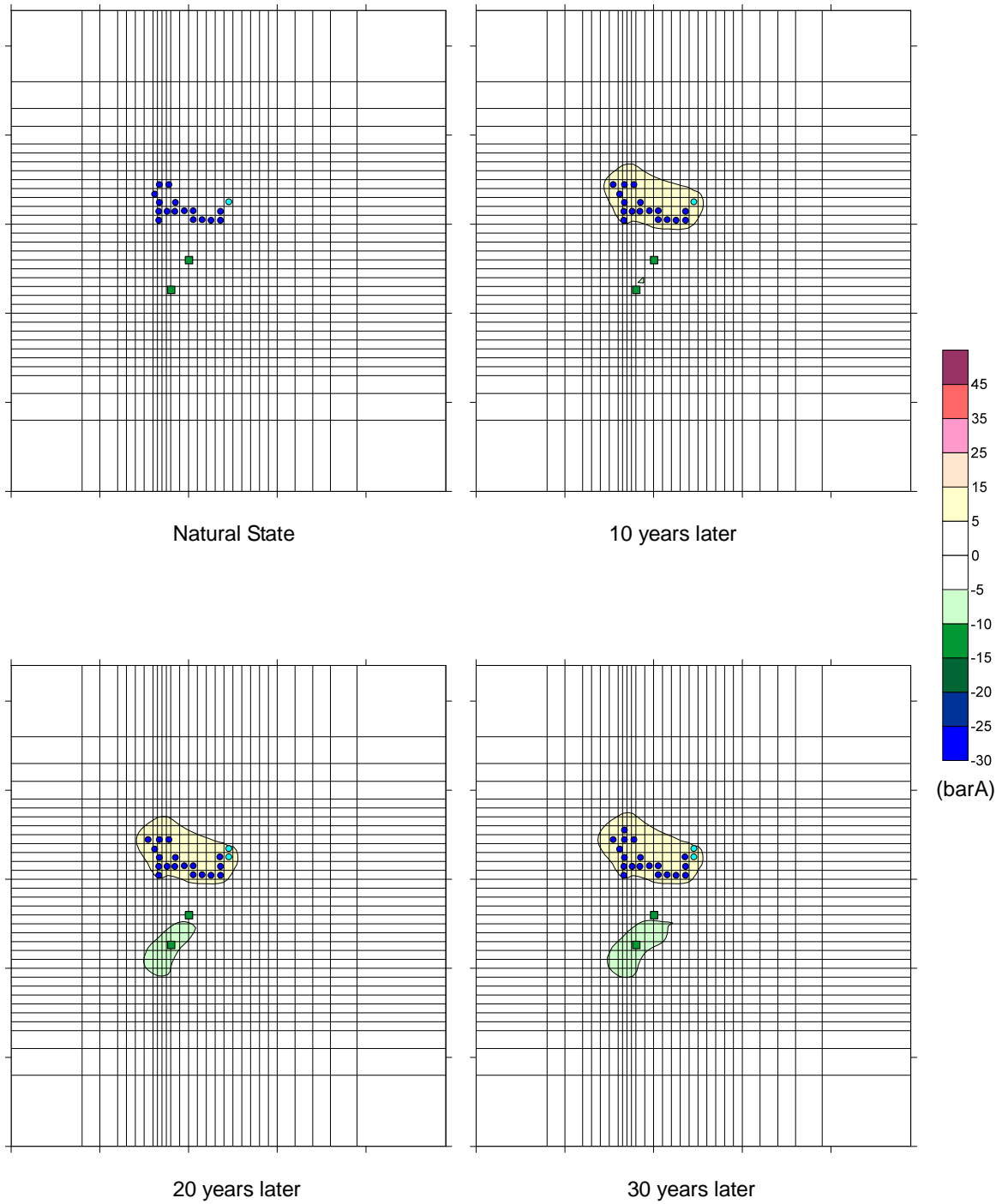


Fig. 3.3-74 Pressure Difference from Steady State in Layer 5 (EL. -100 m asl)

Layer 6 (EL. -200 m ~ -400 m)

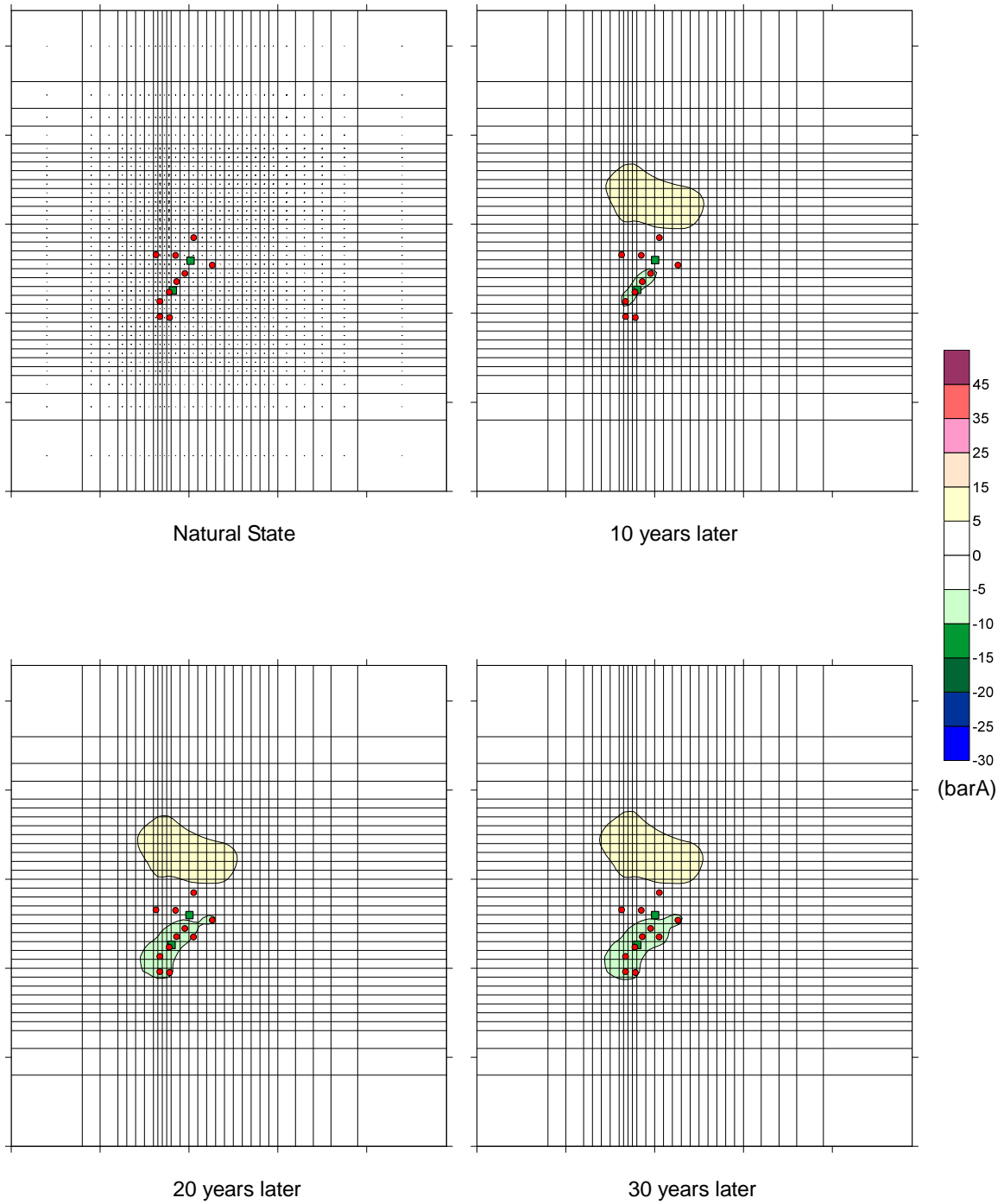


Fig. 3.3-75 Pressure Difference from Steady State in Layer 6 (EL. -300 m asl)

Layer 7 (EL. -400 m ~ -600 m)

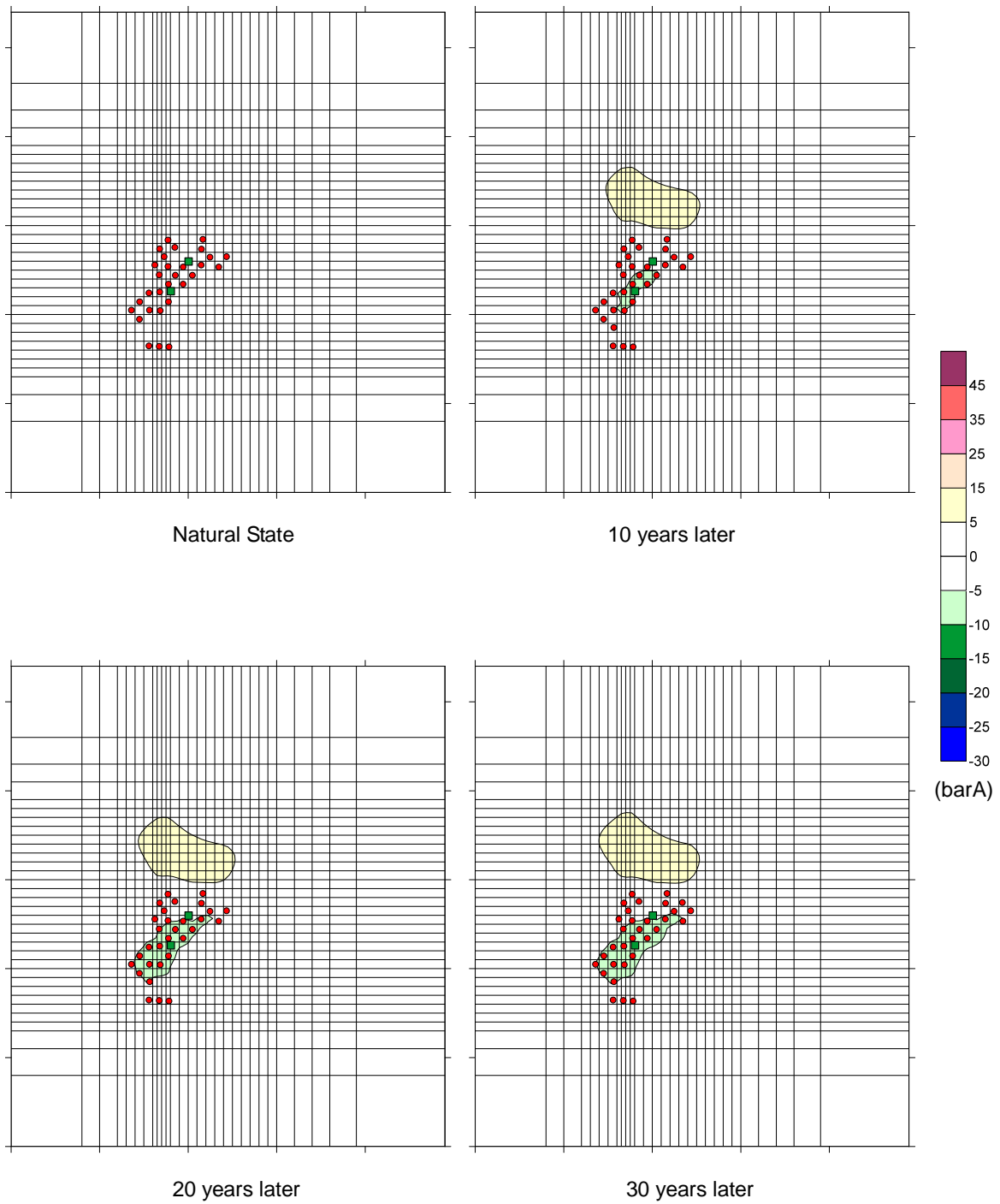


Fig. 3.3-76 Pressure Difference from Steady State in Layer 7 (EL. -500 m asl)

Layer 8 (EL. -600 m ~ -800 m)

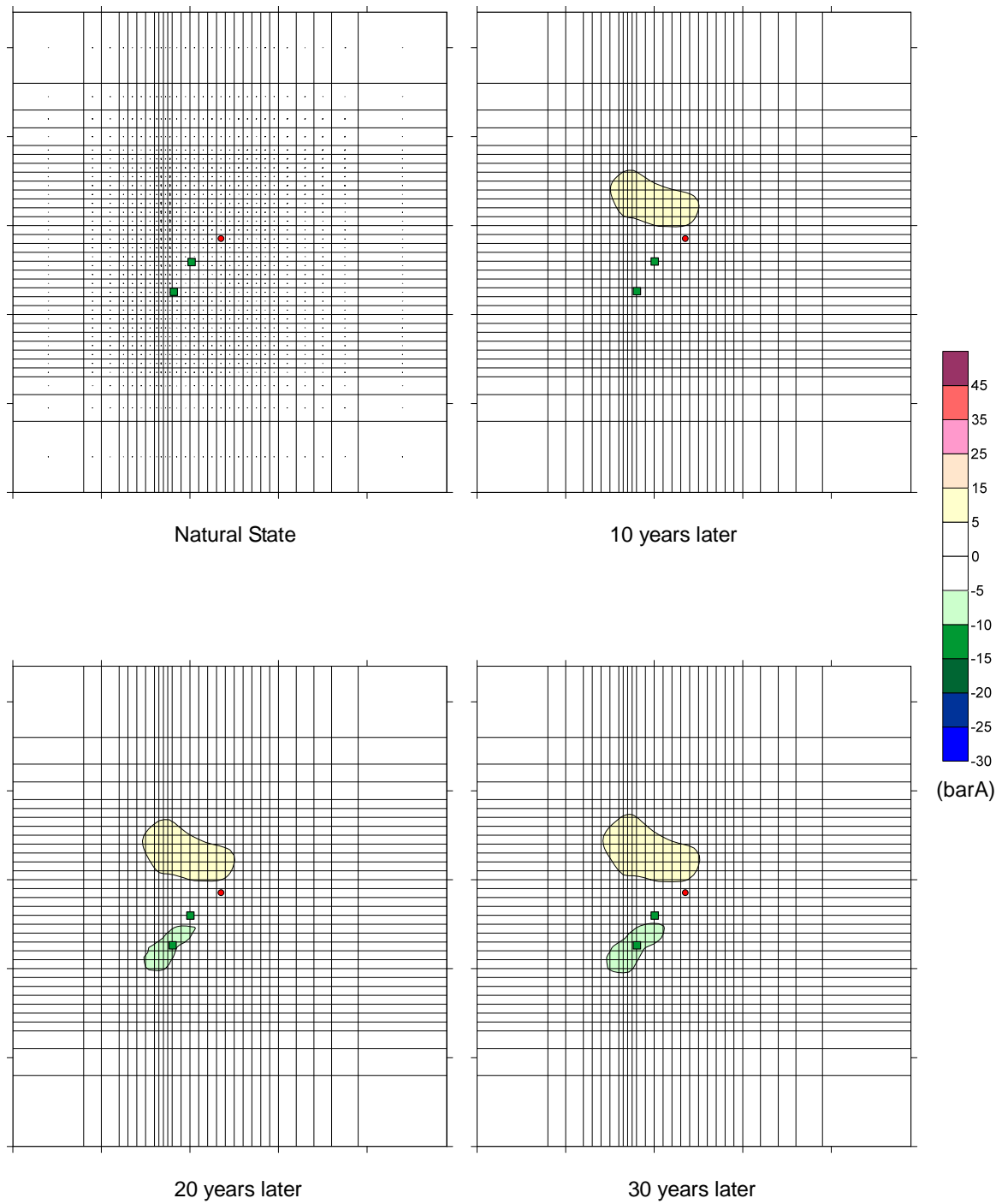


Fig. 3.3-77 Pressure Difference from Steady State in Layer 8 (EL. -700 m asl)

Layer 5 (EL. 0 m ~ -200 m)

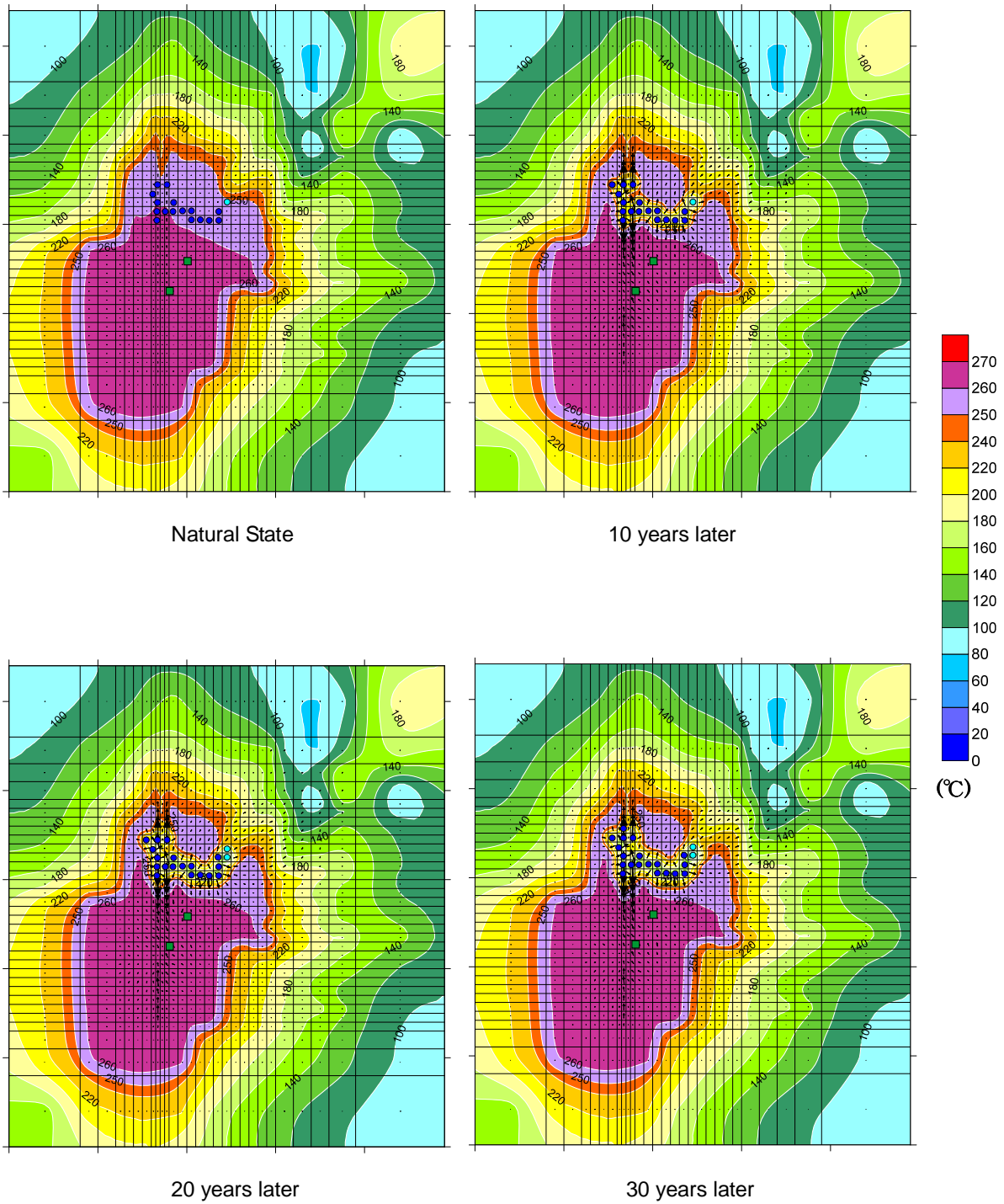


Fig. 3.3-78 Forecasted Temperature Distributions in Layer 5 (EL. -100 m asl)

Layer 6 (EL. -200 m ~ -400 m)

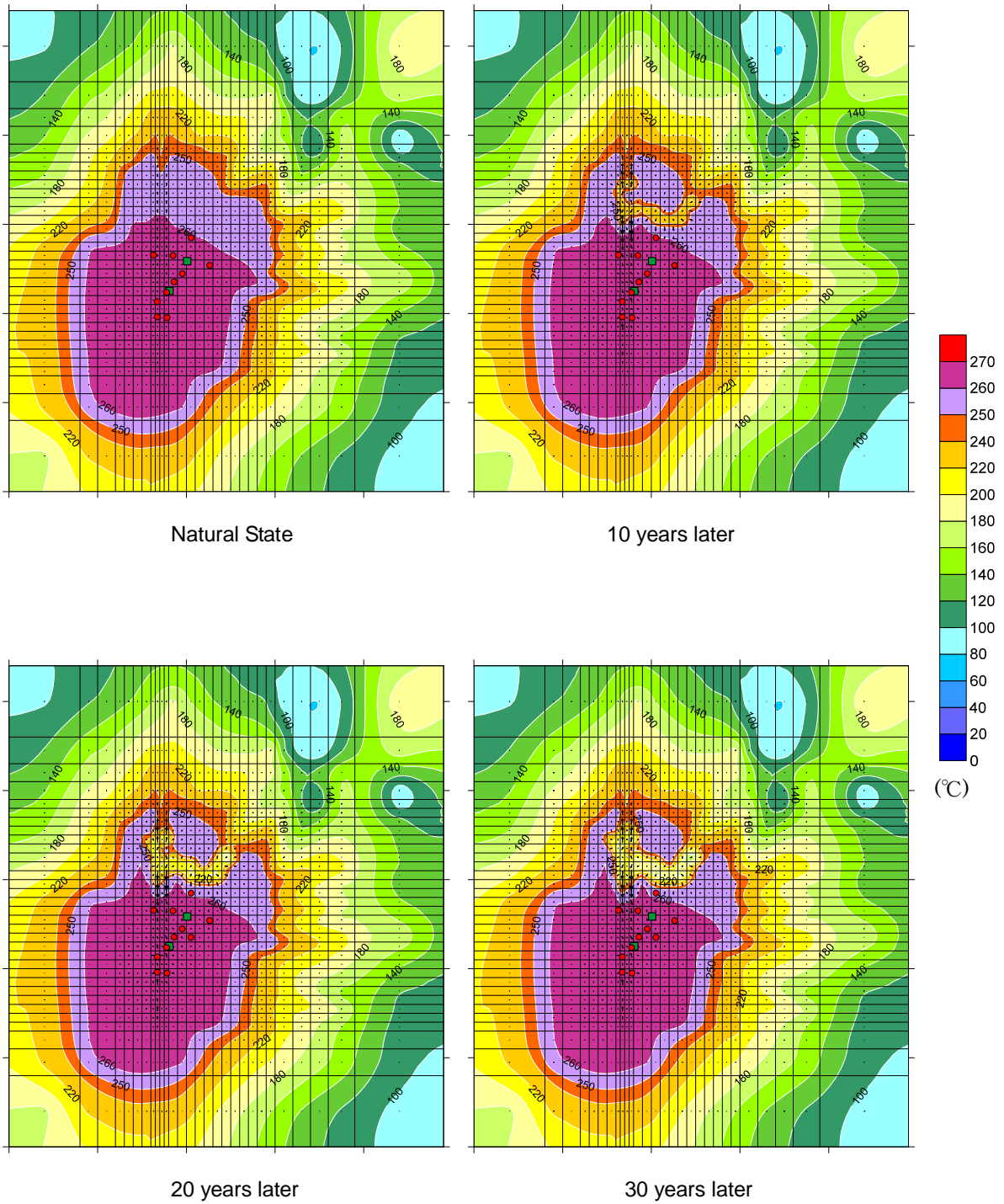


Fig. 3.3-79 Forecasted Temperature Distributions in Layer 6 (EL. -300 m asl)